

EXPRESSION OF IONOTROPIC GLUTAMATE RECEPTORS IN NEOCORTICAL MICROCIRCUITS

Txomin Lalanne

Integrated Program in Neuroscience
McGill University, Montreal, Quebec, Canada

August 2015

A thesis submitted to McGill University in partial fulfillment of the
requirements of the degree of Doctor of Philosophy

© Txomin Lalanne 2015

Table of contents

Table of contents	2
List of figures	5
List of tables	7
Preface	8
Acknowledgments	10
Résumé	11
Summary	13
List of abbreviations	15
Chapter I: Introduction	16
The visual neocortex	16
Inhibitory neurons of the visual neocortex	19
L5 Basket and Martinotti cells have distinct features	20
Properties of basket and Martinotti cells	22
Synaptic transmission	24
Excitatory transmission: glutamate receptors	28
The NMDA receptor.....	29
The AMPA receptor	32
Synaptic plasticity	36
Spike-timing-dependent plasticity	37
Mechanisms of STDP	40
Variability of STDP	42
Plasticity of PC-IN synapses	43

Main question	45
Chapter II: Methods	47
Experimental strategy	47
Relevance of main techniques	48
Quadruple whole-cell recordings	48
Two-photon laser-scanning microscopy	51
Using quadruple whole-cell recordings to study spike-timing-dependent plasticity in acute neocortical slices	55
Introduction	56
Materials	57
Protocol	59
Troubleshooting	66
Discussion	70
Recipes	71
Acknowledgments	73
Chapter III: Results	79
Synapse-specific expression of calcium-permeable AMPA receptors in neocortical layer 5	79
Abstract	80
Impact statement	80
Introduction	81
Results	84
Discussion	91
Materials and methods	100
Acknowledgements	114
Additional information	114
Funding	114

Author contribution	115
Ethics	115
Figures.....	116
Supplemental Figures.....	130
Additional discussion (not included in manuscript).....	134
Additional Figures (not included in the manuscript).....	136
Target-specific expression of presynaptic NMDARs	139
Summary	139
Results.....	139
Discussion	141
Synapse-specific long-term plasticity	148
Summary	148
Results.....	149
Discussion	151
Chapter IV: Concluding remarks.....	157
Appendices	160
Appendix 1: List of publications	160
Appendix 2: List of posters and presentations	161
Posters	161
Presentations.....	162
References	164

List of figures

Figure 1.1: General organization of the visual neocortex.....	18
Figure 1.2: Simplified view of inhibitory neurons targeting of PCs	21
Figure 1.3: Distinctive features of basket and Martinotti cells	25
Figure 1.4: General structure of AMPA receptors	30
Figure 1.5: AMPA receptors Ca^{2+} -permeability and rectification.....	35
Figure 1.6: Spike-timing-dependent plasticity	39
Figure 1.7: The frequency-dependent and independent microcircuits	45
Figure 2.1. Multiple whole-cell recordings	49
Figure 2.2. Principle and advantages of two-photon microscopy.....	53
Figure 2.3. NPEC-AMPA uncaging	54
Figure 2.4: Recording setup	74
Figure 2.5: Finding connected neurons using quadruple recordings	75
Figure 2.6: Using paired recordings study plasticity.....	76
Figure 2.7: Morphological cell classification from 2-photon images	77
Figure 3.1: Lower GluA2 immunolabeling in Pvalb-positive than in Sst-positive INs	116
Figure 3.2: Morphology classified recorded INs into MCs and two types of BCs....	117
Figure 3.3: Monosynaptic connections from PCs to BCs but not to MCs rectify	119
Figure 3.4: AMPA uncaging currents rectify in BCs but not in MCs	121
Figure 3.5: Rectification of BC mEPSCs is spermine dependent.....	123
Figure 3.6: AMPAR currents decay faster in BCs than in PCs and MCs	125
Figure 3.7: Rapid AMPAR kinetics temporally sharpens BC-mediated inhibition ...	126
Figure 3.8: Axonal morphology classified BCs into two types.....	131

Figure 3.9: PC-BC connections short-term depress whereas PC-MC synapses facilitate	132
Figure 3.10: Both PC-MC and PC-BC connections have postsynaptic NMDARs...	133
Figure 3.11: Naspm decreases the amplitude of PC-MC synapses.....	136
Figure 3.12: PC-PC synapses do not express CP-AMPARs	137
Figure 3.13: Role of CP-AMPARs in the BC-mediated early inhibition	138
Figure 3.14: MNI-NMDA Specifically Acts on NMDARs	144
Figure 3.15: NMDAR blockade in pre but not postsynaptic PCs suppresses EPSPs	146
Figure 3.16: STDP at PC-PC and PC-IN synapses	155
Figure 3.17: STDP at IN-PC synapses.....	156
Figure 4.1: Conclusion	159

List of tables

Table 2.1: Equipment	58
Table 2.2: Composition of artificial cerebrospinal fluid	71
Table 2.3: Composition of intracellular solution.....	72
Table 3.1: Synaptic properties of BCs and MCs	128
Table 3.2: Intrinsic Properties of BCs	129
Table 3.3: All INs were morphologically identified	130

Preface

I describe here the work that allowed us to demonstrate the synapse-specific expression of calcium-permeable AMPA receptors – whose properties influence synaptic transmission and plasticity – at excitatory connections onto the most abundant inhibitory neuron type in layer 5 of the mouse visual neocortex, the basket cell. In contrast, those receptors were not expressed at excitatory connections onto another major type of inhibitory neuron, the Martinotti cell. Furthermore, because we previously demonstrated the synapse-specific expression of presynaptic NMDA receptors at excitatory inputs onto Martinotti but not basket cells (Buchanan et al., 2012), we set out to explore the functional consequences of synapse-specific receptor expression on synaptic transmission and plasticity by combining multiple whole-cell recordings and photo-uncaging as well as two-photon laser-scanning microscopy, digital reconstruction to identify inhibitory neuron types, computer modeling, and dynamic clamp.

The thesis contains two manuscripts that have been either accepted or submitted for publication and are complemented by unpublished results. The first publication (in press, Cold Spring Harbor Laboratory Protocols) focuses on the techniques, and provides details on the equipment and main experimental protocol employed for multiple whole-cell recordings of morphologically identified neocortical inhibitory neurons and explains the procedure to record synaptic transmission and plasticity. The second manuscript details the rationale, the experimental approach and the results demonstrating the synapse-specific expression of calcium-permeable AMPA receptors. Furthermore, the work published in 2012 (Buchanan et al., 2012),

to which I contributed, provides evidence of the synapse-specific expression of presynaptic NMDA receptors in the same neocortical microcircuit. The unpublished results that complement the synapse-specific expression of both AMPA and NMDA receptors consist in an attempt to link these receptors to long-term synaptic plasticity.

I performed the vast majority of the experiments and data analysis presented in this thesis. Contributions that are not mine are clearly stated in the corresponding sections.

Acknowledgments

I express my sincere gratitude to Dr. Sjöström for the invaluable guidance he provided me with throughout my PhD.

I am also grateful all members of the Sjöström lab for their help, particularly Dr. Therese Abrahamsson, who's continuous advice and support has been critical. I also thank the members of my PhD advisory committee, Dr. Jean-Claude Lacaille and Dr. Rudiger Krahe for their comments, advice and support.

Beyond the laboratory, I would like to thank my family and particularly my parents for all the efforts they made to allow me to pursue PhD at McGill University, and Anthony for his patience and unconditional support.

Résumé

La transmission synaptique, mais aussi le développement et la réorganisation constante des circuits nerveux, ou plasticité synaptique, dépendent de la composition en récepteurs et canaux ioniques des éléments pré et postsynaptiques. Notamment, au niveau des connexions entre neurones excitateurs les récepteurs NMDA jouent un rôle fondamental dans l'induction de la plasticité à long terme, qui elle-même sous-tend théoriquement l'apprentissage et la mémoire en permettant l'entrée de calcium dans la cellule postsynaptique, activant une cascade de signalisation aboutissant au renforcement de la connexion. Étant donné que les récepteurs NMDA sont ouverts lors de la combinaison d'une dépolarisation postsynaptique et de la libération présynaptique de glutamate, ils jouent le rôle de détecteurs de coïncidence aux synapses excitatrices.

La complexité des circuits du néocortex ainsi que la grande diversité de neurones inhibiteurs qui s'y trouve rendent leur étude difficile. La plasticité des connexions excitatrices sur les neurones inhibiteurs est de fait moins bien connue mais il est clair qu'elle varie avec le type cellulaire et dans certains cas ne requiert pas de récepteurs NMDA. En effet, certains neurones inhibiteurs de l'hippocampe, de l'amygdale ou encore du cervelet expriment très peu voire aucun récepteur NMDA. Le calcium nécessaire à l'induction de plasticité pourrait provenir de récepteurs AMPA perméables au calcium, mais le pattern d'expression de ces récepteurs par les différents types de neurones inhibiteurs n'est pas clairement établi, notamment du fait de leur diversité et de la difficulté à les distinguer.

Ici, nous avons combinés des enregistrements quadruples en configuration cellule-entière avec la microscopie 2-photons ainsi que le décaageage optique de AMPA afin de déterminer l'expression des récepteurs AMPA perméables au calcium ainsi que des récepteurs NMDA aux synapses excitatrices sur deux type majeurs de neurones inhibiteurs néocorticaux : les cellules en panier et les cellules de Martinotti. Nous avons ainsi pu déterminer que les récepteurs AMPA perméables au calcium sont spécifiquement exprimés aux synapses sur les cellules en panier mais pas sur les cellules de Martinotti. La combinaison de modèle informatique et de d'enregistrements « dynamic clamp » nous a par ailleurs permis d'identifier une fonction possible des récepteurs dans les circuits de la couche 5 du neocortex. Nous avons par le passé démontré l'expression de récepteurs NMDA présynaptiques spécifiquement aux synapses sur les cellules de Martinotti mais pas celles sur les cellules en panier. Finalement, nous explorons les conséquences possibles de cette double expression spécifique de deux types majeurs de canaux ioniques sur la plasticité synaptique, en particulier la plasticité « spike-timing-dependent ». Au final, ces travaux aideront à déterminer comment et pourquoi la plasticité synaptique diffère d'un type de neurone inhibiteur à un autre et donc de mieux comprendre d'une part comment se forment les circuits néocorticaux, et d'autre part comment l'information est traitée dans ces réseaux.

Summary

Synaptic transmission as well as the constant reorganization of connections between neurons — known as synaptic plasticity — depend on the composition of synaptic ion channels and receptors. At excitatory connections onto excitatory cells, NMDA receptors play a critical role in long-term plasticity. Upon glutamate binding, NMDA receptors allow the entry of calcium into postsynaptic compartments, which initiates a cascade of reactions leading to the strengthening of the connection. Because postsynaptic NMDA receptors are only open when the postsynaptic cell is depolarized and the presynaptic cell has released glutamate, NMDA receptors act as coincidence detectors.

The complexity of the neocortical circuitry and the diversity of the inhibitory neuron population make it difficult to study the plasticity of a precise, well-defined synapse type involving inhibitory neurons. As a consequence, plasticity of excitatory connections onto inhibitory neurons has been less studied and seems more variable, not always requiring NMDA receptors. Indeed, some inhibitory neuron types in the hippocampus, amygdala and cerebellum express little, if any, NMDA receptors. Yet synapses onto these interneurons undergo plasticity, and there is evidence that the calcium required to trigger this plasticity may arise from calcium-permeable AMPA receptors. The gating properties of calcium-permeable AMPA receptors are almost opposite to that of NMDA receptors: calcium-permeable AMPA receptors are open at negative membrane potentials but are closed at positive. Indeed, this may explain why synaptic plasticity in interneurons often is quite different. However, the precise expression pattern of calcium-permeable AMPA receptors in neocortical inhibitory

neurons remains poorly studied, perhaps due to the challenge posed by their clear identification.

Here, we combined multiple whole-cell recordings with uncaging and two-photon laser-scanning microscopy to determine the pattern of expression of calcium permeable AMPA receptors and NMDA receptors in two major neocortical layer 5 inhibitory neuron types: basket and Martinotti cells. We found that excitatory connections onto basket but not onto Martinotti cells expressed calcium-permeable AMPA receptors. Combining computer modeling and dynamic clamp recordings, we showed that the presence of calcium-permeable AMPA receptors may help sharpen response latencies and durations in basket cells. Moreover, we previously demonstrated that presynaptic NMDA receptors are specifically expressed at excitatory connections onto Martinotti cells but not onto basket cells. Finally, we explored the possible consequences of synapse specific expression of AMPA and NMDA receptors for long-term synaptic plasticity. My work will help determine how and why plasticity differs between inhibitory neuron types and it will improve our understanding of information processing in neocortical microcircuits.

List of abbreviations

2PLSM: 2-photon laser-scanning microscopy

AMPA: α -amino-3-hydroxy-5-methylisoxazol-4-propionate

AMPAR: AMPA receptor

AP: action potential

AP5: (2R)-amino-5-phosphonovaleric acid

bAP: backpropagating AP

BC: basket cell

CP-AMPAR: calcium-permeable AMPAR

CI-AMPAR: calcium-impermeable AMPAR

DNQX: 6,7-dinitroquinoxaline-2,3-dione

EPSC: excitatory postsynaptic current

EPSP: excitatory postsynaptic potential

GABA: γ -aminobutyric acid

IN: inhibitory neuron

KAR: kainate receptor

LTD: long-term depression

LTP: long-term potentiation

MC: Martinotti cell

Naspm: 1-naphthyl-acetyl spermine

NMDA: N-methyl-D-aspartic acid

NMDAR: NMDA receptor

PC: pyramidal cell

preNMDAR: presynaptic NMDAR

STDP: spike-timing-dependent plasticity

TEA: tetraethyl ammonium

TTX:

tetrodotoxin

Chapter I: Introduction

The visual neocortex

The visual neocortex is one of the best-described brain areas. Although very complex, its circuitry is relatively well known. As a consequence, the visual neocortex serves as a good model to study the mechanisms of synaptic transmission and plasticity. It possesses a clear columnar and laminar organization, six different layers (L1 to L6) being distinguished by their cellular population and density (Mountcastle, 1997, Callaway, 1998, Harris and Mrsic-Flogel, 2013). Most of the sensory inputs to primary cortices, including visual cortex come from the thalamus, which projects mainly to L4. Most connections from L4 are towards L2 and L3, which are in turn connected to L5. L5 is the main output from the neocortex to subcortical structures. This simplified view of the neocortical circuitry is schematically described in **figure 1.1.** and has recently been updated by Constantinople and Bruno, who demonstrated that although most sensory inputs from the thalamus target L4, they also project significantly to L5 and L6. Using in vivo recordings and pharmacology, they showed that sensory-evoked responses in L5 and L6 are independent from L4 activation and arise directly from the thalamus (Constantinople and Bruno, 2013). Interestingly, Rubio-Garrido et al. (2009) showed that L1 is an important target of thalamic inputs to the neocortex, while they found few inputs to L4. Those recent insights into thalamocortical projections can be reconciled by taking into account the fact that thalamic inputs to the neocortex can be divided into two categories, with a group preferentially targeting L4 and to some extent L5 and L6, and another group of projections mostly targeting L1. In the end, although the classical hierarchical view

of information processing in neocortical circuits may be correct, it has become much more nuanced over the past decade, in particular because of technical improvements (Harris and Shepherd, 2015).

About 80% of cells in the visual neocortex are excitatory pyramidal cells (PCs), which use glutamate as a neurotransmitter (Beaulieu and Colonnier, 1985). PCs are present in L2 to L6 and are easy to recognize by their characteristic morphology: they possess a large pyramidal soma (about 25 μm in diameter), with a thick apical dendrite extending up to L1 (except for L6 PCs which only go up to L2/3) where it ramifies to produce a dense local dendritic arborisation (DeFelipe and Farinas, 1992). This morphology allows trans-laminar L5 PCs to be innervated by neurons in all neocortical layers (Kätzel et al., 2011). The general connectivity of L5 neocortical PCs is around 11% (Thomson et al., 1993, Markram, 1997, Thomson et al., 2002). However, connectivity in the neocortex is not random and PCs are organized in clusters, within which cells tend to respond to similar visual properties and which present higher connectivity rates (Ko et al., 2011).

Although neocortical PCs are present in L2/3 to L6 and constitute the majority of excitatory cells in the neocortex, other excitatory cell types exist. Those cells seem to be restricted within specific lamina. For example, the spiny stellate cells seem to be expressed solely in L4 (although mostly in the auditory cortex in rodents), where they receive most of the thalamic sensory inputs, although most excitatory connections onto them are from other L4 spiny stellate cells (da Costa and Martin, 2011). Similarly, glutamatergic non-pyramidal cells have been described in L6 (Andjelic et al., 2009). The present work focuses only on L5 and excitatory cells were all visually identified as PCs.

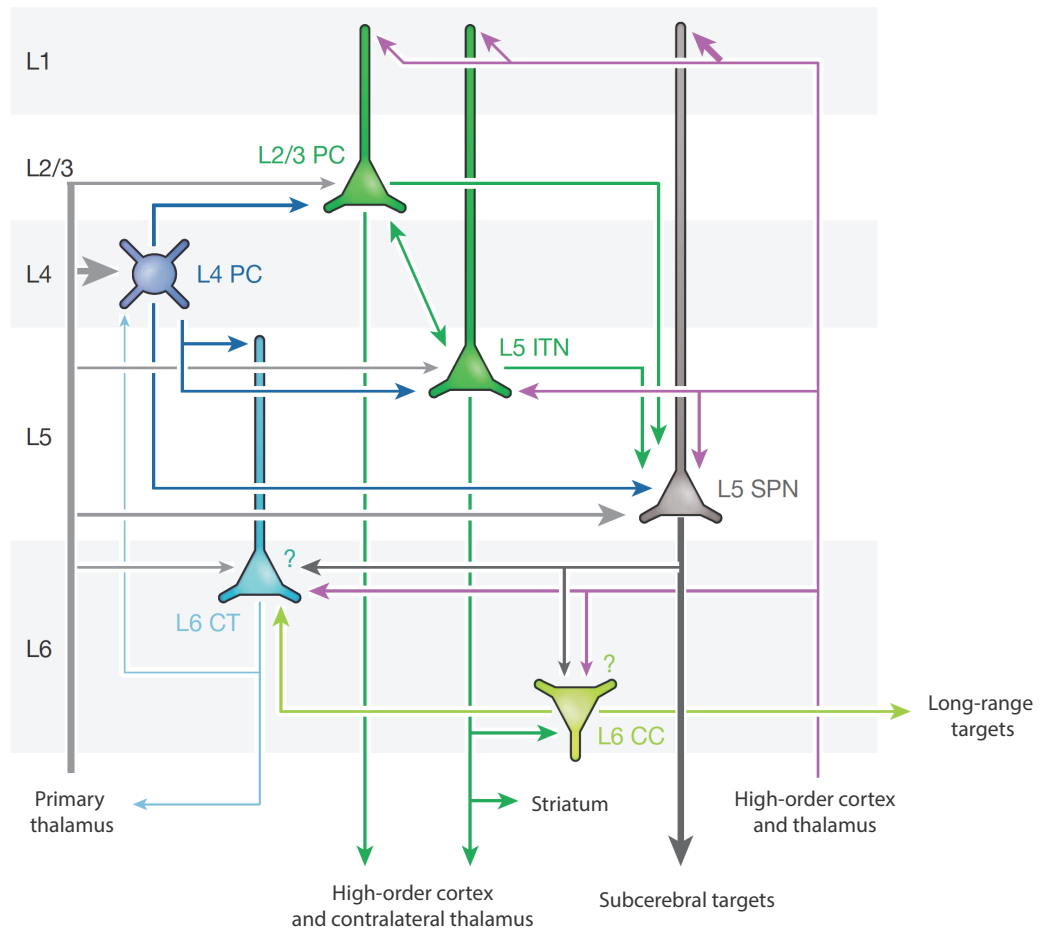


Figure 1.1: General organization of the visual neocortex

Schematic view of the visual neocortical circuitry (with respect to PCs). Most primary sensory inputs arrive from the thalamus in L4 but also to L5 and L2/3 to a smaller extent. L4 projects to both L5 and L2/3 while L2/3 mainly targets L5. The major output is from L5 PCs, which project to subcortical structures, particularly the thalamus. A parallel pathway, conveying information from higher order thalamic inputs target mostly L1, and very little L4. From (Harris and Mrsic-Flogel, 2013).

Inhibitory neurons of the visual neocortex

The remaining 20% of neuronal cells in the neocortex are inhibitory neurons (INs) using γ -aminobutyric acid (GABA) as a neurotransmitter (Hendry et al., 1987). They encompass a very diverse group of neurons both morphologically and electrophysiologically (Somogyi et al., 1998, Markram et al., 2004). Morphologically, INs are mostly identified by their axonal arborization, but also dendritic morphology, soma shape and spine number and size. Electrophysiologically, firing pattern is key to identify INs along with other cellular electrophysiological parameters such as membrane potential (V_m), action potential (AP) threshold, spiking frequency, and AP width and duration (Ascoli et al., 2008). INs also present distinct patterns of expression of three Ca^{2+} binding proteins: calbindin, calretinin and parvalbumin (Pvalb), as well as four peptides: vasoactive intestinal peptide, somatostatin (Sst), neuropeptide Y and cholecystinin. These factors constitute a third classification criterion (Demeulemeester et al., 1991, Kawaguchi and Kubota, 1997). For many IN types however, none of these criteria is perfect and expression patterns are often overlapping or incomplete. For example, two INs with the same pattern of protein expression may have different morphologies and/or different electrophysiological properties (Cauli et al., 1997, Karube et al., 2004). The diversity of IN subtypes and the relatively low efficiency of those identification criteria are such that some have even wondered whether there is any classification possible at all, and have suggested that maybe INs are a continuum rather than a set of classes (Parra et al., 1998). IN categorization thus poses a challenge, yet it is essential to identify cells across studies. To help overcome this hurdle and to provide a common basis for future work, the Petilla nomenclature was established in 2008 (Ascoli et al., 2008, DeFelipe et al., 2013). Two IN types are particularly well defined, making them

relatively easy to identify (Toledo-Rodriguez et al., 2005): basket cells (BCs) and Martinotti cells (MCs) (**see figure 1.3**).

Interestingly, connectivity from INs onto PCs seems to be higher than between PCs or from PCs to INs, at least for Sst-positive cells (around 50%) (Fino and Yuste, 2011). Furthermore, INs are not equally distributed in the neocortical layers and, because their axons arborize in cell-type specific ways, they usually target specific dendritic compartments of L5 PCs (Kätzel et al., 2011, Jiang et al., 2013). MCs, for example, specifically target the distal dendrites of PCs (Silberberg and Markram, 2007). BCs, however, are specialized in inhibiting the soma and proximal dendrites (Somogyi et al., 1998, Wang et al., 2002). Therefore the prevalent view is that inhibition in the neocortex is not random but highly specific, (Gupta et al., 2000, Kätzel et al., 2011, Jiang et al., 2013). To illustrate this specificity, a schematic view of IN targeting of specific PCs compartments is presented in **figure 1.2**. INs also inhibit each other, and it has recently been shown that connectivity between neocortical INs can be close to 100%. This innervation, however, is cell-type dependent, with e.g. Sst-positive cells preferentially innervating all IN types except themselves. Pvalb-expressing cells, on the other hand, seem to preferentially target other Pvalb-positive INs (Pfeffer et al., 2013).

L5 Basket and Martinotti cells have distinct features

Typically, nearly 100% of MCs express Sst, but never Pvalb (Toledo-Rodriguez et al., 2005). Both large and nest BCs, on the other hand, express Pvalb, which means a majority of BCs are positive for Pvalb (Markram et al., 2004). MCs also have a characteristically ascending axon going up to layer 1 where it can extend horizontally a few millimeters, whereas BCs typically have a locally ramified

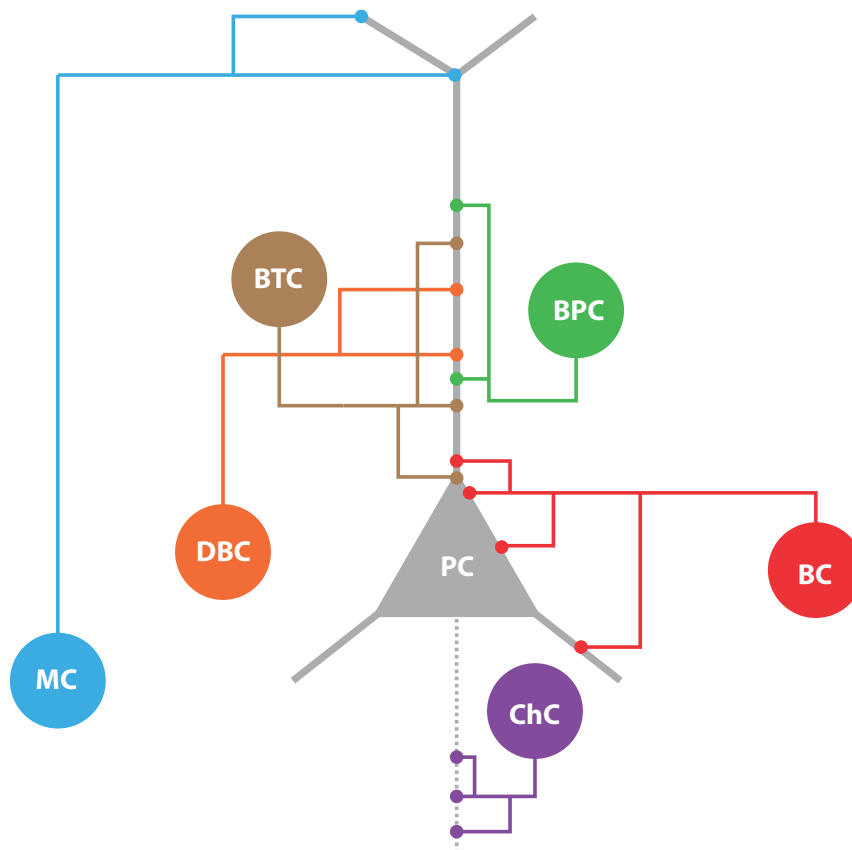


Figure 1.2: Simplified view of inhibitory neurons targeting of PCs

Non-exhaustive list of the different IN types present in L5 of the mouse visual neocortex (MC: Martinotti cell, BC: basket cell, DBC: double-bouquet cell, ChC: chandelier cell, BPC: bipolar cell and BTC: bitufted cell). Colored lines represent the axon. Filled circles denote the location of inhibitory synapses onto a PC (grey). Because of their specific axonal morphology, each IN is specialized in targeting a specific subcompartment of PCs. For example, MCs (blue, ~20% of all L5 INs) preferentially inhibit the distal dendrites of PCs in L1, whereas BCs (red, ~50% of all L5 INs) contact their soma and proximal dendrites, mainly in L5, and ChC (purple) preferentially target the axon hillock.

axon that is restricted to L5 (Kawaguchi and Kubota, 1997). In keeping with their morphological structure, MCs mostly inhibit the distal apical dendritic arbor of PCs, while BCs preferentially target the soma and proximal dendrites (Silberberg and Markram, 2007, Kätzel et al., 2011).

Moreover, MCs have a low spiking threshold and accommodating firing pattern, whereas BCs have a high spiking threshold and fast non-accommodating firing pattern (Kawaguchi and Kubota, 1996, Markram et al., 2004, DeFelipe et al., 2013). Finally, excitatory synapses onto MCs are strongly short-term facilitating whereas those onto BCs are short-term depressing (Buchanan et al., 2012, Blackman et al., 2013), and this can be used as an additional criterion to identify cell type. In the end, it appears that because they present essentially mutually exclusive features, a combination of different techniques permits a clear identification of BCs and MCs, whose main features are illustrated in **figure 1.3**.

To aid in the targeting of BCs and MCs, transgenic mouse lines exist that express eYFP specifically in Pvalb (Chattopadhyaya et al., 2004) or Sst-positive cells (Oliva et al., 2000). These mouse lines are very useful to target BCs and MCs, which identity can then be confirmed by electrophysiological measurements and morphology quantification (see **figure 1.3**, **figure 2.7** and **figure 3.2**).

Properties of basket and Martinotti cells

Some important functions of MCs and BCs have been described. For example, even though they represent only around 20% of the neocortical IN population (Gonchar and Burkhalter, 1997), Sst-positive INs have been shown to be very efficient at regulating PCs activity thanks to their dense connectivity (Fino and Yuste, 2011). Furthermore, the short-term facilitating PC-MC synapse give rise to

both a strong temporal and spatial summation that results in a widespread inhibition (Kapfer et al., 2007, Berger et al., 2010). Because of these particularities, a small number of PCs activating a small number of MCs can result in a very strong inhibition. Interestingly, it has also been shown that Sst-positive cells in L2/3 of the somatosensory cortex seem to be the only neuronal type active during passive wakefulness, during which they provide tonic inhibition of neighboring cells and are however quiet when sensory information arrives (Gentet et al., 2012). Regarding Pvalb-expressing INs, which account for approximately half of the neocortical IN population (Celio, 1986, Kisvarday, 1992), Atallah et al. (2012) selectively activated and inhibited those cells in the visual cortex and observed that they were able to modulate PCs activity without affecting their selectivity for visual information, and thus suggest that they are able to modulate the gain. PV-expressing INs are also critical in the generation of gamma oscillations (Cardin et al., 2009). A given cell type may have different function depending on the circuit it belongs to, and INs functions are likely to be circuit-dependent. An example of well described and simple circuits involving INs are the frequency-dependent disynaptic inhibition (FDDI) and the frequency independent disynaptic inhibition (FIDI) microcircuits, involving MCs and BCs respectively (Silberberg and Markram, 2007). As illustrated in **figure 1.7**, the motifs consist of the inhibition of a PC, or group of PCs, by MCs for FDDI and BCs for FIDI, themselves being stimulated by another group of PCs. FDDI relies on the short-term facilitating PC-MC synapses, whose release probability is low, whereas FIDI requires the short-term depressing PC-BC synapse, whose release probability is high. As a consequence, MC inputs must be activated at sufficiently high frequency in order to produce APs, which means MCs may thus act to shut down excessive excitatory activity. The feed-forward inhibition resulting from PC1

activation is thus in two temporally distinct phases mediated by BCs and MCs, respectively, as evidenced by a work by Pouille and Scanziani (2001), who demonstrated that the time window for integration (EPSPs to simplify) is broader in the distal dendrites compared to the soma and proximal dendrites of PCs. This is due to the rapid feed-forward inhibition mediated by BCs on the soma compared the slower MC-mediated inhibition on distal dendrites (Pouille and Scanziani, 2001). Finally, the short-term depressing PC-BC and facilitating PC-MC synapses optimally transfer information at low and high frequencies, respectively (Fortune and Rose, 2001, Fuhrmann et al., 2002), highlighting other functional differences between MCs and BCs.

Synaptic transmission

Most of the cells in the neocortex communicate via chemical synapses, although electrical connections (gap junctions) are also widespread, particularly between some IN types, such as BCs or between astrocytes (Galarreta and Hestrin, 1999, Fukuda and Kosaka, 2000). Here, we focus only on chemical synapses, which transform the electrical signal of a cell into a chemical one, so it can be transmitted to the postsynaptic cell. This way of communication has several advantages compared to purely electrical communication. Notably, not only it allows the control of the amplitude of the signal, but also the modulation of the sign of this signal, which can be excitatory or inhibitory. The chemicals that transmit the information are the neurotransmitters, among which the amino acids glutamate and GABA are ubiquitous in the central nervous system and mediate fast excitatory and inhibitory signaling, respectively. The repartition of ions between the internal and external parts of the neuronal membrane results in a negative resting potential (negative voltage inside compared to outside). The

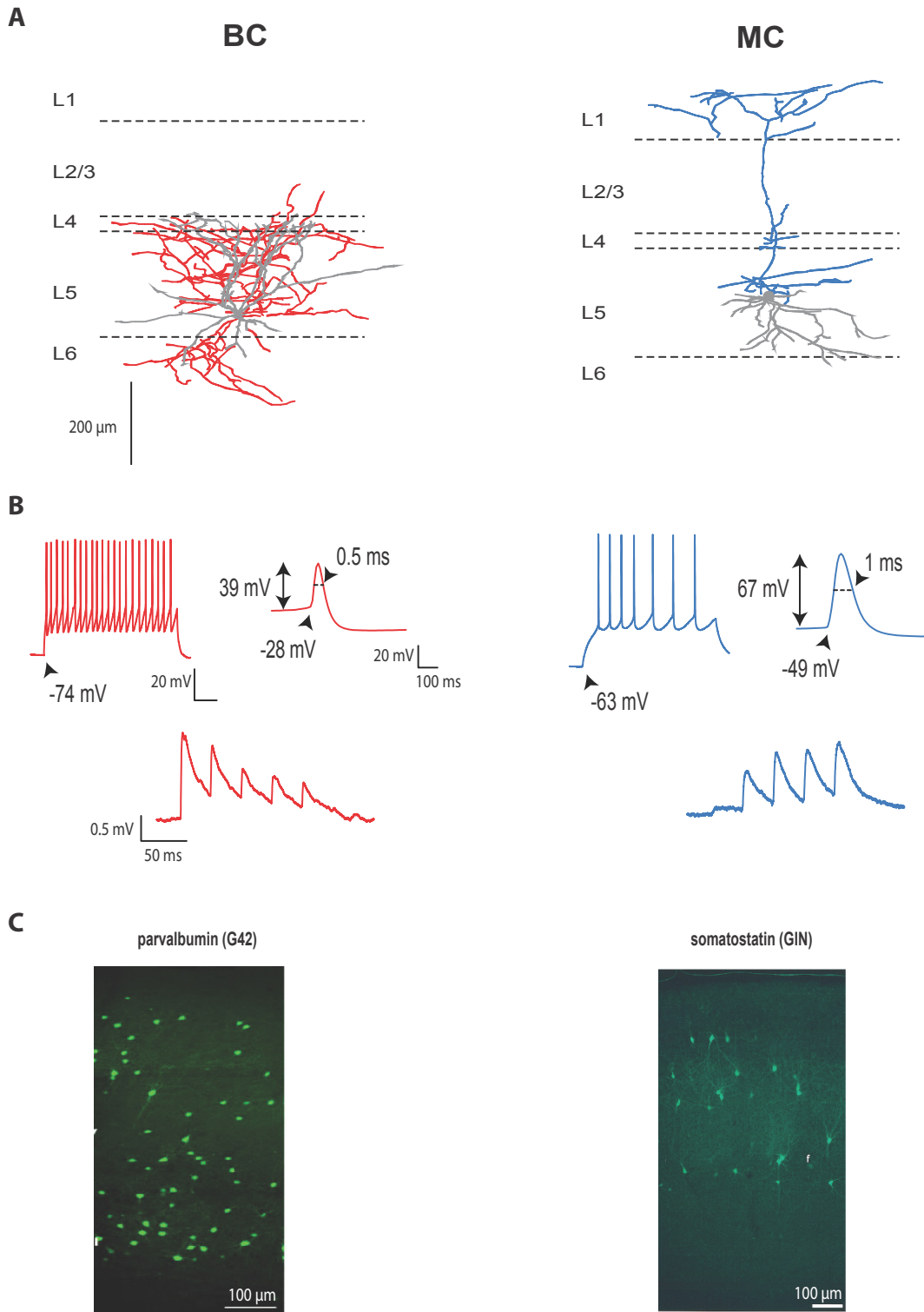


Figure 1.3: Distinctive features of basket and Martinotti cells

(A) Sample reconstruction of a BC (left) and a MC (right). Cortical layers (L1-L6) are indicated by horizontal dashed lines. The BC axon (red) is mostly restricted within L5, whereas that of the MC (blue) extends up to and ramifies within L1.

(B) Main electrophysiological distinctions between BCs and MCs, including firing pattern (top left), AP height, threshold and half-width (top right), and short-term plasticity of excitatory connections onto BC (bottom, red) and MC (bottom, blue). Scale bars apply to both BCs and MCs.

(C) To facilitate the targeting of BCs and MCs mouse lines expressing eYFP in Pvalb-positive cells (left, G42 line, (Chattopadhyaya et al., 2004) and in Sst-positive cells (right, GIN line, (Oliva et al., 2000) have been created.

predominant mechanism for fast excitatory synaptic transmission in the mammalian CNS is the depolarization (more positive potential) of the postsynaptic membrane by activation of three main types of ionotropic glutamate receptors that are described below. Conversely, GABA-mediated inhibitory synaptic transmission involves the activation of two main types of ionotropic GABA receptors.

A synaptic current can thus be excitatory (EPSC, for excitatory postsynaptic current), corresponding to a depolarization of the membrane potential skewed towards the threshold for AP generation or inhibitory (IPSC), hyperpolarizing the membrane and reducing the likelihood of an AP to occur by furthering the membrane potential from the AP threshold. In a simplified view, channels that allow the entry of Ca^{2+} and Na^{+} in the neuron have an excitatory effect at resting membrane potential, while channels allowing the entry of Cl^{-} hyperpolarize and thus inhibit the cell. Importantly, for each channel, the excitatory or inhibitory effect depends not only on the binding of the neurotransmitter, but also on several other parameters, including the reversal potential of the ions and thus on the ionic concentration inside and outside the cell, according to the Nernst equation:

$$E_x = -RT/Z_x F \cdot \ln ([X]_i/[X]_o)$$

Where the equilibrium potential (E) of a given ion (X) depends on the temperature (T), the universal gas constant (R), the charge of the ion (Z) and the concentrations of the ion inside and outside the cell ($[X]_i$ and $[X]_o$, respectively). For example, in tissue from young animals, it is known that the binding of GABA on its receptors can have an excitatory effect, due to the important intracellular chloride concentration that affects the direction of the ionic flux. GABA and glutamate are

thus not inhibitory or excitatory by themselves, but by the movements of ions they contribute to create across the membrane.

This mode of communication is well conserved throughout evolution and, even though there are a number of differences, the basic mechanism does not differ between excitatory and inhibitory chemical synapses. Indeed, in both cases neurotransmitters are encapsulated in vesicles, which are aggregated at the presynaptic terminal. A local depolarization of the presynaptic cell membrane potential, e.g. by an AP, activates voltage-dependent calcium channels that produce an increase in intracellular Ca^{2+} concentration. This Ca^{2+} then triggers the fusion of some vesicles with the cell's membrane and thus the release of the neurotransmitters in the synaptic cleft, allowing them to act on their postsynaptic targets (Nicoll, 1988, Kochubey et al., 2011, Kaeser and Regehr, 2014). The excess of neurotransmitter is recaptured by specific transporters expressed on the presynaptic side and are either degraded or recycled. This transformation of the signal at chemical synapses heavily depends on specific pre and postsynaptic composition in receptors, transporters, ion channels, adhesion proteins and other molecules that form what is called the postsynaptic density.

Excitatory transmission: glutamate receptors

Both slow metabotropic and fast ionotropic receptors, with subfamilies, exist for glutamate and all have excitatory effects. Here, we focus on the ionotropic receptors, which are responsible for the fast excitatory communication between neurons. Three types of ion channels responsive to glutamate have been identified and named according to specific agonists: the AMPA, NMDA and Kainate receptors (Cotman et al., 1988, Collingridge and Lester, 1989, Monaghan et al., 1989, Smart and Paoletti, 2012). Another receptor with sequence similarity to AMPARs, NMDARs

and KARs have been identified, but little is known about it and no clear evidence exists that it contributes to synaptic transmission by binding to glutamate: the delta receptor (Kakegawa et al., 2007, Ady et al., 2014).

The structure of the three channels is similar, they are tetramers assembled in the endoplasmic reticulum as dimers that then pair up together (Ayalon and Stern-Bach, 2001). Each subunit is made of a modular structure containing four semi-autonomous regions: the amino-terminal domain (ATD), the ligand binding domain (LBD), the trans-membrane domain (TMD) and the carboxyl-terminal domain (CTD), as illustrated in **figure 1.4** (Meyerson et al., 2014, Sobolevsky, 2015). Here, we focus on NMDARs and AMPARs. These receptors gate channels that produce a flux of cations (Na^+ , K^+ and/or Ca^{2+}), and have a reversal potential of ~ 0 mV (Traynelis et al., 2010).

Importantly, to decipher specific functions and precise location of these receptors, it is critical to isolate currents from AMPARs, NMDARs or KARs. In order to do that, pharmacological agents exist, such as D-(-)-2-amino-5-phosphonopentanoic acid (D-AP5) to block NMDARs, 2,3 diox-6-nitro-1,2,3,4-/-terahydrobenzo[f]quinox/-aline-7-sulphonamide (DNQX) to block AMPAR and KARs, or 2,3-dihydroxy-6-nitro-7-sulfamoyl benzo[f]quinoxaline-2,3-dione (NBQX) that more specifically target AMPAR-mediated currents (Traynelis et al., 2010).

The NMDA receptor

Although the structure of NMDARs is as described above, important differences in the channel's conductance and kinetics arise from the diversity of subunit types (Moriyoshi et al., 1991, Kutsuwada et al., 1992, Monyer et al., 1992). This diversity itself comes from seven genes that encode the subunits: GRIN1,

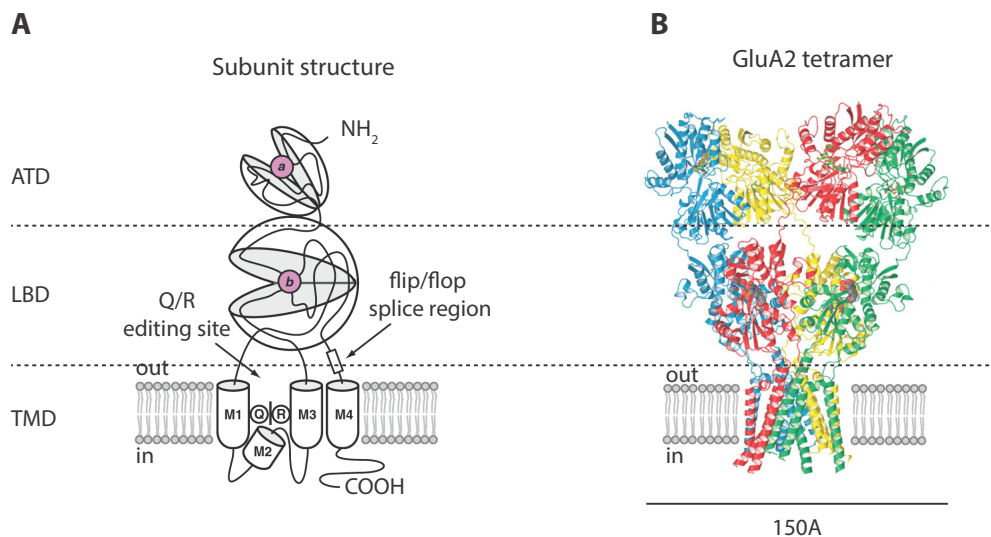


Figure 1.4: General structure of AMPA receptors

(A) Schematic representation of an AMPAR subunit, composed of three main modular domains: the amino-terminal domain (ATD), the ligand-binding domain (LBD), the transmembrane domain (TMD), which constitutes the channel pore. Note the position of the flip/flop and Q/R editing sites, which both critically affect the properties of the receptor.

(B) Tetrameric structure of the AMPAR (recombinant GluA2 homomer in this case) showing the general arrangement of the subunits as dimers of dimers. Each subunit is in a different color. Adapted from (Fleming and England, 2010, Traynelis et al., 2010)

GRIN2A-D and GRIN3A-B (Ikeda et al., 1992, Monyer et al., 1992, Ishii et al., 1993), (for review, see Traynelis et al., 2010).

Voltage-dependence

When recording the current through NMDARs at different membrane potentials, an outward-rectifying current/voltage (IV) relationship appears, which means no or little current exist for negative potentials. This IV relationship, however, becomes linear if depleting the bath of Mg^{2+} ions, because NMDARs are blocked by Mg^{2+} (and Zn^{2+} to a lesser extent) at negative membrane potentials (Nowak et al., 1984, Mayer and Westbrook, 1987, Ascher and Nowak, 1988). As discussed below, this property has important implications for synaptic plasticity, and it is known that NMDARs play a critical role in this phenomenon by acting as detectors of coincident activity: they can only be opened by nearly simultaneous presynaptic glutamate release and postsynaptic depolarization (Cotman et al., 1988, Bliss and Collingridge, 1993). Indeed, the most studied and commonly used plasticity paradigm, developed by the Canadian psychologist Donald Hebb (Hebb, 1949), can be summarized by “cells that fire together, wire together” (Carla Shatz, 1992), meaning that the response amplitude in the postsynaptic neuron, or synaptic strength, is increased when the presynaptic cell repeatedly contributes to evoking APs in the postsynaptic cell. This is due to the fact that NMDARs are open by a depolarization (removal of magnesium block), and can thus flux Ca^{2+} only when the postsynaptic cell is depolarized in a short time window from glutamate release by the presynaptic cell. Interestingly, this critical function of NMDARs seems to only make sense if they are present on the postsynaptic cell (Duguid and Sjöström, 2006), and it is thus not entirely surprising that they have long been thought to be expressed postsynaptically

only. However, as discussed in the following section, NMDARs are also expressed presynaptically at many synapse types.

Presynaptic expression of NMDARs

Recently, there has been increasing interest and debate regarding the existence of presynaptic NMDARs (preNMDARs). Putative preNMDARs have been observed in e.g. spinal cord (Bardoni et al., 2004), cerebellum (Casado et al., 2002, Duguid and Smart, 2004), amygdala (Humeau et al., 2003), and neocortex (Berretta and Jones, 1996, Sjöström et al., 2003). Accumulating evidence also suggests that preNMDARs play important roles in regulating both spontaneous and evoked neurotransmission (Sjöström et al., 2003, Bardoni et al., 2004, Duguid and Smart, 2004). They have also been shown to be critical for LTD (Casado et al., 2002, Sjöström et al., 2003) and LTP (Humeau et al., 2003) induction. As detailed below, there have been various discrepancies in the identification of preNMDARs with for example a research group observing preNMDARs at synapses onto granule cells in the cerebellum (Casado et al., 2000, Casado et al., 2002), while others did not (Shin and Linden, 2005). This is likely due at least in part to their synapse-specific expression (Buchanan et al., 2012), which highlights the importance of clearly identifying cell types.

The AMPA receptor

AMPA receptors mediate most of the fast excitatory transmission in the brain (Trussell and Fischbach, 1989, Colquhoun et al., 1992, Jonas and Sakmann, 1992). As with NMDARs, the four subunits of the AMPARs are diverse (Keinanen et al., 1990). They arise from four different genes, GRIA1 to GRIA4. However, from the

transcription to the insertion of the receptors to the membrane, several modifications may happen that can affect the properties of the channels considerably, for example ion-selectivity, permeability, and channel kinetics. Importantly, the RNA subunits undergo post-transcriptional modifications. First, AMPAR subunits exist in 2 splicing variants, named “flip” and “flop” (Salussolia and Wollmuth, 2012), which site is indicated in **figure 1.4**. These splicing variants notably affect the kinetics of the channels. Another modification of the subunits dramatically modifies their properties: the edition of the Q/R site, see **figure 1.4** and (Sommer et al., 1991). On the GluA2 subunit, this modification exchanges a glutamine for a positively charged arginine in the transmembrane domain, which later forms part of the channel pore. This positive charge, which is present in most AMPARs, prevents the passage of Ca^{2+} . Hence, the absence of GluA2 leads to critical changes in the receptor properties, as described below. Finally, the GluA2 edition site is also important for the receptors assembly and stoichiometry, and particularly it favors the insertion of GluA2 in AMPARs by retaining the GluA2 subunit in the endoplasmic reticulum longer than the other subunits (Greger et al., 2003). Thus, most AMPARs contain the GluA2 subunit and have similar properties, outlined below.

GluA2 edition and Ca^{2+} -permeability

The presence of the arginine in the channel pore of AMPARs containing the edited GluA2 subunit allows small ions such as K^+ and Na^+ to cross the channel. However, Ca^{2+} is unable to go through due to the arginine’s positive charge and hence most AMPARs are impermeable to Ca^{2+} (Hume et al., 1991, Sommer et al., 1991, Greger et al., 2003). Although most AMPARs contain the GluA2 subunit, GluA2-lacking receptors are widespread throughout the brain and have notably been

observed at excitatory connections onto inhibitory neurons (Mahanty and Sah, 1998, Kullmann and Lamsa, 2007, Oren et al., 2009). These receptors cannot prevent the passage of Ca^{2+} because of the absence of the positive charge that is provided by the Arginine in the transmembrane domain of GluA2 subunit. Therefore, GluA2-lacking AMPARs are Ca^{2+} -permeable (CP) (Hume et al., 1991, Jonas et al., 1994). Because Ca^{2+} plays critical roles in plasticity, CP-AMPARs are critical in regulating e.g. long-term synaptic plasticity of excitatory connections onto various INs types (Kullmann and Lamsa, 2007, Lamsa et al., 2007b, Oren et al., 2009). Interestingly, although CP-AMPARs allow enough Ca^{2+} to enter the cells and trigger various events including long-term plasticity, their permeability to Ca^{2+} is ~5 times less than that of NMDARs (Burnashev et al., 1995, Schneggenburger, 1996). The permeability to Ca^{2+} relative to that of Na^+ and K^+ is $P_{\text{Ca}}/P_{\text{Na,K}} = 2.3$ for GluA2-lacking, CP-AMPARs (GluA1 homomers), compared to ~10 for NMDARs. For comparison, the same ratio for GluA2-containing AMPARs is ~0.3 (for review, see Traynelis et al., 2010).

Ca^{2+} permeability and voltage dependence

The Ca^{2+} permeability of CP-AMPARs is accompanied by another property that also critically impacts the receptor's functioning: its voltage dependence. When GluA2-containing AMPARs display a linear IV curve, CP-AMPARs show an inward-rectifying IV relationship (Donevan and Rogawski, 1995, Kamboj et al., 1995). In other words, CP-AMPARs present almost opposite Ca^{2+} -permeability to NMDARs: when NMDARs require a depolarization to relieve their blockade at negative potentials by Mg^{2+} , CP-AMPARs are blocked at positive, depolarized potentials and require a hyperpolarization together with glutamate binding to flux Ca^{2+} . The

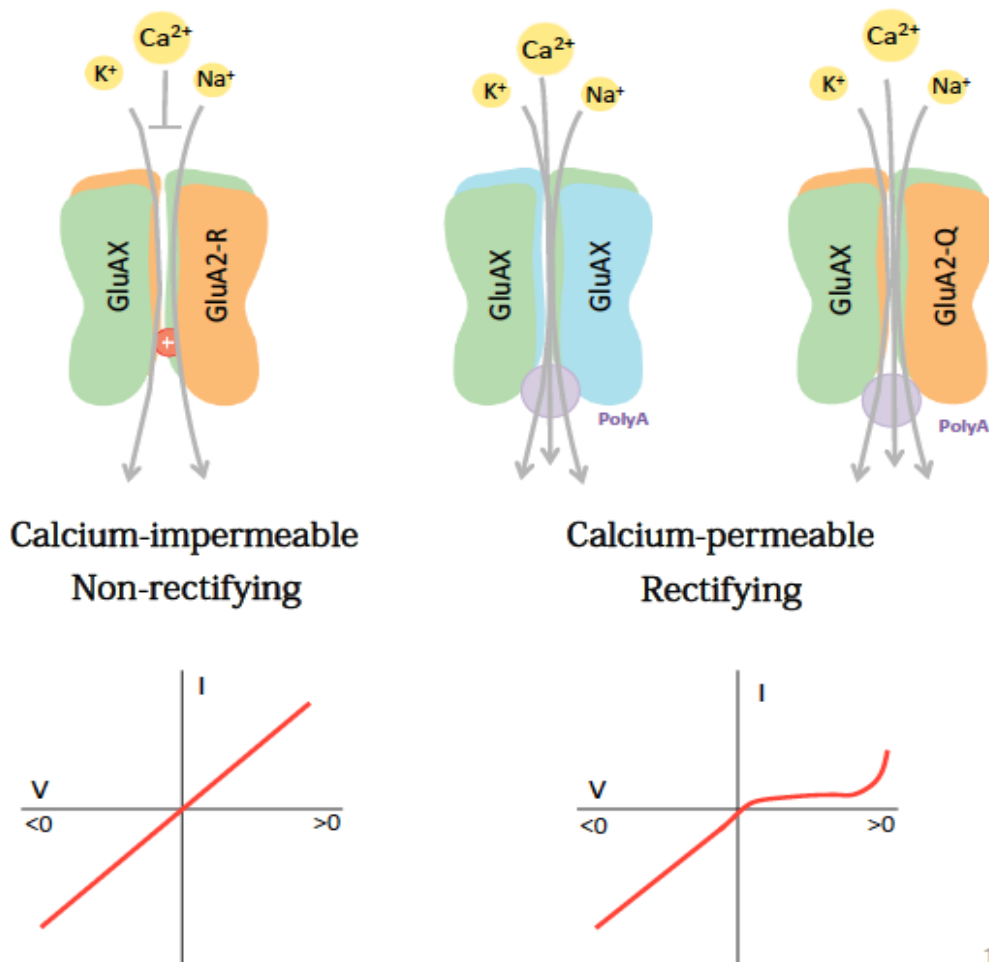


Figure 1.5: AMPA receptors Ca^{2+} -permeability and rectification

Top: GluA2-containing AMPARs (left) are Ca^{2+} -impermeable, due to the positive charge of the arginine that replaces the glutamine in the channel pore after RNA editing. This results in insensitivity to polyamines and a linear IV curve (bottom left). In contrast, GluA2-lacking AMPARs (middle) do not carry that positive charge and are thus permeable to Ca^{2+} . Their IV curve is inward-rectifying due to their blockade by polyamines at positive potentials (bottom right). AMPARs containing the unedited version of the GluA2 subunit (right) are rare, and also permeable to Ca^{2+} . GluAX denotes any AMPA receptor subunit but GluA2.

blockade of CP-AMPARs at positive potentials is due to intracellular polyamines, such as spermine (Washburn and Dingledine, 1996, Bowie et al., 1998). Other polyamines include putrescine and spermidine, but they are present in smaller concentrations in cells and are less efficient as spermine to block CP-AMPARs (Watanabe et al., 1991). The precise mechanism of this voltage-dependent block by spermine is unclear, although some evidence suggests spermine is inserted in the pore thanks to the absence of the positive charge carried by the arginine present in GluA2-containing receptors. Interestingly, spermine also has allosteric effects on NMDARs, but whether it is a positive or negative regulator of the receptor is unclear (Lerma, 1992, Ragnarsson et al., 2002, Turecek et al., 2004).

Synaptic plasticity

Chemical synapses are able to increase or decrease in strength for short (Zucker and Regehr, 2002, Abbott and Regehr, 2004) or long periods of time (Bliss and Lømo, 1973). This long-term modification of synaptic weight, mainly via insertion of AMPARs, is thought to underlie learning and memory (Morris et al., 1986, Nabavi et al., 2014). The idea that causality and associativity are critical in the functioning of the mind is very ancient, but it was difficult to transpose it to biology before understanding the basic structure of the brain. Indeed, the discontinuous nature of nerve cells forming the brain was only demonstrated in 1894 notably by the work of Ramón y Cajal and it was in 1897 that Sherrington proposed the term “synapsis”. At the same time, Lugaro and Tanzi proposed that memory formation could result from new connections between neurons or from the plasticity of those connections, thus introducing the concept of synaptic plasticity (for review, see Markram et al., 2011). In 1949, the notion of causality was notably proposed as a possible way to induce plastic synaptic changes by Donald Hebb, who hypothesized that when two neurons

are connected, if the presynaptic one repeatedly and persistently participates in evoking APs in the postsynaptic cell, the response amplitude in the postsynaptic cell should be increased, and that this would be a way of storing a memory trace of the stimulus that caused the correlated activity in the first place (Hebb, 1949). This concept was later demonstrated and is now known as long-term potentiation (LTP) (Bliss and Lømo, 1973). This experimental paradigm is based on the idea that a high-frequency stimulation of the presynaptic cell allows the near-coincidence of postsynaptic depolarization and presynaptic AP and is usually termed Hebbian plasticity. Hebb's theory was originally developed to explain how cells assemblies could be created to retain memories (or form engrams), based on the idea that more and stronger connections would be formed between cells pertaining to a given assembly compared to synapses across different assemblies. In addition to its implications for learning and memory, Hebbian plasticity is now considered a key component of development, allowing connections in the brain to form, last, and constantly reorganize. In the classical model, long-term plasticity is usually rate based, high-frequency stimulation of the synapse leading to LTP while low-frequency stimulation induces long-term depression (LTD) of the synapse (for review, see Collingridge et al., 2010). However, during the past 50 years, several experimental plasticity paradigms have emerged that may coexist at a given synapse with rate-based plasticity (Sjöström et al., 2001), (for review, see Abbott and Nelson, 2000). The next section describes one such paradigm.

Spike-timing-dependent plasticity

A recently described paradigm, emphasizing the precise timing and order of firing between neurons rather than their frequency (Gerstner et al., 1996, Markram et al., 1997), has gained interest in the past two decades, notably due to observations

of its relevance *in vivo* and efficiency in computer modeling (Clopath et al., 2010, Müller-Dahlhaus et al., 2010, Richards et al., 2010, Roberts and Leen, 2010). Although spiking frequencies vary with e.g. behavior or cell type, STDP induction is possible using a physiological range of spiking frequencies ranging from 0.1 to 100 Hz (Sjöström et al., 2001, Nelson et al., 2002, O'Connor et al., 2010) and evidence suggesting it occurs *in vivo* in several species, including humans have been found (Wolters et al., 2005, Müller-Dahlhaus et al., 2010, Testa-Silva et al., 2010, Pawlak et al., 2013). Furthermore, as other forms of plasticity, it is referred to as Hebbian because it requires the coincidence of activity in the pre and postsynaptic cells in a small (tens of milliseconds) time window (Markram et al., 1997, Bi and Poo, 1998). This experimental paradigm has thus been called spike-timing-dependent plasticity (STDP) (Song et al., 2000). Timing is indeed very important in that it may indicate causality: in a simplified view, if a neuron is consistently activated at the same, short latency after an AP in another cell, then that second cell may have something to do with the activation of the first one. STDP thus turns out to be a very interesting paradigm that possibly explains at least some forms of learning. For example, Meliza and Dan (2006) have demonstrated *in vivo* the dependence of the neuronal receptive field specificity on the timing between a visually-caused depolarization and an AP induced via a whole-cell recording electrode. Another interesting aspect of STDP is that with the reverse order, i.e. when the timing is not correlated or when the response in the second cell appears before the AP in the first one, then the synapse's weight is decreased and the absence of causality can also be "seen" by the neurons. This ability of STDP to make neuron "learn" and also "forget" has been experimentally demonstrated by Pawlak et al. (2013). By pairing with different

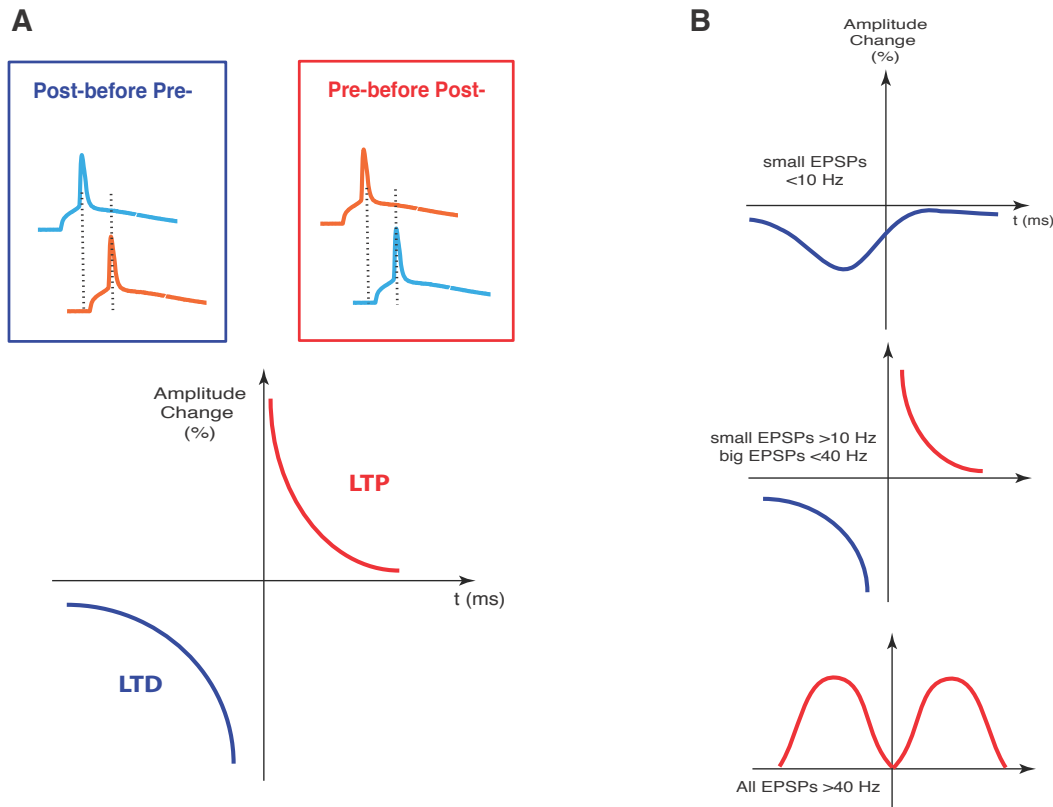


Figure 1.6: Spike-timing-dependent plasticity

(A) Principle of STDP at L5 PC-PC connections in the mouse visual cortex: when two cells are connected, an AP in the presynaptic cell in a time window of tens of milliseconds before an AP in the postsynaptic cell leads to LTP of the synapse, whereas the reverse order results in LTD.

(B) Frequency dependence of STDP showing that at 50 Hz only LTP is induced regardless of the timing, while only LTD can be obtained with frequencies below 10 Hz. Also, note that STDP may depend on the baseline amplitude of the response, with small EPSPs being less likely to undergo LTP. Adapted from (Buchanan and Mellor, 2010). Even though this reference relates to the hippocampus, similar frequency-dependence of STDP has been observed in the neocortex (Sjöström et al., 2001).

timings the response of a neuron to a visual stimulation with current injection in vivo, they were able to tune or “untune” a neuron for a given position of a visual cue in the visual field. Interestingly, another evidence of the relevance of STDP in vivo sheds light on anti-Hebbian STDP, i.e. the potentiation of a connection by a non coincidence of activity or its depression via coincident activity, has also been observed in vivo (Roberts and Leen, 2010). The authors demonstrate that in the sensory system of the weakly electric fish distortions of the electromagnetic field caused by the movement of the fish itself are cancelled by an anti-Hebbian mechanism. Indeed, the motor commands are taken into account by the sensory system and the movement that consistently causes and thus precedes those “images” that would modify the perception of the fish are cancelled.

Mechanisms of STDP

STDP has now been widely studied at PC-PC synapses (Markram et al., 1997, Bi and Poo, 1998), and several molecular pathways involved have been identified (for review, see Feldman, 2012). In a simplified view, an AP in the presynaptic cell preceding a spike in the postsynaptic cell by a few tens of ms leads to LTP whereas the reverse order leads to LTD. The amplitude and duration of the induced plasticity vary depending on the precise timing between the two events and by changing them one can produce a STDP curve for a given induction frequency (illustrated in **figure 1.6**). Most of the molecular actors involved are the same as for classical rate-based plasticity, including the NMDARs, AMPARs, and voltage-dependent calcium channels (Bender et al., 2006). Although all mechanisms have not yet been elucidated, the molecular pathways underlying LTD seem to be more diverse than those for LTP. For example, it has been shown that LTD can be dependent (Froemke et al., 2005) or independent of postsynaptic NMDARs

(Sjöström et al., 2003). The postsynaptic NMDAR-independent pathway involves a retrograde endocannabinoid signal and requires presynaptic NMDARs (Rodriguez-Moreno and Paulsen, 2008). Since STDP does not require high-frequency stimulation for LTP however, one important mechanistic difference compared to rate-based plasticity is the source of postsynaptic depolarization that is required.

Although it has been criticized (Lisman and Spruston, 2005), it is now generally accepted that the postsynaptic depolarization in STDP arises from a back-propagating AP (bAP) (Letzkus et al., 2006). The bAP consists in the propagation of an AP from the soma of a cell towards its dendrites. Indeed, even though dendrites mostly allow a passive propagation of the APs, the bAP can serve as postsynaptic depolarization at least for synapses relatively close to the soma. For synapses further away, where the bAP is not enough, other mechanisms, such as Na⁺ dendritic spikes (or bursts) (Golding et al., 2002) or synaptic cooperativity (Hardie and Spruston, 2009), have been shown to be potential contributors for plasticity. However, STDP is by definition dependent on APs in the pre and postsynaptic cells. Nevertheless, as a consequence of the need for bAPs, STDP at PC-PC synapses is known to vary with the dendritic location of the connection on the postsynaptic dendritic arbor, because the amount of postsynaptic depolarization caused by an AP differs between e.g. proximal vs. distal dendrites. Therefore, “pre-before-post” firing leads to LTP at proximal synapses, but to LTD or no plasticity at distal synapses (Letzkus et al., 2006, Sjöström and Häusser, 2006). Although this is in agreement with the view that bAPs are passively traveling from the soma towards the dendrites resulting in a decreasing gradient of depolarization and a delayed postsynaptic activity relative to the distance from the soma, both being critical in STDP induction, it is important to note that bAPs are not completely passive (Stuart and Sakmann,

1994, Stuart and Häusser, 2001), and that local dendritic events can also participate in increasing the amount of postsynaptic depolarization in distal dendrites, such as dendritic spikes (Golding et al., 2002).

Variability of STDP

With an increasing number of investigations on STDP, it clearly appeared that it is a very diverse phenomenon. Importantly, STDP seems to be cell type-specific (Lu et al., 2007, Tzounopoulos et al., 2007, Fino and Venance, 2010) and varies between brain regions (Tzounopoulos et al., 2004). Furthermore, as mentioned above, the requirement for a bAP leads to a variability of STDP with the dendritic location of the synapse (Letzkus et al., 2006). STDP is also sensitive to the frequency of induction (Sjöström et al., 2001, Buchanan and Mellor, 2010). Notably, at least at L5 PC-PC connections, it seems that low frequencies during a STDP induction protocol (below approximately 10 Hz), favor the induction of LTD by broadening the corresponding timing window. In contrast, at high frequencies (at and above approximately 40 Hz), LTP is more likely to be induced regardless of the timing. For frequencies in between, the sign and amplitude of plasticity of L5 PC-PC connections in acute brain slices depends on the precise timing and order of pre-and postsynaptic firing (see **figure 1.6**). Interestingly, STDP also depends on the baseline EPSP amplitude (Buchanan and Mellor, 2007). Finally, neuromodulation seem to critically affect STDP. It has indeed been demonstrated that neuromodulation can gate STDP and even completely change the sign of the plasticity induced with a given protocol (Seol et al., 2007, Huang et al., 2012, Huang et al., 2013).

Plasticity, including STDP, is critical for neuronal functioning, allowing synapses to form and modulate their strength over time, circuits to establish,

maintain or change, and memory to be formed (Morris et al., 1986, Nabavi et al., 2014). Understanding synaptic plasticity is thus necessary to improve our comprehension of how the brain develops and processes information. So far, plasticity has mostly been studied at excitatory connections onto excitatory cells. Although we know that plasticity depends on cell type, plasticity at excitatory connections onto INs remains largely unexplored, in part due to the challenge posed by INs diversity and identification. It is thus crucial to understand the synaptic composition and plasticity rules governing PC-IN synapses.

Plasticity of PC-IN synapses

Although little is known about plasticity of excitatory connections onto INs, some studies have clearly demonstrated that STDP depends, among other factors, on IN type (Tzounopoulos et al., 2004, Kullmann and Lamsa, 2007, Lu et al., 2007, Tzounopoulos et al., 2007, Huang et al., 2013). Given the diversity of INs and the challenge that their identification represents, it is perhaps not surprising that diverse results have been obtained, because studying cell-type specific STDP requires a clear identification of the cell types at hand. However, most studies pool results from INs subtypes based on their electrophysiological properties, a parameter that may be less reliable than morphology and that usually encompasses several cell types (Kawaguchi and Kubota, 1997, Ascoli et al., 2008, DeFelipe, 2013). Nonetheless, it appears that STDP of excitatory connections onto different INs can lead to LTP, LTD or no plasticity at all. For example, Lu et al. (2007) found only LTD at L2/3 excitatory inputs onto L2/3 fast-spiking INs regardless of the timing, but both LTP and LTD of the same inputs onto non-fast-spiking cells in the neocortex (Lu et al., 2007). Another factor that may critically affect STDP at those synapses is neuromodulation, with the same neuromodulator able to affect differently cell types. For example, the

Kirkwood laboratory has shown that neuromodulation is able to gate STDP at excitatory connections onto some INs and plays critical roles in the outcome of a given induction protocol (Seol et al., 2007, Pawlak et al., 2010, Huang et al., 2013).

More relevant to our study, due to their voltage dependence properties almost opposite to that of NMDARs, CP-AMPARs seem to provide a particular form of plasticity for PC-IN connections. Notably, they are involved in non-Hebbian plasticity. For example, the induction of LTP at excitatory inputs onto O-LM cells of the hippocampus requires concomitant hyperpolarization of the postsynaptic cell (thus removing the polyamine block of CP-AMPARs) and the presynaptic release of glutamate (Kullmann and Lamsa, 2007). Interestingly, a mechanism involving CP-AMPARs but leading to LTP of excitatory inputs onto INs in the absence of postsynaptic hyperpolarization has been observed in the basolateral amygdala (Mahanty and Sah, 1998), where excitatory synaptic transmission onto INs seems entirely mediated by CP-AMPARs and tetanic stimulation leads to LTP in an NMDAR-independent yet Ca^{2+} -dependent manner. CP-AMPARs are also highly expressed in cerebellar stellate cells, where Ca^{2+} influx through them after 50 Hz stimulation of parallel fiber inputs has been shown to induce an activity-dependent modification in synaptic composition, switching from CP- to CI-AMPARs (Liu and Cull-Candy, 2002). Although the role of CP-AMPARs in synaptic transmission and plasticity at excitatory inputs onto INs is well established, not much is known about their pattern of expression by different IN types in the neocortex.

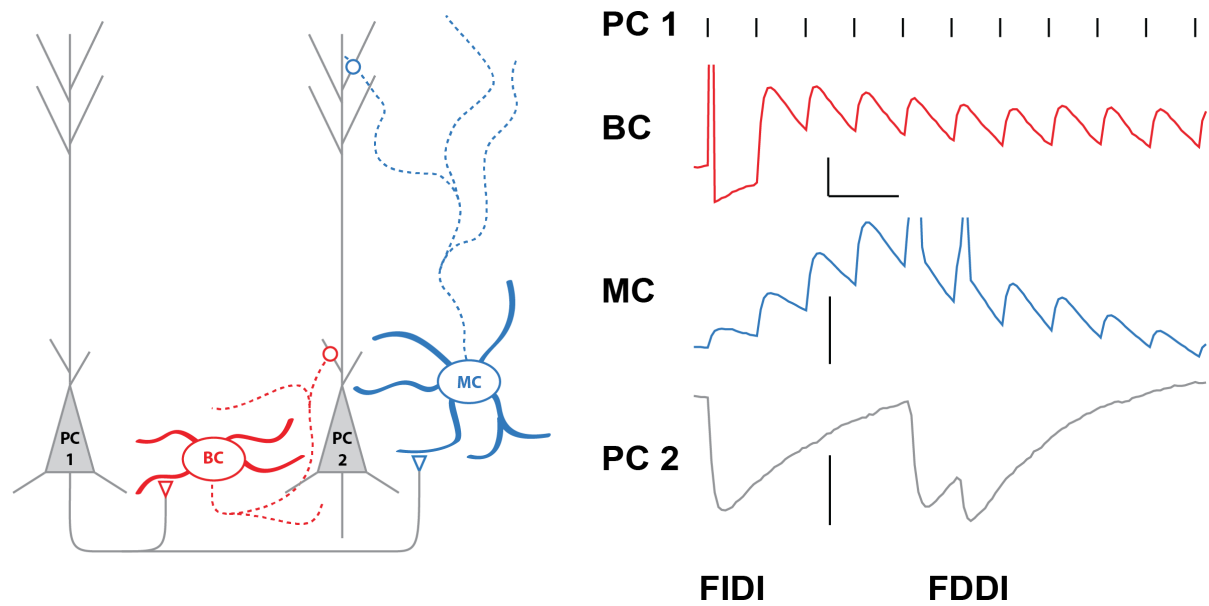


Figure 1.7: The frequency-dependent and independent microcircuits

Left: A group of PCs (grey, “PC1”) simultaneously target BCs (red, scale bar: 10 mV, 20 ms) and MCs (blue, scale bar: 10 mV) to the point of eliciting feed-forward inhibition onto another group of PCs (grey, “PC2”, scale bar: 0.5 mV). Right: Computer simulation where the short-term facilitating PC-MC synapse requires a high frequency stimulation to elicit APs in the MC, but the short-term depressing PC-BC synapse rapidly results in APs, followed by subthreshold EPSPs. This results in two temporally distinct inhibitions onto PC2, the early one being mediated by BCs, and the late one by MCs. These two microcircuits are respectively called frequency-independent disynaptic inhibition (FIDI) and frequency-dependent disynaptic inhibition (FDDI). Adapted from (Buchanan et al., 2012).

Main question

Based on the knowledge available on CP-AMPARs, it seems that they are widely expressed by INs in various brain structures. However, given the diversity of the IN population and the difficulty to identify them, it remains unclear whether all INs express CP-AMPARs or if they are restricted to some IN types. In other words, are CP-AMPARs expressed similarly by all neocortical INs? And do they underlie specific functions in neocortical microcircuits? To answer these questions, we combined electrophysiological and imaging techniques allowing us to assess the presence of CP-AMPARs at the synaptic level, between clearly identified pre and postsynaptic cells. We also show that PC-PC long-term plasticity differs from PC-IN plasticity, which is likely related to the synapse's molecular composition.

Chapter II: Methods

Experimental strategy

INs represent about 20% of the neocortical cellular population (Beaulieu et al., 1992). Moreover, they are more diverse than PCs and are not easily targeted only by the shape of their soma. BCs can be relatively easy to target given they represent half the IN population (Gonchar and Burkhalter, 1997, DeFelipe et al., 2013) by focusing on small rounded somata. For MCs, we relied in part on the GIN mouse line (Oliva et al., 2000), expressing eYFP in Sst-expressing cells, which are mostly MCs in visual neocortex L5 (Toledo-Rodriguez et al., 2005, Silberberg and Markram, 2007, Buchanan et al., 2012). The identity of the cells was then confirmed by their morphology (see **figure 2.7 and** (Blackman et al., 2014) and, when applicable, their firing pattern (see **figure 1.3**). Quadruple recordings in the whole-cell configuration allow us to observe up to twelve monosynaptic connections simultaneously between different cell types (see **figure 2.1 and figure 2.5**) monitor the status of the cells by constantly determining the input resistance, the series resistance, the resting membrane potential (see **figure 2.6**) and the injected current. Finally, a fluorescent dye can be introduced into the recorded cells during the experiments, so their morphology can be acquired via 2PLSM. In the end, this approach gives us access to precise data on both cell and synapse physiology and allows us to assess possible synapse-specific phenomena, even within the diverse IN population because we combine several identification criteria. Here, I first introduce the techniques employed and then explain how to use the combination of quadruple-whole-cell recordings and 2PLSM to study STDP in the neocortex under the form of

a manuscript accepted for publication in Cold Spring Harbor Laboratory Protocols that details the approach, the procedure and provides the most likely solutions to a range of possible technical issues.

Relevance of main techniques

Quadruple whole-cell recordings

For complex structures or for the examination of presynaptic events, extracellular stimulations might not be sufficient, since the presynaptic cell cannot be identified. Furthermore, using extracellular stimulation makes it difficult to be certain that a presynaptic action potential (AP) occurred. In 1968, Hugues and Tauc were among the first to perform dual recordings (Hughes and Tauc, 1968), but it is only more recently that researchers have begun recording whole-cell from pairs of connected neurons (Miles and Poncer, 1996). In more recent years, the paired-recording technique has been further refined, producing large databases of neuronal connectivity motifs and connective weight distributions (Barbour et al., 2007) that reveal important information about e.g. information storage capacity of the brain (Varshney et al., 2006) and functional specificity of connectivity (Ko et al., 2011). Because the method gives access with precision to both the pre- and postsynaptic cells, paired recordings have enabled great advances in the understanding of the mechanisms of synaptic transmission and plasticity, particularly those requiring an extreme temporal precision such as STDP (Markram et al., 1997, Sjöström et al., 2001). The access to the presynaptic side is of particular importance when characterizing presynaptic mechanisms of e.g. regulation of vesicle release or plasticity (Rodriguez-Moreno and Paulsen, 2008, Buchanan et al., 2012). Pre- and postsynaptic mechanisms can be dissected to a greater detail using paired

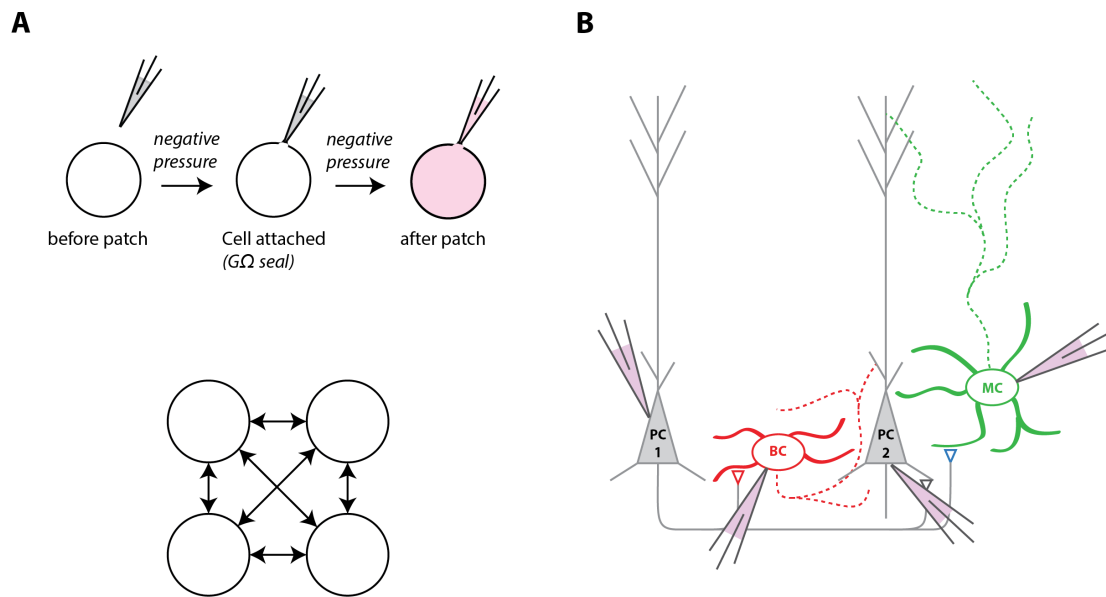


Figure 2.1. Multiple whole-cell recordings

(A) Top: Schematic depicting the principle of whole-cell recordings. Once the pipette touches the cell to be patched, a light negative pressure application leads to the formation of a high-resistance seal (cell-attached configuration). A second negative pressure application ruptures the membrane, allowing continuity between the intracellular milieu and the solution in the pipette (whole-cell configuration). This solution diffuses into the cell during the recording and can be used to introduce e.g. fluorescent dyes specifically in the recorded cells. Bottom: To overcome the relatively low neocortical connectivity rate, we performed quadruple whole-cell recordings, allowing us to test up to twelve connections simultaneously.

(B) Diagram depicting the patch of four cells, including one MC (green) targeted by the expression of eYFP (GIN mouse line), one BC targeted by its non-pyramidal, small rounded soma and two PCs targeted thanks to their large pyramidal soma and the presence of an apical dendrite.

recordings by including pharmacological agents specifically into one or the other cell via the intracellular solution.

Finding monosynaptically connected cells in a structure with low connectivity such as the neocortex (Thomson et al., 2002, Song et al., 2005, Lefort et al., 2009), is the main limitation of the paired recording technique, since the acquisition of data can be slow. In the past ten years, there have been several attempts to overcome this obstacle and several methods allow the experimenter to assess the connectivity before patching the cells. The most common consists of searching for connections by patching a few cells in the whole-cell configuration, and creating loose seals on other cells with a third pipette (Feldmeyer et al., 1999). The experimenter can test candidate presynaptic cells with a loose patch recording by injecting a current and monitoring the others for post-synaptic responses. Once a connection is found, the pipette is carefully replaced with a new pipette, and the cell is re-patched in the whole-cell configuration. This approach can be extremely useful, although re-patching a cell can be challenging. Another strategy can be to retrogradely label presynaptic neurons, as developed by the Callaway laboratory. The idea consists in using a rabies virus that retrogradely crosses single synapses and thus labels presynaptic neurons. Those presynaptic neurons can then be patched (Wickersham et al., 2007, Osakada and Callaway, 2013). Finally, another recent attempt to facilitate finding connected neurons relies on optogenetics. An optic fiber locally delivers laser light onto cells expressing light-sensitive ion channels (Sun et al., 2014). Therefore, once a cell is patched, the laser can activate selected neurons and the experimenter thus “scans” the preparation for putative presynaptic cells that can then be patched.

Despite those recent advances, which present their own challenges, paired recordings are still state of the art when it comes to study synaptic mechanics and they have evolved from dual recordings to up to twelve simultaneous recordings (Debanne et al., 2008, Molnar et al., 2008, Jiang et al., 2013, Perin and Markram, 2013) and have also been performed *in vivo* (Jiang et al., 2013). The evolution towards simultaneous recordings from multiple cells is due to the rather low neuronal connectivity of e.g. the neocortex. Indeed, the number of connections tested increases as $n(n-1)$ with the number of cells patched, n . However, simultaneous recordings from an increased number of cells cause more spatial constraints of the set up. Quadruple whole-cell recordings — which allow the test of twelve connections simultaneously — represent a good compromise, as they require only modest spatial constraints while at the same time providing relatively high yields of connected cell pairs.

Two-photon laser-scanning microscopy

As mentioned above, paired recordings of INs should be combined with morphological reconstruction and classification, either from biocytin histology or 3D imaging stacks obtained with 2PLSM (Blackman et al., 2014, Ferreira et al., 2014). Although biocytin staining is state of the art and provides a superior precision than 2PLSM, the level of details provided by 2PLSM is more than enough to clearly identify a cell as BC or MC based on their dendritic and axonal morphology. Furthermore, 2PLSM has advantages over biocytin staining for this particular project. The morphology is indeed acquired right after the recordings, which is much faster than the process required to reveal biocytin staining (Blackman et al., 2014). Furthermore, maintaining a good connectivity with paired recordings requires the experimenter to patch as deep as possible in the slice so dendrites and axons are

not too severed by the slicing, and the near infrared wavelengths employed with 2PLSM allow good signal to noise ratio up to several hundreds of microns into light-scattering tissue such as acute brain slices. However, because of these longer wavelengths, resolution is not as good as with confocal microscopy. Also, the small cross-section of 2-photon microscopy requires high intensities of excitation to generate a signal, which is notably achieved by the short pulses (~100 fs) produced by the lasers. Because some dyes have particularly small 2-photon cross section, this also results in them being very poorly excited by 2-photon microscopy even though they might work very well with confocal imaging (For review, see Svoboda and Yasuda, 2006).

In the end, although both techniques can be expensive to set up, quadruple whole-cell recordings and 2PLSM thus represent an excellent combination to study the synapse-specific expression of CP-AMPARs in inhibitory neurons in acute slices of mouse neocortex. Further details on the experiments performed to identify CP-AMPARs at those synapses are provided in the manuscript in **Chapter III**. Together, the two manuscripts thus give clear and detailed information on all the procedures we followed.

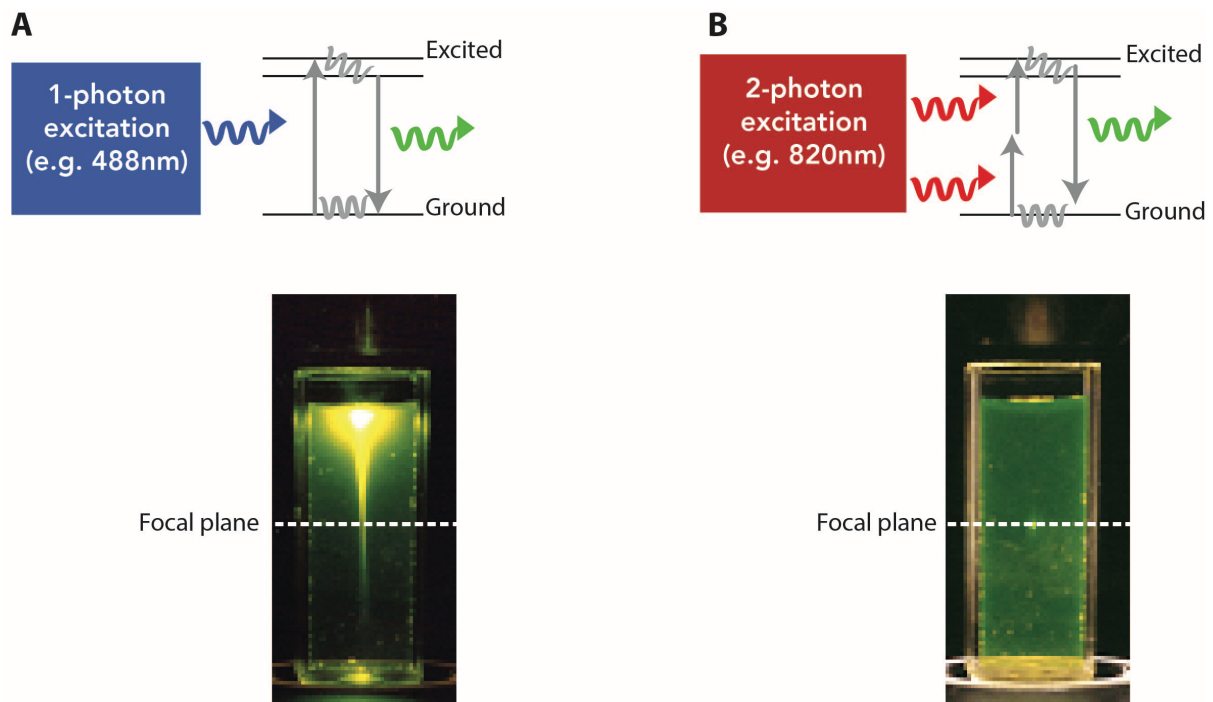


Figure 2.2. Principle and advantages of two-photon microscopy

(A) With one photon excitation, only one photon (blue) of a given wavelength (and thus specific energy) is required to make electrons (grey) reach an excited, unstable state of energy (vertical lines). When the electrons go back to their preferential, more stable state, they release energy, which is the fluorescence that is seen (green).

(B) The chief difference with two-photon excitation is the requirement for 2 photons (red) each carrying a smaller energy than the photon in A. In the end their energy combined allow the electrons to reach the same excited state and then emit fluorescence (green). As illustrated in the picture (bottom), an important consequence is that with two-photon excitation only electrons present at the focal plane can be excited, considerably reducing background noise. Other advantages of the technique relative to this project are developed in the Methods section. Images are from Dr. Webb's laboratory website (Cornell University, USA).

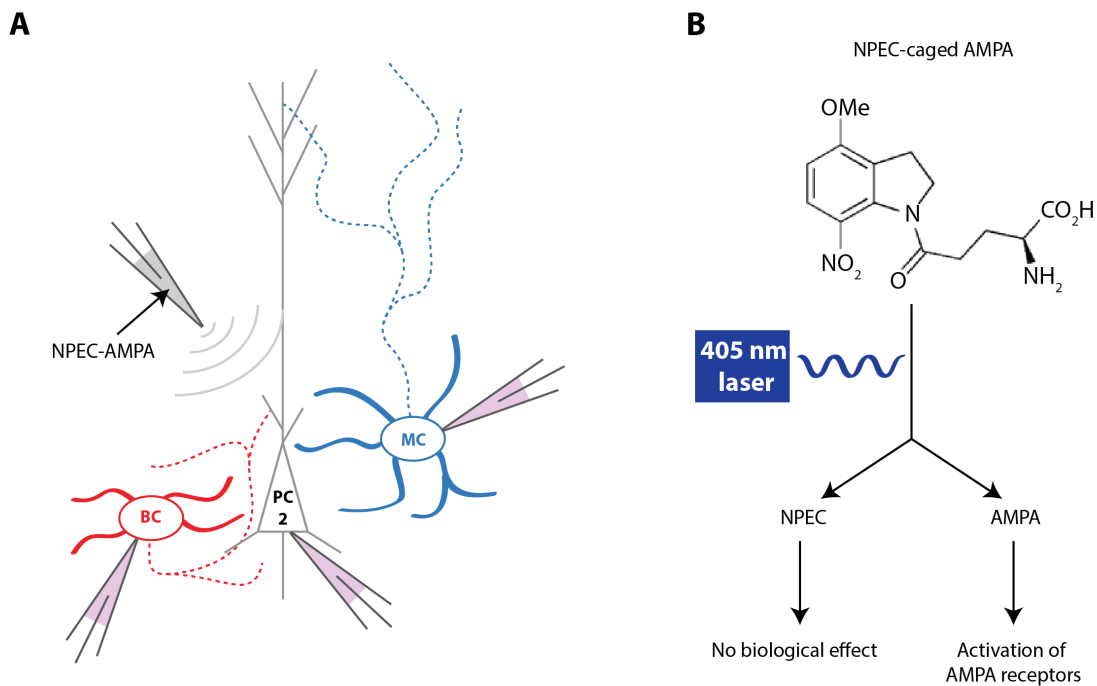


Figure 2.3. NPEC-AMPA uncaging

(A) Three cells are patched, ideally one BC one PC and one MC, while the fourth pipette is used to puff NPEC-AMPA close to the dendrites and soma of the recorded cells.

(B) Principle of AMPA uncaging from NPEC-AMPA: the link between the NPEC molecule and the AMPA is photolysed by one (0.1-2 ms-long) pulse from a 405 nm laser, thus allowing AMPA to act on its targets, while the NPEC molecule has no known biological activity.

Using quadruple whole-cell recordings to study spike-timing-dependent plasticity in acute neocortical slices

In press (Cold Spring Harbor Laboratory Protocols)

Txomin Lalanne^{1,2}, Therese Abrahamsson¹, and P. Jesper Sjöström^{1,4}

1) Centre for Research in Neuroscience, Department of Neurology and Neurosurgery, The Research Institute of the McGill University Health Centre, Montreal General Hospital, Montréal, Québec, H3G 1A4, Canada

2) Integrated Program in Neuroscience, McGill University, 3801 University Street, Montreal, Quebec H3A 2B4, Canada

4) Correspondence: jesper.sjostrom@mcgill.ca

Prof P J Sjöström

Centre for Research in Neuroscience

Department of Neurology and Neurosurgery

The Research Institute of the McGill University Health Centre

Montreal General Hospital

1650 Cedar Ave, room L7-225

Montreal Quebec H3G 1A4, Canada

Office: +1-514-934-1934, ext. 44561

Mob: +1-438-826-1971

FAX: +1-514-934-8216

Introduction

Using extracellular field recordings, electrophysiologists have made great strides in the study of synaptic plasticity in e.g. hippocampus. With the neocortex, however, it has not been quite as straightforward. Although lots has been learned about neocortical plasticity by stimulating in the white matter or in layer 4 (Kirkwood et al., 1993, Kirkwood and Bear, 1994, Kirkwood et al., 1995), neocortical extracellular stimulation experiments often suffer from the shortcoming that it is difficult to know which synapse types were recorded from.

With paired recordings, however, the experimenter knows precisely what neuronal types are being stimulated and recorded from (Miles and Poncer, 1996, Debanne et al., 2008). Paired recordings are thus particularly needed for the study of neocortical circuits, where multiple cell types exist side by side and where plasticity is known to be synapse specific (Buchanan et al., 2012, Blackman et al., 2013). To benefit maximally from paired recordings, they should therefore ideally be combined with morphological reconstruction and classification, either from biocytin histology or 3D imaging stacks obtained with 2-photon laser-scanning microscopy (2PLSM) (Blackman et al., 2014, Ferreira et al., 2014). In addition, paired recordings provide pharmacological access to both the pre and the postsynaptic cell, thus enabling wash-in of drugs or dyes into the transmitting or recipient neuron (Kaiser et al., 2004, Koester and Johnston, 2005, Rodriguez-Moreno and Paulsen, 2008, Buchanan et al., 2012). Finally, paired recordings also enable precise timing of spikes in connected neurons, which is absolutely essential for the spike-timing-dependent plasticity (STDP) experimental paradigm (Markram et al., 1997, Sjöström et al., 2001).

Unfortunately, neocortical connectivity is sparse — typically only 10-40% of neighboring excitatory cells are monosynaptically connected (Song et al., 2005, Lefort et al., 2009, Ko et al., 2011) — which makes paired recordings slow and painstaking. Fortunately, the number of connections tested scales favorably with the number of cells recorded: with n neighboring cells simultaneously patched, the number of connections tested is $n(n-1)$. As n increases, more manipulators are required, resulting in considerable spatial and financial constraints. Still, several studies have been reported with 7-12 simultaneous whole-cell recordings (Lefort et al., 2009, Perin et al., 2011). Because quadruple recordings sample twelve possible connections simultaneously with reasonable spatial constraints and at a relatively realistic cost, we suggest that $n = 4$ recordings represent an ideal choice for the majority electrophysiology labs.

Here, we provide a quadruple whole-cell recording protocol to study synaptic plasticity of neocortical connections, with a special focus on STDP. We also show how to morphologically identify recorded cells from 2PLSM stacks.

Materials

Reagents

Carbogen gas (95% O ₂ /5% CO ₂)	MgCl ₂
D-Glucose	CaCl ₂
HEPES	NaGTP
KCl	NaH ₂ PO ₄
K-Gluconate	NaCl
NaHCO ₃	Na-Phosphocreatine
KOH	Sucrose
MgATP	Bleach

Table 2.1: Equipment

Item	Source
Anti-vibration air table	Newport, TMC, Thorlabs
Motorized microscope with XY stage	Scientifica (SliceScope Pro), Luigs and Neumann (Infrapatch 380)
IR-sensitive CCD camera	Watec (WAT902H), TILL Photonics (VX55)
Micromanipulator	Scientifica (MicroStar) (Figure 2.4A), Luigs and Neuman (MLE/MRE 3axes Mini25)
Stabilizing pipette rod holder	Scientifica (Figure 2.4A and B)
Electrodes holders and silver wire	Harvard Apparatus (2037760664) (Figure 2.4B)
Water immersion objective	Olympus (40x: LUMPLFLN40XW, (Figure 2.4B), 60x: LUMPLFLN60XW)
Patch clamp amplifier	Dagan Corporation (BVC-700A) (Figure 2.4C) Molecular Devices (MultiClamp 700B or Axopatch 200B)
Electrode tracking software	Scientifica (LinLab). Wavemetrics (Igor Pro) or MathWorks (MATLAB) for custom written programs
Recording acquisition software	Molecular Devices (pClamp), AxoGraph (AxoGraphX). Wavemetrics (Igor Pro) or MathWorks (Matlab) for custom written programs
Software for morphological reconstructions	Neuromantic (http://www.reading.ac.uk/neuromantic/), Neurolucida (MBF Bioscience), Imaris (Bitplane)
Software for morphometry	L-Measure (http://cng.gmu.edu:8080/Lm/), Fiji (http://fiji.sc/Fiji)
Data acquisition board	National Instruments (PCI-6229) (Figure 2.4C)
Contrast enhancement	Luigs and Neumann DGC tube, Scientifica Dodt contrast, or Olympus DIC. Dodt contrast can also be custom-built from Thorlabs parts.
Borosilicate capillary	Harvard Apparatus (G150F-4)

glass tubing	
Inline heater, sensor and temperature controller	Scientifica (HPT-2A), Warner instruments (SH-27B)
Three-way stopcocks	Cole-Parmer (EW-30600-23), VWR (89134-220)
Pipette puller	Narishige (PC-10), Sutter Instruments (P-97, P-1000), Harvard Apparatus (PMP-102), AutoMate Zeitz DMZ
Patch-pipette filler	Advanced Instruments (MF28G67-5), Eppendorf ("microloader", 930001007)
Slice holder	Harvard Apparatus, Warner Instruments, or custom made from platinum wire with nylon strands held in place by cyanoacrylate glue (Figure 2.4B).
Faraday cage	Custom made, Luigs and Neumann, Scientifica
Oscilloscope	Tektronix (TDS2024C, Figure 2.4C), Picotech (3406A/B)
Vacuum system or pump	Charles Austen (Dymax5), Masterflex (HV7791620), Gilson (Minipuls 3)

Protocol

Setup the experiment

1. Prepare ACSF and internal solution as described in the Recipes section and dissect the brain slices (see Protocol 1 and Davie et al., 2006). Ensure that ACSF is circulating in the recording chamber and that the temperature is 31-34°C. ACSF should circulate at a rate of ~1 drop/sec (~2 ml /min).
2. Hold down the slice in the recording chamber (**Figure 2.4B**) with the slice holder. To ensure that layer-5 (L5) pyramidal cells (PCs) were not damaged during dissection, visualize their apical dendrites as far up to L1 as is possible. Select the cells you aim to patch, keeping in mind that connectivity is higher

for cells located closer together than 100 μm (Holmgren et al., 2003, Perin et al., 2011) and for neurons deep in the slice (Ko et al., 2011). Cells that appear smooth are usually healthier than those that are of high contrast.

3. Fill pipettes with internal solution and insert them into the electrode holders. Ensure pressure tubing and wires are attached to electrode holders. Clamp pipettes with a rod (**Figure 2.4A**) to stabilize recordings. Apply positive pressure with a 20-ml syringe or by mouth. Close a three-way stopcock to maintain pressure.

Patch-clamp protocol

4. Place electrodes just above the region of interest in the slice. Null amplifier offsets and measure pipette resistances. Use a software solution to semi-automate electrode movements (e.g. *Follow* software from Scientifica or custom scripts). With computer assistance, you save time and reduce the risk of damaging pipettes and/or the tissue.
5. Approach the first cell to be patched. Voltage clamp the pipette to 0 mV and apply a -5-mV test pulse running at 30-40 Hz with 50% duty cycle to monitor pipette resistance with an oscilloscope. Verify the positive pressure — as you advance the pipette through the slice, the positive pressure should push tissue aside. Approach the cell slowly, ideally along the diagonal axis of the pipette while circumventing other cells — do not go straight through other cells, as this makes the tip dirty, which makes the formation of a $G\Omega$ seal difficult or

impossible. If the test pulse readout suddenly drops, the tip was blocked, either by dirt inside the pipette or by brain tissue. When the pipette tip is located $\sim 10 \mu\text{m}$ from the cell, reduce positive pressure: open the three-way stopcock, then reapply and hold positive pressure quickly by mouth. Advance the pipette tip a few microns into the cell until you can see a dimple form. Quickly release the pressure and gently apply light negative pressure to gradually form a $\text{G}\Omega$ seal without rupturing it (point 7 below). As seal resistance increases beyond $\sim 100 \text{M}\Omega$, switch holding voltage from zero to -70mV , as this helps establish the $\text{G}\Omega$ seal. Once the $\text{G}\Omega$ seal is formed, remove the negative pressure.

6. Repeat point 5 for the other three electrodes. As you bring the next pipette down into the tissue with positive pressure, the tissue moves, thus requiring continual readjustments of the previous electrodes. Ideally, the tip of the pipettes should follow any movement of the cell so that the pipette tip remains at the same position relative to the cell as when it was first patched.
7. Once four $\text{G}\Omega$ seals have been established, go into whole-cell configuration. Doing this in quick succession on all four cells ensures that intracellular components necessary for plasticity induction are not dialyzed unequally from the different cells (Malinow and Tsien, 1990, Sjöström et al., 2001). Gradually apply gentle suction until the patch is ruptured while monitoring the oscilloscope test pulse. Patch rupture is evidenced by a sudden increase in test pulse current step. The negative pressure ramp may have to be repeated a few times. If the seal does not rupture, try hyperpolarizing the cell to -140

mV until rupture (see Troubleshooting). Switch to current clamp and remove negative pressure.

8. Once broken through, assess quality of whole-cell recordings. The resting membrane potential and the input resistance should for visual neocortex L5 PCs of postnatal day 14-16 (P14-P16) rats be mean \pm s.d. = -65 ± 3.4 mV and 110 ± 45 M Ω , respectively (n = 325, P.J.S. unpublished), although the distribution of the latter parameter has a long tail extending beyond 300 M Ω , and both values vary with age (Sjöström et al., 2001). The series resistance should be as low as possible, but is as a rule of thumb not less than double the pipette resistance. In practice, series resistances as high as 20-30 M Ω are satisfactory for plasticity experiments carried out in current clamp, but voltage clamp is badly affected by high and variable series resistance. A typical P14 visual neocortex L5 PC will produce a single spike after a 5-ms-long 1.3-nA current injection. Spikes should be millisecond-wide at half-height — if broader, the series resistance is too high, which results in artificial spike broadening by temporal filtering.

Identify connected pairs of neurons

9. Search for connections by evoking spikes in all four cells (**Figure 2.5B**, top), staggered by at least 500 ms to avoid accidental STDP induction (Sjöström et al., 2001). Generate spike-triggered averages of 10-40 postsynaptic sweeps to ensure that weak connections are not missed. Verify that connections found

are monosynaptic: response latency and temporal jitter should be sub-millisecond (**Figure 2.5C** and **2.5D**).

Induce plasticity

10. Once connections have been identified, start the STDP protocol. First, a baseline period of 10 minutes or more should be acquired. Next, STDP is elicited by repeated pre- and postsynaptic spike pairings at the desired frequency and timing. A second post-pairing baseline period then follows, which is maintained for at least 30 minutes but ideally longer (**Figure 2.6B**). At L5 PC connections, repeated pre-before-postsynaptic spike pairings at a timing difference of $\Delta t = +10$ ms result in potentiation if the frequency or depolarization is high enough, whereas the opposite temporal order may elicit depression (Sjöström et al., 2001) (**Figure 2.6C**, bottom).

Analyze acquired data

11. Use a dedicated analysis software, since data analysis is time consuming and highly repetitive. Software can be purchased (e.g. pClamp, or AxoGraph X), but customization (in e.g. Igor PRO or MATLAB) maximizes flexibility and speed. For a lab course, Microsoft Excel is quite adequate.

12. Discard recordings with unstable baseline. To avoid bias in the data selection, it is important to apply the same stability criterion to all recordings. One suitable requirement is that the baseline should not change more than e.g.

10% (Markram et al., 1997). An alternative is to apply a t-test to the differences of the means of the two baseline period halves. A stable baseline is indicated by a non-significant p-value. Similarly, Pearson's r for response amplitude versus time should not be significant.

13. Apply quality-control criteria. Recordings should consistently be discarded or truncated if resting membrane potential, perfusion temperature, or input resistance venture outside bounds. The specifics of these bounds are somewhat arbitrary but can be: input resistance should not change more than 30%, resting membrane potential not more than 8 mV, and temperature should remain within 31-34°C (Sjöström et al., 2001) (**Figure 2.6C**). In voltage clamp, also monitor series resistance: it should e.g. be less than 25 MΩ, not change more than 20%, and/or the change should be indistinguishable compared to control experiments (Sjöström et al., 2003).

14. Quantify the magnitude of plasticity. Measure plasticity as the change in EPSP amplitude after the induction protocol compared to before, expressed in percentage terms. Ignore the first several minutes after the induction, as other forms of plasticity may be active during this period, e.g. post-tetanic potentiation (Zucker and Regehr, 2002). We typically compare the responses starting ten minutes after the induction until the end of the recording, to the entire pre-pairing baseline (Sjöström et al., 2001, 2003) (**Figure 2.6C**).

15. Morphologically classify recorded cells. Image the entire volume in which recorded neurons arborize (**Figure 2.7A**). Use software such as Neuromantic, NeuroLucida, or Imaris to reconstruct neurons from 2PLSM image stacks (Blackman et al., 2014), carefully distinguishing dendrites from axons by the presence of spines (**Figure 2.7B**). L-measure provides numerical morphometry measurements (Scorcioni et al., 2008). To obtain ensemble averages, create arbor density maps (Buchanan et al., 2012) (**Figure 2.7C**) or carry out Sholl analysis (Sholl and Uttley, 1953) (**Figure 2.7D**). To save time, Sholl analysis is possible to carry out directly on bitmap images using Fiji (Ferreira et al., 2014).

16. Repeat experiments. If you wish to produce a complete STDP curve or to examine the rate dependence of plasticity, repeat experiments in different paired recordings while varying the timing or rate during the induction (Sjöström et al., 2001). Make sure that the induction occurs roughly the same time after rupture of the patch, to avoid plasticity washout (Malinow and Tsien, 1990). It is generally not appropriate to repeat different inductions in sequence in the same connected pair, since depression of previously potentiated synapses is not necessarily the same as depressing a naïve connection (Massey and Bashir, 2007). (Sjöström et al., 2001)

Troubleshooting

Seals and recordings are of poor quality

1. Pipette resistance has to be in the right range. Seals form more easily with high pipette resistance (4-6 M Ω), although as a consequence, it may be harder to rupture the patch, and the resulting series resistance will be higher. If the patch does not rupture when applying negative pressure, try hyperpolarizing the cell to -140 mV. With this approach, be ready to quickly switch from voltage to current clamp as soon as whole-cell mode is established, to avoid killing the cell with the large negative current that results from clamping it to -140 mV. With a G Ω seal that resists rupture even at this point, you can try more aggressive tricks such as applying large negative pressure with a 20-ml syringe, or using the amplifier's "buzz" function. These tricks, however, are rarely successful, but represent a last resort. With lower pipette resistance (3-4 M Ω), the pipette tip will be larger, so the series resistance will be lower, but sealing may be more difficult. Once a seal has been established, breaking through to go whole-cell is easier, however. The use of large pipette tips with low pipette resistance is thus recommended for voltage clamp experiments. For quadruple whole-cell recordings in current clamp, however, it is typically more important to establish good seals with high success rate on all four cells, since failure to record from one out of the four cells reduces the number of tested connections from 12 to 6 — a 50% reduction in yield of connections.

2. Pipette tips may be dirty. Remove visible debris with large positive pressure using a 50-ml syringe. If this fails then change the pipette — patching with dirty tips is a waste of time. To reduce clogging of the pipette from the inside, always filter the internal solution with a nylon syringe filter (Nalgene, item #176). Sonicating it may also help.
3. Pressure may be too low. Leaky pressure lines should be replaced. Apply positive pressure before the pipette enters the ACSF. In the absence of positive pressure, specks of dirt stick to the pipette tip, making patching much more difficult.
4. External/internal solutions may not be optimal. The difference in internal and external solution osmolality determines the ease of patching. For rat slices, internal osmolality should be ~294 mOsm (adjusted with sucrose), while the ACSF should be ~320 mOsm (adjusted with D-glucose). For mouse slices, osmolalities should be 17 mOsm higher (Bourque, 2008).
5. Animal age may not be optimal. For rat slices, P13-P16 is the ideal age, while for mice it is 1-2 days younger. Although cell health is often inferior in slices from older animals, cells might not have acquired mature properties in slices from young animals. With older animals, cardiac perfusion or high-sucrose dissection solution may improve slice quality (Moyer and Brown, 1998).
6. Slice quality may have deteriorated. Replace the slice with a new one, or dissect a new animal. Slices generally decline faster at 31-34°C than at room

temperature. In P14 rat slices may be usable up to 10 hours after dissection, while P18 slices may last no more than 5 hours. Mouse slices deteriorate faster than rat slices do.

Connected pairs of neurons cannot be found

1. The slice may not have been cut at an optimal angle. A slice with L5 PC apical dendrites reaching layer 1 is likely to have well-preserved connectivity.
2. Patch cells deeper into the slice. Although visibility and rate of successful patching drop below 80 μm , there are returns in terms of higher connectivity rates (Ko et al., 2011). A reasonable trade-off is to patch 50-80 μm deep.
3. Use a train of presynaptic spikes and average more sweeps to better visualize weak postsynaptic responses.

Electrical problems with recordings

1. Recordings may be noisy. Make sure headstages and bath chamber are grounded. Do not ground the same device several times, as this creates ground loops resulting in more noise. Ground all devices to the same grounding point to avoid grounding loops. Noisy devices should be disconnected, substituted, or moved farther away.
2. Voltages may slowly drift due to slow polarization of electrodes. To slow down voltage drift, increase electrode surface area by covering electrodes in

chloride. Leave them in bleach for 10 minutes, or pass a positive current through electrodes immersed in 1M NaCl until they turn white.

3. Series resistance may be too high. The $G\Omega$ seal may not have been completely ruptured. Apply a light negative pressure. If the problem persists, increase pipette tip diameter.

Recordings are not stable

1. Make new intra and/or extracellular solutions.
2. The slice may not have been cut in the right orientation, so that recorded cells are damaged. Pick a new slice from the incubation chamber. Turning the slice over may also help.
3. Stimulation frequency may be too high, so the synapse may not have enough time to recover from short-term depression. For single EPSPs, use an inter-stimulus interval of 7-10 seconds. A train of five EPSPs at 30-50 Hz, requires 15-18 seconds for full recovery (Varela et al., 1997, Buchanan et al., 2012).
4. Verify that the perfusion temperature is stable and set correctly. Deterioration can be very rapid at 37°C. Temperature variations cause fluctuations in EPSP amplitude and passive properties.

It is difficult to obtain LTP or LTD

1. Intracellular components necessary for plasticity induction may get dialyzed if induction occurs too long after breakthrough (Malinow and Tsien, 1990). Avoid a baseline longer than 15 minutes.
2. Verify that both pre- and postsynaptic cells spike during the induction.
3. Verify the quality of recordings by monitoring the membrane potential, input resistance, series resistance and bath temperature, as appropriate.
4. Average across 5-8 paired recordings; do not make too much of the outcome of individual connections.

Discussion

Although the quadruple patch-clamping technique may be expensive to set up and difficult to master, it has several advantages. It provides millisecond temporal precision, which is important for the STDP paradigm (Markram et al., 1997, Sjöström et al., 2001). It enables dissection of pre- from postsynaptic mechanisms by wash-in of drugs and dyes (Kaiser et al., 2004, Koester and Johnston, 2005, Rodriguez-Moreno and Paulsen, 2008, Buchanan et al., 2012). Finally, it enables morphological identification of connected cells, which is essential for studying synapse specificity (Buchanan et al., 2012, Blackman et al., 2013).

With multiple whole-cell recordings, the statistics of local connections can also be studied. For example, neocortical pyramidal cells are reciprocally connected to a greater degree than expected from a uniformly random distribution (Song et al.,

2005, Lefort et al., 2009). This may result from Hebbian plasticity, so that cells coding for similar information are relatively strongly wired together (Ko et al., 2011). The juvenile cerebellar Purkinje cell network, on the other hand, is solely built from chains of unidirectionally connected neurons (Watt et al., 2009). This forms a substrate for travelling waves of activity, which may help wire the circuit up in early development (van Welie et al., 2011).

Multiple whole-cell recordings represent a financial hurdle, however. A cheaper alternative is to search for presynaptic cells using a “loose patch” while whole-cell recording the postsynaptic cell (Feldmeyer et al., 1999, Barbour and Isope, 2000). Because this method may subject the postsynaptic cell to prolonged periods of dialysis of intracellular components, it may however not be useful for long-term plasticity experiments due to LTP washout (Malinow and Tsien, 1990).

In the end, quadruple whole-cell recording is technically similar to patching single cells. With this protocol, an experimentalist capable of reliably patching individual cells should not find multiple whole-cell recordings too difficult.

Recipes

Table 2.2: Composition of artificial cerebrospinal fluid

Prepare a 10x stock solution in double-distilled water (ddH₂O) made from:

Compound	Concentration (mM)
NaCl	125
KCl	2.5

NaH ₂ PO ₄	1.25
NaHCO ₃	26

The 10x solution should be diluted 10-fold on the day of the experiment, bubbled for 10 min with carbogen and supplemented with:

Compound	Concentration (mM)
MgCl ₂ (1M stock)	1
CaCl ₂ (1M stock)	2
Glucose	~26

Adjust osmolality to ~320 mOsm with D-glucose for rat and ~338 mOsm for mouse.

Table 2.3: Composition of intracellular solution

Prepare a 1M solution of HEPES in ddH₂O and adjust the pH to 7 with KOH (3M).

In 30 ml of ddH₂O, add:

Compound	Concentration (mM)
KCl	125
KGluconate	2.5
1M HEPES	10

Adjust the volume to 45 ml and verify that pH ~7.

To the previous solution, add:

Compound	Concentration (mM)
MgATP	4
NaGTP	0.3
NaPhosphocreatine	10

The pH should be re-adjusted to 7.2-7.4 with KOH and osmolality should be corrected to 294 mOsm (rat) with sucrose. Filter the solution using a nylon filter (pore size 0.2 μ m) and make 1-ml aliquots. Store at -20°C for up to several months. Verify the osmolality each experiment day.

Acknowledgments

The authors thank Alanna Watt, Elvis Cela, Jerome Maheux, and Andrew Chung for help and useful discussions. This work was funded by CFI Leaders Opportunity Fund #28331 (P.J.S.), CIHR OG 126137 (P.J.S.), CIHR New Investigator Award (P.J.S.), NSERC DG 418546-2 (P.J.S.), and by an RI MUHC studentship award (T.L.).

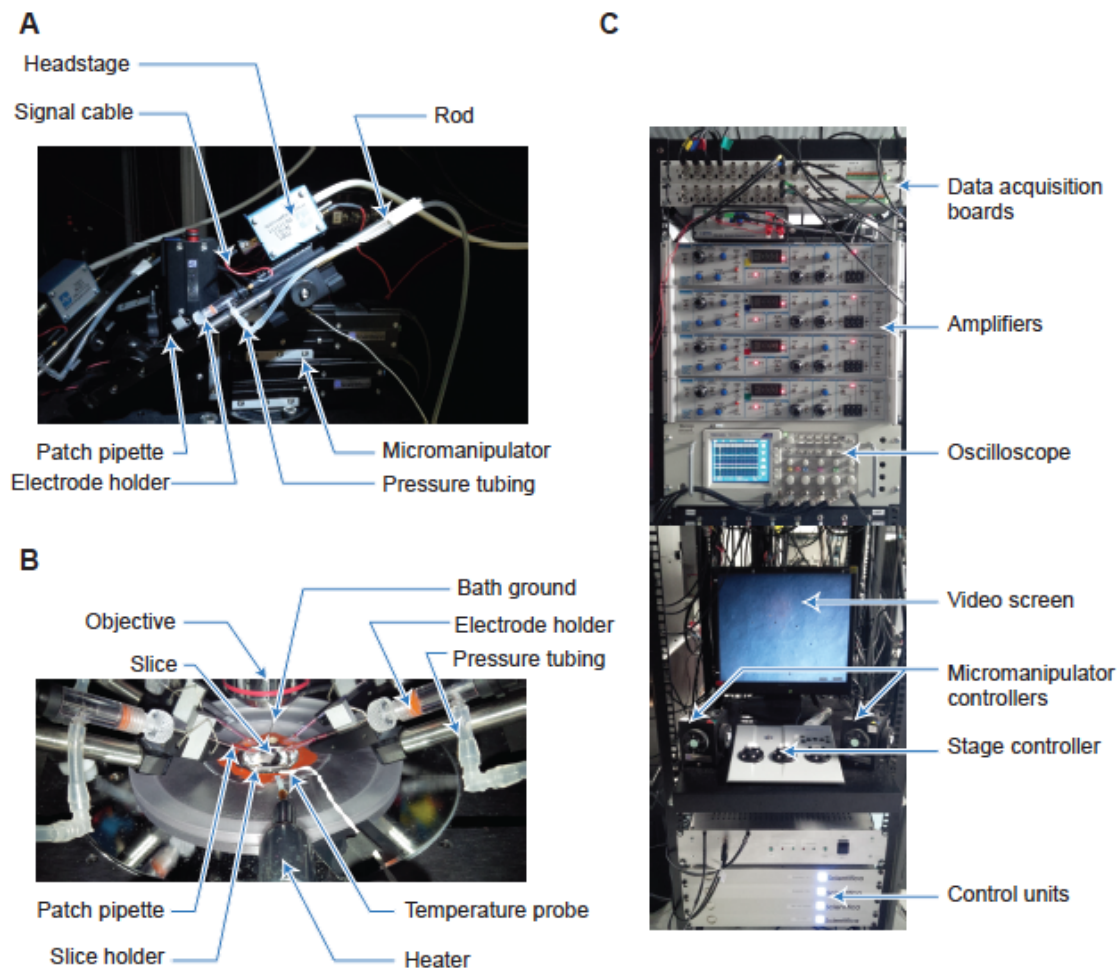


Figure 2.4: Recording setup

(A) Motorized micromanipulator with patch pipette. With this design, the rod is slid away from the chamber for pipette exchange; other designs may rotate or swing backwards. The mode of pipette exchange determines the total number of manipulators that can be fit.

(B) Perfusion chamber during quadruple whole-cell recording. Pipettes are filled with enough intracellular solution to touch the electrode wire. Glass pipettes are clamped to the rod to minimize movements. The temperature probe and the bath ground should be fully immersed in ACSF.

(C) Acquisition boards provide communication between computer and amplifiers. Recording channels and manipulators are color-coded (see oscilloscope screen) for simplicity. Video screen shows a Ddtd-contrast-enhanced image of the slice. Microscope stage, objective, and manipulators are remotely controlled to minimize the risk of disrupting ongoing recordings.

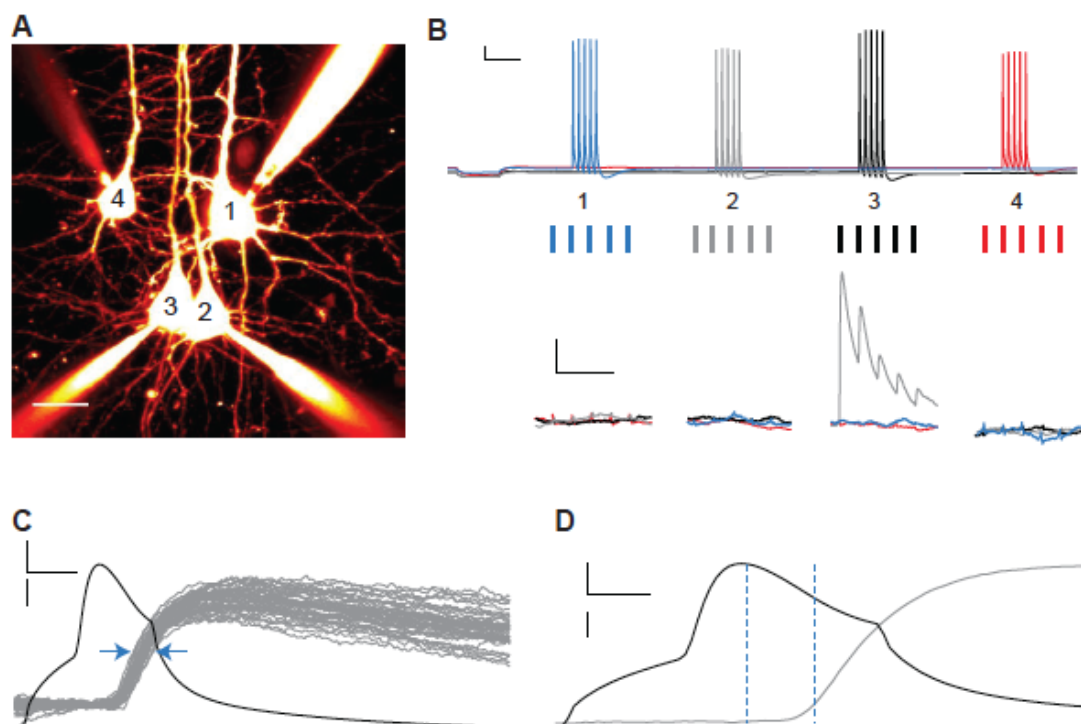


Figure 2.5: Finding connected neurons using quadruple recordings

(A) Flattened 2-photon-imaging stack of four neighboring L5 PCs filled with Alexa 594 (scale bar: 25 μm).

(B) 30-Hz trains are evoked (top, scale bars: 200 ms, 10 mV) to identify responding postsynaptic cells (bottom, scale bars: 100 ms, 0.25 mV). Sweeps should be repeated 10-40 times every 10-20 seconds, and are then averaged. Note short-term depressing connection from cell 3 (black) to cell 2 (gray).

(C) Monosynaptic connections have a jitter of less than 1 ms (blue arrows); larger jitter suggest that the responses are polysynaptic. Fifty spike-triggered traces from cell 2 are represented (scale bars: 2 ms, 20 mV/300 μV).

(D) Monosynaptic connections also have sub-millisecond latency between presynaptic spike and 10% of EPSP peak (vertical dashed lines). EPSP trace is a spike-triggered average of 50 sweeps, while the presynaptic action potential is represented by a single sweep (scale bars: 1 ms, 20 mV/200 μV).

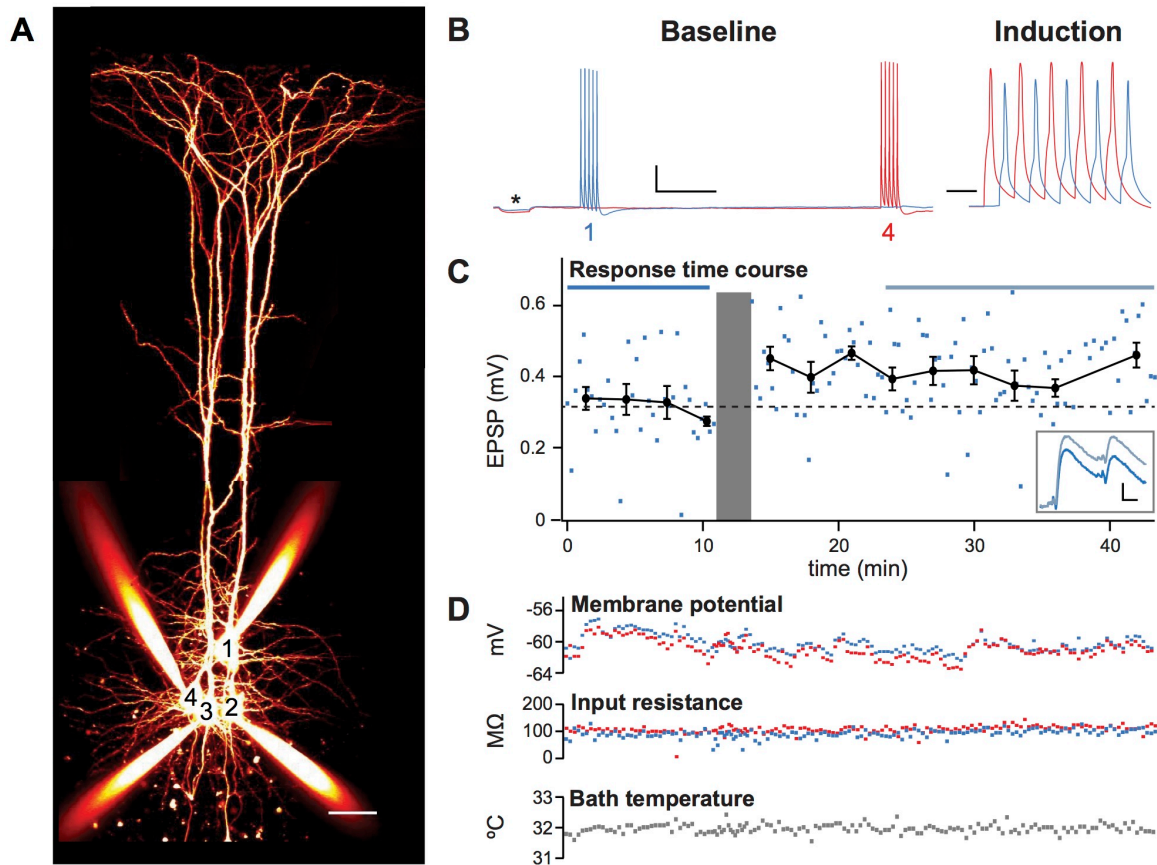


Figure 2.6: Using paired recordings study plasticity

(A) Quadruple whole-cell recording in which PC 4 was connected to PC 1 (scale bar: 50 μm).

(B) During the 10-min baseline period, 30-Hz trains were repeated every 18 seconds in the connected pair of neurons. These bursts were temporally separated to avoid accidental induction of plasticity (Sjöström et al., 2001). During the induction, 5 APs at 50 Hz were repeated 15 times every 15 seconds. The timing difference, Δt , was +10 ms. After the induction, the baseline pattern was repeated again (scale bars: 500 ms/20 ms, 20 mV). Asterisk denotes a 250-ms-long test pulse of -50 pA, used to monitor input resistance.

(C) Time course of the first EPSP in the 30-Hz train shows LTP. The induction is illustrated by gray area. Horizontal blue lines (top) represent time periods over which averages (inset) were taken (scale bars: 10 ms, 0.1 mV).

(D) As a measure of recording quality, resting membrane potential, input resistance, and bath temperature were monitored throughout experiment.

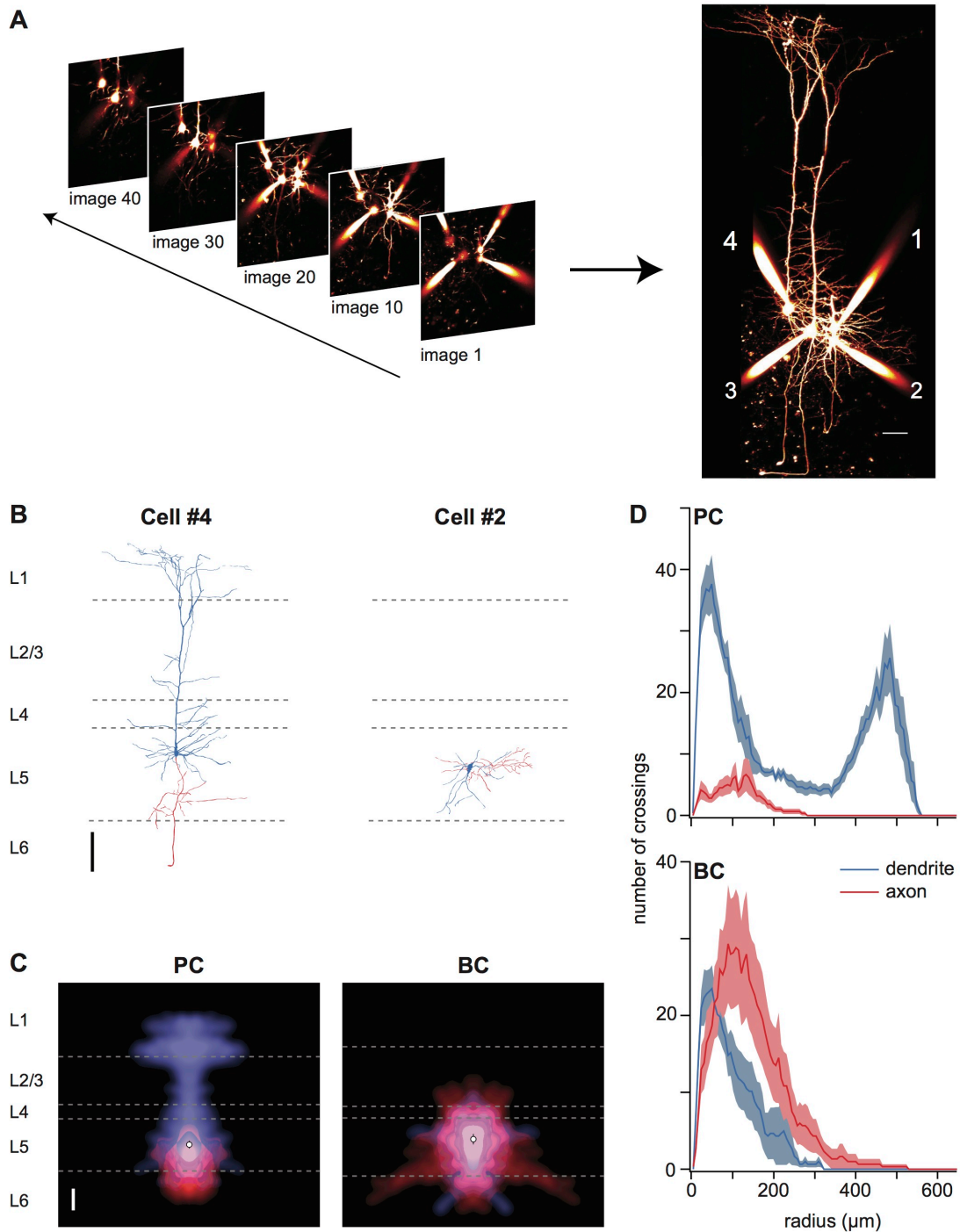


Figure 2.7: Morphological cell classification from 2-photon images

(A) A stack of 2-photon slices provides a 3D representation of recorded neurons filled with Alexa-594. Each slice is an average of two to four 512×512-pixel frames collected. Maximum-intensity projections are assembled for full morphological view (scale bar: 50 μm).

(B) Digital reconstruction of cell 4 (top) shows that this is a neocortical L5 pyramidal cell, whereas the morphology of cell 2 (bottom) is characteristic of a basket cell (scale bar: 100 μm). Reconstructions were carried out using Neuromantic (Blackman

et al., 2014). Dendrites (blue) were distinguished from axons (red) by presence of spines. Dashed grey lines represent layer boundaries, as determined from simultaneously acquired laser-scanning Dodt contrast images.

(C) Morphology density map (Buchanan et al., 2012) of six PCs (left) highlights the characteristic apical dendrite, with an axonal arborisation that remains chiefly localized to L5. The corresponding map of six basket cells (right) shows axonal and dendritic arbors that both remain confined to L5. Average soma location indicated by open circle (scale bar: 100 μm).

(D) Sholl Analysis (Sholl and Uttley, 1953) of six PCs and six basket cells provide quantitative cell classification criteria from axonal and dendritic branching patterns.

Chapter III: Results

Synapse-specific expression of calcium-permeable AMPA receptors in neocortical layer 5

Submitted to Journal of Physiology

Txomin Lalanne^{1,2,*}, Julia Oyrer^{3,*}, Adamo Mancino¹, Erica Gregor¹, Andrew Chung¹, Louis Huynh¹, Sasha Burwell¹, Jérôme Maheux¹, Mark Farrant³ and P. Jesper Sjöström^{1,3,4}

1) Centre for Research in Neuroscience, Department of Neurology and Neurosurgery, The Research Institute of the McGill University Health Centre, Montreal General Hospital, Montreal, Quebec, H3G 1A4, Canada

2) Integrated Program in Neuroscience, McGill University, 3801 University Street, Montreal, Quebec, H3A 2B4, Canada

3) Department of Neuroscience, Physiology and Pharmacology, University College London, Gower Street, London, WC1E 6BT, UK

4) Correspondence: jesper.sjostrom@mcgill.ca

*) These authors contributed equally to this work.

Abbreviated title: Synapse-specific CP-AMPA expression

Address for editorial correspondence:

Prof P J Sjöström

Centre for Research in Neuroscience

Department of Neurology and Neurosurgery

The Research Institute of the McGill University Health Centre

Montreal General Hospital

1650 Cedar Ave, room L7-225

Montreal Quebec H3G 1A4, Canada

Office: +1-514-934-1934, ext. 44561

Mob: +1-438-826-1971

FAX: +1-514-934-8216

Abstract

AMPA-type glutamate receptors (AMPA) lacking the GluA2 subunit are calcium permeable (CP), and contribute to synaptic plasticity in several hippocampal interneuron types, but their precise role in neocortex is not well described. We explored the presence of CP-AMPA receptors at pyramidal cell (PC) inputs to Martinotti cells (MCs) and basket cells (BCs) in layer 5 of developing mouse visual neocortex. Immunolabeling suggested greater GluA2 expression in MCs than in BCs. Based on spermine-dependent rectification and the CP-AMPA blocker Naspm, a differential presence of CP-AMPA receptors at PC-BC and PC-MC synapses was confirmed electrophysiologically, using paired recordings, NPEC-AMPA uncaging, and mini recordings. CP-AMPA receptor expression in BCs was in addition correlated with rapidly decaying synaptic currents. Modeling predicted that this reduces spike latencies and sharpens responses in BCs, which we verified experimentally using dynamic clamp. The synapse-specific expression of CP-AMPA receptors may thus critically influence both plasticity and information processing in neocortical microcircuits.

Impact statement

The synapse-specific expression of calcium-permeable AMPA receptors at pyramidal to basket cell connections in neocortical layer 5 may sharpen basket cell-mediated feed-forward inhibition.

Introduction

Synaptic calcium transients critically regulate synapse development, functioning, and plasticity. The involvement of *N*-methyl-D-aspartic acid receptors (NMDARs) and voltage-gated calcium channels in mediating calcium transients is well established (Sjöström and Nelson, 2002, Sjöström et al., 2008). But α -amino-3-hydroxy-5-methyl-4-isoxazolepropionic acid receptors (AMPARs) that either contain an unedited version of the GluA2 subunit or lack it completely are also calcium permeable (CP) (Hume et al., 1991), and are able to trigger long-term plasticity (Kullmann and Lamsa, 2007).

While NMDARs are blocked by extracellular Mg^{2+} ions at hyperpolarized membrane potentials, GluA2-lacking CP-AMPARs are blocked by endogenous intracellular polyamines at depolarized potentials (Bowie and Mayer, 1995, Donevan and Rogawski, 1995, Kamboj et al., 1995, Koh et al., 1995). This results in a characteristic inward-rectifying current/voltage (IV) relationship, which can be used to identify CP-AMPARs. Subunit composition also determines the kinetic properties of AMPARs. For example, CP-AMPARs typically have faster desensitization rates than GluA2-containing AMPARs (Hume et al., 1991, Traynelis et al., 2010, Sobolevsky, 2015) as well as higher single-channel conductance (Swanson et al., 1997).

In the hippocampus, CP-AMPARs have been identified at excitatory inputs onto PCs (Rozov et al., 2012, Mattison et al., 2014) but are primarily associated with excitatory inputs onto inhibitory neurons (IN), where they elicit long-term plasticity (Lamsa et al., 2007b, Camire and Topolnik, 2014). However, the precise pattern of expression of CP-AMPARs in neocortical INs is not as well described. One reason for this may be the complexity of the neocortical circuitry, as neocortical IN classification remains a challenge (DeFelipe et al., 2013). INs are generally classified

by morphology, by firing pattern, and by genetic markers (Markram et al., 2004, Ascoli et al., 2008, DeFelipe et al., 2013, Kepecs and Fishell, 2014), such as parvalbumin (Pvalb) and somatostatin (Sst) (Toledo-Rodriguez et al., 2005). In L5, two key IN types are fast-spiking Pvalb-positive basket cells (BCs), and accommodating Sst-expressing Martinotti cells (MCs). These IN types have strikingly different morphologies: classically, BC axons are largely intralaminar (although see Buchanan et al., 2012), whereas MC axons ascend and ramify extensively up to L1 (Kawaguchi and Kubota, 1996, 1997, Markram et al., 2004, Silberberg and Markram, 2007, Buchanan et al., 2012). Excitatory inputs onto these two IN types also have very different short-term dynamics: those onto MCs short-term facilitate, whereas those onto BCs rapidly depress once activated (Silberberg and Markram, 2007, Buchanan et al., 2012, Blackman et al., 2013). As a consequence of these prominent features, BCs and MCs are relatively easy to distinguish when compared to other neocortical IN types. In addition, BCs are also the most numerous, accounting for approximately half of all INs (Markram et al., 2004), while MCs make up for their lower numbers by strongly and efficiently inhibiting PCs (Berger et al., 2010).

The above-mentioned differences in morphology and synaptic properties have important implications for MC and BC function in the local circuit. The strong facilitation of excitatory inputs onto MCs, for example, enables delayed-onset feedback inhibition (Silberberg and Markram, 2007) that increases rapidly with the number of excitatory synapses recruited so that PCs can via MCs efficiently limit their own spiking activity (Kapfer et al., 2007, Berger et al., 2010). MCs inhibit PC dendrites, and are particularly efficient at shutting down dendritic calcium spikes, spiking output, as well as plasticity in PCs (Murayama et al., 2009, Bar-Ilan et al., 2012, Gidon and Segev, 2012). The short-term depressing excitatory inputs onto

BCs, on the other hand, ensure that this cell type mediates early-onset feed-forward inhibition of PCs. This occurs largely perisomatically (Kawaguchi and Kubota, 1997, Buchanan et al., 2012), where BC inhibition can act rapidly to shorten the integrative time window for excitation (Pouille and Scanziani, 2001, Mittmann et al., 2005). In combination, early-onset perisomatically targeting BCs and late-onset dendritically targeting MCs can thus remap a temporal high-frequency pattern of excitation into a spatial pattern of inhibition, such that the soma is inhibited first and dendrites later (Pouille and Scanziani, 2004, Blackman et al., 2013). We have previously demonstrated that presynaptic NMDARs enhance the delayed-onset MC-mediated feedback inhibition of PCs by specifically boosting PC inputs to MCs during high-frequency firing (Buchanan et al., 2012). Whether specific glutamate receptor types similarly assist in early-onset BC-mediated inhibition is not known, however.

Here, we looked for CP-AMPA receptors at synapses from PCs onto BCs and MCs in L5 of mouse visual neocortex. We found that CP-AMPA receptors were expressed at PC-BC but not at PC-MC synapses. We also observed that CP-AMPA receptor-containing synapses onto BCs were associated with significantly more rapid decay kinetics, which helps shorten spike latencies and sharpen response durations in BCs. We propose that synaptic CP-AMPA receptors in BCs, by virtue of their relatively rapid kinetics, may help sharpen the BC-controlled integration time window for excitation in PCs (Pouille and Scanziani, 2001) to temporally sharpen information processing in neocortical microcircuits.

Results

Differential GluA2 labeling of Pvalb and Sst-positive INs

In order to assess the relative expression of GluA2 in BCs and MCs within L5 of the mouse visual neocortex, we first examined the pattern of GluA2 immunoreactivity in these INs, identified by the presence of Pvalb and Sst, respectively. In slices from P21 wild-type (WT) mice, we quantified immunolabeling in neocortical L5, which was identified by the presence of large PC somata. Unsurprisingly, L5 PCs were immunoreactive for GluA2 (Kumar et al., 2002). While Pvalb-positive somata showed little immunolabeling for GluA2 (**Figure 3.1A**), Sst-positive somata were strongly labeled, although less so than those of PCs (**Figure 3.1B**). Quantification of somatic GluA2 fluorescence normalized to that of PCs confirmed a much greater labeling of Pvalb- positive cells (normalized intensity 0.55 ± 0.08 for Pvalb versus 0.14 ± 0.002 for Sst; $n = 3$ and 4 , $p < 0.05$) (**Figure 3.1C**). This suggests a differential expression of CP-AMPARs in layer-5 BCs and MCs.

Morphology classified recorded INs into MCs and two types of BCs

To examine whether the cell-dependent expression of GluA2 was reflected in the properties of synaptic currents, we performed a series of experiments using whole-cell recording (see below). This required reliable targeting and classification of recorded cell.

L5 PCs were readily targeted using contrast-enhanced infrared video microscopy because of their large pyramidal somata and conspicuous apical dendrites. BCs were similarly targeted by their relatively small and rounded cell bodies or by fluorescence in acute slices from the Pvalb-positive G42 mouse line

(Chattopadhyaya et al., 2004), visualized by two-photon laser scanning microscopy (2PLSM). To target MCs by fluorescence, we used the Sst-positive GIN transgenic mouse line (Oliva et al., 2000), which solely labels MCs in neocortical L5 (Fino and Yuste, 2011, Buchanan et al., 2012). Alternatively, MCs were targeted in slices from WT mice by their large and characteristically ovoid somata (Silberberg and Markram, 2007).

Every single recorded neuron was classified *post hoc* by morphology (**Figure 3.2** and **table 3.1**). Recorded neurons were manually reconstructed from 2PLSM imaging stacks and morphometry was carried out (see 'Materials and methods' and Buchanan et al., 2012, Blackman et al., 2014).

BCs were additionally independently morphologically classified into two subtypes using software clustering (see 'Materials and methods' and **Figure 3.8**). Axons of type-1 BC preferentially ramified in L2/3, whereas axons of type 2 branched chiefly in L5, as previously shown (Buchanan et al., 2012, Ferreira et al., 2014). The type-1 and type-2 BCs were found at indistinguishable rates in slices from Pvalb-positive G42 (3 out of 11) and WT mice (7 out of 70, $p = 0.11$, Chi-squared test).

Whenever possible, cell type was additionally verified by synaptic dynamics (**Table 3.1** and **Figure 3.9**). Excitatory inputs to BCs characteristically showed short-term depression, whereas excitatory connections to MCs exhibited strong short-term facilitation (Buchanan et al., 2012, Blackman et al., 2013). In a subset of recordings, BCs were also identified by their characteristic high-threshold fast-spiking pattern (**Table 3.2**) (Buchanan et al., 2012).

Synaptic current properties suggest the presence of CP-AMPARs at PC-BC but not at PC-MC or at PC-PC connections

We first performed whole-cell recordings of connected PC-IN and PC-PC pairs (**Figure 3.3A**). Once a connection was found, the postsynaptic IN was held at different membrane potentials ranging from -100 mV to $+50$ mV while action potentials (APs) were evoked in the presynaptic PC. Recordings were performed using an intracellular solution containing added spermine (see 'Materials and methods'). For PC-BC connections, the IV relationship was inward rectifying (**Figure 3.3A, B, D**) with a low rectification index (RI) (**Figure 3.3E**), reflecting the predominance of CP-AMPARs. In contrast, the IV relationship of PC-MC connected pairs was linear (**Figure 3.3C-E**), suggesting a predominance of CI-AMPARs. At PC-PC connections, synaptic currents exhibited non-rectifying IV relationship ($RI_{+40/-40} = 1.1 \pm 0.1$, $n = 4$ pairs, $p = 0.69$ for comparison to 1, data not shown), which was different compared to PC-BC pairs ($p < 0.001$, Bonferroni adjusted). The RIs of PC-PC and PC-MC connections were indistinguishable ($p = 0.75$).

Although we analyzed the initial component of the excitatory postsynaptic currents (EPSCs), we were concerned that NMDARs might distort our analysis. We therefore blocked NMDARs with AP5, but RI at both PC-BC and PC-MC synapses was unaffected (**Figure 3.3F**). Taken together, these results suggest a synapse-specific expression of CP-AMPARs at PC-BC but not PC-MC or PC-PC synapses.

As an aside, the $NMDA_{+50}/AMPA_{-60}$ ratio was 3-fold smaller at PC-BC than at PC-MC connections (**Figure 3.9A, B**). This suggests that PC-MC synapses express more NMDARs relative to AMPARs than do PC-BC synapses. It does not, however, imply that PC-BC synapses express no NMDARs. Indeed, long-latency synaptic currents at PC-MC as well as at PC-BC connections had an IV relationship

characteristic of NMDARs that was abolished by AP5 (**Figure 3.9C, D**), suggesting that both these synapse types possess postsynaptic NMDARs.

We reasoned that if CP-AMPARs are indeed present at PC-BC synapses, the blocker 1-naphtyl acetyl spermine (Naspm) (Koike et al., 1997) should decrease the amplitude of PC-BC EPSCs. Consistent with this prediction, we found that after Naspm wash-in, PC-BC EPSCs were reduced, while control recordings remained stable (**Figure 3.3F, G**), confirming the presence of CP-AMPARs. The absence of complete blockade hints at a possible combined expression of calcium-impermeable (CI) and CP-AMPARs at PC-BC synapses (see 'Discussion').

Currents evoked by AMPA uncaging rectify in BCs but not in MCs or PCs

Calcium-permeable kainate receptors are expressed presynaptically at excitatory inputs to Sst-positive INs in the hippocampus, and can be blocked by Naspm (Sun et al., 2009). Such receptors may also be present on inputs to the corresponding neocortical Sst-positive INs, i.e. MCs. To eliminate any contribution from presynaptic kainate receptors and to focus exclusively on the postsynaptic side, we uncaged AMPA by photolysing NPEC-AMPA with brief 405-nm laser pulses. We used ACSF supplemented with TTX to exclude a possible contribution of glutamate due to the suprathreshold activation of neighboring cells. We puffed NPEC-AMPA close to the soma and proximal dendrites of PCs, BCs, or MCs using a patch pipette. Recorded neurons were voltage-clamped at potentials ranging from -100 mV to $+50$ mV and a single 0.1-2 ms laser pulse per voltage step produced a slow current (**Figure 3.4A, B**) characteristic of the slow rate of photolysis of the NPEC cage (Palma-Cerda et al., 2012). The uncaging-evoked current was virtually abolished by

NBQX ($7\% \pm 2\%$ of baseline, $n = 4$ cells, $p < 0.001$ compared to 100%, data not shown), indicating that it was indeed AMPAR-mediated. With AMPA uncaging, we found a marked rectification in BCs (**Figure 3.4D, E**). In contrast, no such rectification was observed in MCs (**Figure 3.4D, E**) or in PCs ($RI_{+40/-40} = 0.9 \pm 0.1$, $n = 5$ cells, versus 1, $p = 0.31$, data not shown). These results are in keeping with the paired recording experiments and confirm the presence of CP-AMPARs in BCs.

We next examined the effect of Naspm on currents evoked by AMPA uncaging in BCs held at -80 mV. Naspm wash-in decreased the amplitude of uncaging-evoked responses while control recordings remained stable (**Figure 3.4F, G**). In contrast, Naspm wash-in did not affect AMPA-uncaging-evoked currents in PCs ($94\% \pm 5\%$ of baseline, $n = 6$ cells, versus 100%, $p = 0.29$, data not shown) or MCs ($94\% \pm 5\%$, $n = 5$ cells, versus 100%, $p = 0.29$; or $p = 0.15$ versus MC mock Naspm controls $103\% \pm 2\%$, $n = 3$, data not shown). These uncaging experiments corroborate the paired-recording results and show that CP-AMPARs are specifically expressed in neocortical L5 BCs but not MCs or PCs. Since NPEC-AMPA uncaging activates synaptic as well as extra-synaptic AMPARs, these experiments furthermore suggest that CP-AMPARs may be selectively expressed in BCs in a cell-wide manner.

CP-AMPARs contribute to miniature EPSCs in BCs

Since paired recordings sample a small fraction of all synaptic inputs onto a cell, it is possible that we missed excitatory inputs onto BCs that do not contain CP-AMPARs. Spontaneous release, however, can arise at any of the synaptic contacts onto a neuron and dendritic filtering should not reduce the chances of detecting spontaneous release events at distal synapses of relatively electrically compact BCs

(Sjöström et al., 2008). Spontaneous release may thus sample relatively globally from all excitatory inputs onto a recorded cell. Moreover, spontaneous and evoked glutamate release may activate non-overlapping populations of receptors and synapses (Atasoy et al., 2008, Sutton and Schuman, 2009, Sara et al., 2011, Peled et al., 2014). To determine whether spontaneously released glutamate activates AMPARs with functional properties similar to those activated in an AP-dependent fashion, we examined the contribution of CP-AMPARs to miniature EPSCs (mEPSCs) recorded in BCs.

To isolate AMPAR-mediated spontaneous currents, we blocked voltage gated Na^+ channels, NMDARs, GABA_A receptors, and GABA_B receptors using TTX, AP5, SR-95531, and CGP 54626 (see 'Materials and methods'). We measured the mEPSC rectification $\text{RI}_{+60/-60}$ both in the presence and absence of intracellular spermine (Bats et al., 2012). This revealed spermine-dependent inward rectification, indicating the activation of synaptic CP-AMPARs by quantal events in BCs (**Figure 3.5A-D**). To verify these findings pharmacologically, we recorded mEPSCs from BCs at -60 mV while washing in Naspm. In agreement with the rectification data, mEPSC-mediated charge transfer was decreased by Naspm (**Figure 3.5E-G**). Taken together, our findings suggest that both spontaneous and evoked glutamate release activates CP-AMPARs in BCs, implying a cell-wide expression.

Rapid AMPAR kinetics reduces spike latency and sharpens responses in BCs

Fast-spiking INs in hippocampus and neocortical layer 2/3, 4, and 6 have previously been associated with AMPARs with relatively rapid decay kinetics (Hestrin, 1993, Geiger et al., 1995, Angulo et al., 1997, Geiger et al., 1997), so we

investigated whether the presence of CP-AMPA receptors at PC-BC connections in L5 was also associated with more rapid synaptic kinetics. Indeed, the decay time constant, τ_{decay} , for PC-BC EPSCs was faster than for PC-MC or PC-PC EPSCs (**Figure 3.6A** and **Table 3.1**). However, the EPSC rise time constants, τ_{rise} , were indistinguishable (PC-PC: 2.2 ± 0.8 ms; PC-BC: 1.8 ± 0.3 ms; PC-MC: 2.0 ± 0.4 ms; $n = 5, 22$ and 9 pairs, respectively; ANOVA $p = 0.86$). We were concerned that this difference in decay time constant was an artifact arising from differential filtering in the different cell types, because BCs have faster membrane time constant, τ_M , than MCs and BCs have (Buchanan et al., 2012). To rule out a contribution from differential membrane time constant filtering, we benefitted from the fact that NPEC-AMPA photolysis is an order of magnitude slower than τ_M in any of these cells (**Figure 3.4B, C**) (Palma-Cerda et al., 2012). In agreement with the paired recordings, AMPA-uncaging-evoked responses decayed faster in BCs than in MCs or PCs (**Figure 3.6B** and **Table 3.1**), suggesting that the difference in kinetics was due to cell-specific AMPAR characteristics rather than to biophysical properties intrinsic to these three cell types.

We explored possible functional consequences of the faster synaptic kinetics in BCs by implementing a simple leaky integrate-and-fire computer model of a BC with a single synaptic input modeled as a double-exponential conductance waveform. We used either $\tau_{\text{decay}} = 3$ ms or $\tau_{\text{decay}} = 5$ ms consistent with the excitatory input kinetics seen in BCs and MCs, respectively (**Figure 3.7A**). The model predicted that rapidly decaying inputs result in EPSPs with faster rise, in shorter spike latencies, and in temporally sharpened responses in BCs (**Figure 3.7B**). To test the model predictions, we next carried out dynamic clamp experiments. We patched BCs and injected conductances mimicking rapidly or slowly decaying excitatory synaptic

inputs ($\tau_{\text{decay}} = 3 \text{ ms}$ or 5 ms) as for the computer model. In agreement with the model, we observed in dynamic clamp more rapidly rising EPSPs ($\tau_{\text{rise}} = 3.5 \pm 0.3 \text{ ms}$ vs. $5.4 \pm 0.8 \text{ ms}$, $n = 5$, $p < 0.05$, paired t-test), shorter spike latencies, and temporally sharpened responses for the rapidly decaying excitatory inputs (**Figure 3.7B, C**). Rapidly decaying EPSCs occurring at CP-AMPA-expressing PC-BC synapses may thus help make BC-mediated early inhibition of PCs even faster.

Discussion

In the present study, we demonstrate a contrasting CP-AMPA expression pattern at excitatory synapses onto two major IN subclasses in L5 of visual neocortex, with BCs but not MCs expressing CP-AMPA. While the somata of Pvalb-positive INs contained little GluA2 immunoreactivity, the somata of Sst-positive INs were more strongly labeled, although less so than PCs. This observation was supported by our electrophysiological data, which showed both rectifying current-voltage relationships and Nasp sensitivity for AMPA-mediated currents in BCs but no rectification in MCs or in PCs. In addition, CP-AMPA-expressing synapses were associated with more rapidly decaying kinetics. Computer modeling predicted that this helps shorten BC response latency and duration, which we verified using conductance clamp.

Interneuron classification

To ensure correct identification of recorded INs, we reconstructed and morphologically characterized all INs. Whenever possible, we also classified them based on firing pattern and short-term plasticity of excitatory inputs. In addition, in a subset of recordings we used two transgenic mouse lines that fluorescently label

cells positive for Pvalb or for Sst (Oliva et al., 2000, Chattopadhyaya et al., 2004). As expected, the morphologies of MCs and BCs were strikingly different, with MCs having characteristic descending dendrites and axonal arbors that ramified into layer 1, while BC morphologies were more compact (Buchanan et al., 2012). In addition, two types of BCs were found: type 1 with an ascending axon and type 2 with axonal ramifications largely confined to L5. The ascending axons of type-1 BCs differed from those of MCs in that they did not penetrate layer 1 (**Figure 3.2**). Even though the axonal branching pattern for type-1 cells was unorthodox for BCs, we opted to denote both cell types as 'BCs', since they both had short-term depressing excitatory inputs and high-threshold fast-spiking pattern characteristic of BCs. The existence of these two BC types is in agreement with our previous studies that also identified these two fast-spiking Pvalb-positive BC types in L5 of mouse visual neocortex (Buchanan et al., 2012, Ferreira et al., 2014). Fast-spiking Pvalb-positive BCs with ascending translaminal axonal arborizations have also been found in neocortical layer 6 (Bortone et al., 2014), suggesting that cross-laminar BC inhibition is a general organizational principle of neocortical microcircuits.

Cell-specific expression of GluA2

In L5 we found greater GluA2 immunoreactivity in Sst-positive cells than in Pvalb-positive cells. Can one equate this directly with MCs and BCs? Many attempts have been made to link molecular expression with anatomical and electrophysiological features of INs (Markram et al., 2004, Ascoli et al., 2008, DeFelipe et al., 2013, Kepecs and Fishell, 2014). Sst is expressed in all MCs (Wang et al., 2004, Toledo-Rodriguez et al., 2005); this is true for assays of protein or mRNA and regardless of neocortical region and layer (Wahle, 1993, Kawaguchi and

Kubota, 1996, 1997, Wang et al., 2004, Toledo-Rodriguez et al., 2005). Accordingly, Sst is considered one of the most specific genetic markers (Toledo-Rodriguez et al., 2005). Pvalb is the next most specific of available molecular markers (Toledo-Rodriguez et al., 2005), being primarily associated with fast-spiking BCs (Cauli et al., 1997, Kawaguchi and Kubota, 1997, Dumitriu et al., 2007). Although Pvalb and Sst are likely to predominantly identify BCs and MCs, respectively, it is important to note that no genetic marker known to date unambiguously identifies a single IN type (Markram et al., 2004, Ascoli et al., 2008, DeFelipe et al., 2013, Kepecs and Fishell, 2014).

In an immunolabeling study of monkey visual neocortex (Kooijmans et al., 2014), Pvalb-positive INs were reported to label strongly for both GluA2 and GluA3, whereas Sst-positive INs showed little or no GluA2 labeling (Kooijmans et al., 2014). This is the opposite of our findings in the mouse. However, in mouse and monkey, different IN classes are defined by different molecular markers (Wahle, 1993, Conde et al., 1994, Gonchar et al., 2007, Xu and Yao, 2010). This raises the possibility that these species differences are not so much about varying GluA2 expression as they are about differences in IN genetic markers.

Target-specific expression of CP-AMPARs

The pronounced rectification of BC mEPSCs, of uncaging-induced currents in BCs, and of PC-BC unitary EPSCs all supported the suggestion from our immunolabeling that CP-AMPARs are expressed in BCs but not in MCs or PCs. However, we obtained an incomplete Nasp block of evoked as well as of spontaneous AMPAR-mediated EPSCs in BCs. One interpretation is that CP and CI-AMPARs are co-expressed at excitatory inputs onto BCs, although with CP-AMPARs

dominating. However, several studies have shown incomplete block with Naspm or the related polyamine spider toxin philanthoxin-433 for both recombinant CP-AMPARs (Washburn and Dingledine, 1996, Jackson et al., 2011) and for native receptors in cells lacking GluA2 (Koike et al., 1997, Sara et al., 2011, Studniarczyk et al., 2013). Also, synaptic responses in BCs in both paired recordings and with AMPA uncaging were virtually abolished at positive voltages by internal spermine. A more parsimonious explanation may thus be that Naspm cannot fully block CP-AMPARs under our experimental conditions. Given the known use-dependence of block (Washburn and Dingledine, 1996, Koike et al., 1997), additional work would be required to settle this issue.

Recently, it has been suggested that spontaneous and evoked glutamate release activate non-overlapping populations of receptors (Atasoy et al., 2008, Sutton and Schuman, 2009, Sara et al., 2011) or can occur preferentially at different sets of synapses (Peled et al., 2014). Our data on BCs, however, suggests that glutamate released in an AP-dependent or AP-independent fashion activates AMPARs with similar properties.

Here we found that CP-AMPARs were similarly expressed at PC synapses onto both type-1 and type-2 BCs. In contrast, we previously reported that PC connections to type-1 but not to type-2 BCs differentially expressed presynaptic NMDARs (Buchanan et al., 2012). Excitatory inputs to translaminal type-1 BCs thus have presynaptic NMDARs and postsynaptic CP-AMPARs, whereas excitatory synapses onto intralaminar type-2 BCs do not have presynaptic NMDARs, even though they too have postsynaptic CP-AMPARs. The functional relevance of this interesting dichotomy is unclear at this stage.

Other studies, in both neocortex and hippocampus, have also identified the presence of CP-AMPA receptors in BCs. Several studies have shown inward rectification and faster kinetics of currents in outside-out somatic patches from BCs in rat dentate gyrus as well as in neocortical fast-spiking non-pyramidal cells in rat frontal neocortex (Geiger et al., 1995, Koh et al., 1995, Angulo et al., 1997). Furthermore, inward rectification has been associated with a relatively low abundance of GluA2 mRNA (Geiger et al., 1995, Angulo et al., 1997). More recently, Wang and Gao (2010) showed that the majority of fast-spiking INs in rat prefrontal neocortex have inwardly rectifying EPSCs, suggesting the presence of CP-AMPA receptors. The existence of CP-AMPA receptors in Pvalb-positive INs in the prefrontal neocortex was confirmed by Tao et al. (2013), who showed a pronounced inward rectification of evoked EPSCs in adult mice.

It has recently been suggested that CP-AMPA receptor expression in INs of the hippocampus reflects the developmental origin of the cells, and may be restricted to those derived from the medial ganglionic eminence (MGE) (Matta et al., 2013). Of note, fate-mapping studies in the neocortex have shown that both Pvalb-positive- and Sst-positive INs originate from the MGE (Wonders and Anderson, 2006, Kessarlis et al., 2014), albeit primarily from ventral and dorsal aspects, respectively (Fogarty et al., 2007, Wonders et al., 2008). Thus, as both L5 BCs and MCs may derive from MGE progenitors, our findings that these two IN types have different AMPA receptor subtypes at their excitatory inputs appears at odds with the picture emerging from the hippocampus. However, it is important to note that gene expression profiling has revealed considerable molecular heterogeneity between the dorsal and ventral MGE (Wonders et al., 2008). As pointed out by (Matta et al., 2013), a purely origin-dependent rule for the expression of CP- versus CI-AMPA receptors is probably too

simplistic, as individual INs have been demonstrated to express CP- and CI-AMPARs at synapses innervated by distinct afferent inputs (Toth and McBain, 1998).

In many cell types, the expression of CP-AMPARs is developmentally regulated. Unfortunately no clear patterns emerge from the literature, with different cell types and different brain regions exhibiting different developmental profiles for CP-AMPARs. Although many studies suggested a developmental decrease in CP-AMPAR expression (Kumar et al., 2002, Shin and Lu, 2005, Osswald et al., 2007, Soto et al., 2007), others have shown expression fluctuating with age (Wang and Gao, 2010). Most relevant to our work, CP-AMPAR expression in Pvalb-positive layer-2/3 INs of mouse visual neocortex was recently shown to increase at P31-P34 compared to P17-19 (Lu et al., 2014). Our experiments were carried out using tissue from 12- to 21-day-old mice. Although this age range spans eye opening at postnatal day 14 — a key developmental milestone for visual neocortex — we found no evidence for developmental changes in BC CP-AMPAR expression.

Functional implications in health and disease

What is the functional significance of differential and synapse-specific CP-AMPAR expression? In the local circuit, MCs and BCs may act as high- and low-pass filters respectively (Blackman et al., 2013): the strong facilitation of excitatory inputs onto MCs enables delayed-onset feedback inhibition (Silberberg and Markram, 2007), whereas the short-term depressing excitatory inputs onto BCs ensure they provide early-onset feed-forward inhibition of PCs (Kawaguchi and Kubota, 1997, Buchanan et al., 2012). This rapid BC-mediated feedforward inhibition act perisomatically on principal neurons such as PCs, to shorten their integrative time window for excitation (Pouille and Scanziani, 2001, Mittmann et al., 2005). In

addition, we found that PC-BC synaptic currents decayed faster than PC-PC and PC-MC connections. Our dynamic clamp experiments confirmed the computer model prediction that rapidly decaying CP-AMPA synaptic currents result in shorter AP latency and sharper response duration in BCs compared to the slower CI-AMPA currents that were characteristic of excitatory inputs to MCs. These findings thus suggest that the specific expression of fast CP-AMPA receptors at PC-BC synapses helps temporally sharpen BC-mediated early inhibition of PCs, to further tighten the integration time window in PCs (Pouille and Scanziani, 2001, Mittmann et al., 2005). These results are in general agreement with a body of literature showing that excitatory inputs onto BCs tend to have faster kinetics than at onto principal neurons (Geiger, Roth et al. 1999).

Although the difference in kinetics of the two excitatory input types onto BCs and MCs may arise from the differential expression of CP-AMPA receptors, other factors — such as subunit composition, auxiliary proteins, glutamate concentration waveform, and receptor splice variants (Lomeli et al., 1994, Koike et al., 2000, Cathala et al., 2005, Milstein et al., 2007, Kato et al., 2010, Jackson et al., 2011) — are known to determine channel kinetics too, and are furthermore likely to differ between IN types (Tao et al., 2013). In addition, we have previously shown that membrane time constants are faster for BCs than for MCs (Buchanan et al., 2012), which also contributes to making BC responses relatively faster. We thus do not argue that inputs to BCs necessarily decay faster solely because they have CP-AMPA receptors, only that the faster decay is correlated with this specific synapse type.

Calcium influx can occur via NMDARs, CP-AMPA receptors or voltage-gated calcium channels. Previous work has shown that synapses onto cells that express CP-AMPA receptors tend to express few NMDARs and exhibit EPSCs with small NMDAR-

mediated components, while those on cells with non-rectifying EPSCs mediated by CI-AMPA receptors tend to exhibit substantial NMDAR-mediated currents (Angulo et al., 1999, Lei and McBain, 2002, Lamsa et al., 2007a, Hull et al., 2009, Wang and Gao, 2010, Scheuss and Bonhoeffer, 2014). Our findings are in agreement with these results and demonstrate that CP-AMPA-containing PC-BC synapses express less NMDAR-mediated current relative to AMPA current, as compared to PC-PC and PC-MC connections, which have CI-AMPA receptors. We also show, however, that the NMDAR-mediated current is by no means absent at PC-BC connections — it is just small relative to the large CP-AMPA-mediated conductance.

Although one might imagine that the differential prevalence of NMDARs and CP-AMPA receptors simply endows different cell types with alternative routes of calcium entry, it may not be this simple. For example, in supragranular fast-spiking Pvalb-positive INs of the mouse, calcium may enter via both routes, with CP-AMPA receptors giving rise to a fast calcium influx and causing depolarization that facilitates an additional, slower calcium influx following NMDAR activation (Goldberg et al., 2003b). Of note, (Goldberg et al., 2004) found that synaptically driven calcium elevations in MCs of the visual and somatosensory cortices of mice — which might be expected to rely on NMDARs — were dependent on AMPA-mediated depolarization and on activation of T-type calcium channels and did in fact not result from activation of NMDARs.

Differences in CP-AMPA receptors, NMDARs, and calcium buffering proteins may also underlie cell-type-specific forms of long-term plasticity. For example, CP-AMPA receptors elicit NMDAR-independent anti-Hebbian LTP at excitatory inputs onto hippocampal INs (Kullmann and Lamsa, 2007, Oren et al., 2009, Nissen et al., 2010, Szabo et al., 2012). The differential expression of CP-AMPA receptors among neocortical

INs suggests the existence of specific plasticity rules at PC-BC and PC-MC synapses. Such differential plasticity of IN excitatory inputs would have important repercussions for information storage in neocortical microcircuits (Lamsa et al., 2010). Future work is needed to investigate this possibility.

Dendritic spines serve as biochemical compartments in spiny neurons (Sjöström et al., 2008). BCs do not generally have many dendritic spines — indeed, spines are found at ~7-fold higher density in MCs than in BCs (Kawaguchi et al., 2006). BCs, however, express the slow calcium-binding protein Pvalb (Hof et al., 1999), which contributes to their high endogenous calcium-buffering capacity (Lee et al., 2000, Goldberg et al., 2003a, Aponte et al., 2008). This buffering has been shown to compartmentalize dendritic calcium signals in BCs while leaving fast CP-AMPA-mediated calcium transients relatively unaffected locally (Goldberg et al., 2003a, Aponte et al., 2008). BCs might thus additionally need CP-AMPA receptors together with the Pvalb calcium buffer to achieve a degree of calcium compartmentalization in the absence of dendritic spines.

In summary, we propose that the synapse-specific CP-AMPA expression may be a general organizational principle of local circuits, not just in neocortex, but also in other brain regions where BCs mediate early-onset inhibition (Blackman et al., 2013). Our findings are important for our understanding of brain functioning not just in health but also in disease, since the disordered regulation of CP-AMPA receptors has been associated with a wide range of neurological conditions, such as stroke, epilepsy, and neurodegeneration (Cull-Candy et al., 2006, Kwak and Weiss, 2006). In particular, several early studies suggested that CP-AMPA receptors contribute to excitotoxicity and cell death (reviewed in Wright and Vissel, 2012). In this view, known as the GluA2 hypothesis, a pathological switch to the expression of CP-

AMPARs following neurological insult may enhance glutamate toxicity because of elevated calcium influx (Pellegrini-Giampietro et al., 1997). Although much additional work is needed to investigate the potential roles of CP-AMPARs in long-term plasticity and in different disease states, our study offers a novel perspective on CP-AMPARs by highlighting just how tightly regulated their synapse-specific expression is in neocortex.

Materials and methods

Animals

Experiments were performed using tissue from mice aged between postnatal days 12 and 21 (P12-21). Most recordings were from C57BL/6 wild-type mice (WT). To target MCs genetically, we employed the GIN mouse line (Jackson Labs 3718, Oliva et al., 2000). To target BCs genetically, we used the G42 mouse line (Jackson Labs 7677, Chattopadhyaya et al., 2004).

Immunolabeling

P21 WT mice were anesthetized with isoflurane and transcardially perfused with 0.1 M PBS (pH 7.4) followed by 4% paraformaldehyde. Brains were removed and postfixed overnight in 4% paraformaldehyde and transferred to 10% sucrose (wt/vol). Brains were dissected and 40- μ m-thick visual neocortex slices were cut and collected in PBS. Slices were incubated for 90 min in 20% normal goat serum (NGS) (vol/vol), 1% bovine serum albumin (BSA) (wt/vol) and 0.5% Triton (vol/vol). Slices were then incubated overnight at 4°C with the primary antibodies (mouse anti-Pvalb Swant 235 at 1:500, rat anti-Sst Millipore MAB354 at 1:100, and rabbit anti-GluA2 Frontier Institute GluR2C-Rb-Af1050 at 1:200) in a carrier solution containing 2%

NGS, 1% BSA and 0.5% Triton. Slices were washed in carrier solution and incubated 1 h at room temperature with the secondary antibodies (1:250). Secondary antibodies were as follows: Alexa Fluor 488 Goat Anti-Mouse IgG Jackson Immuno Research 115-545-062, Alexa Fluor 647 Goat Anti-Rabbit IgG Jackson Immuno Research 111-175-144, Alexa Fluor 555 Goat Anti-Rat IgG Life Technologies A-21434 and Alexa Fluor 488 Goat Anti-Rabbit IgG Life Technologies A-11008. Slices were again washed three times, incubated in DAPI (1:1000) at room temperature for 10 min and washed in PBS for 15 min before being mounted using anti-Fade gold (Invitrogen P36930) and kept in the dark at 4°C until imaging. Primary and secondary antibodies were initially tested for optimal dilution, with reference to previously published studies (Shimuta et al., 2001, Fukaya et al., 2006, Xu et al., 2006, Gonchar et al., 2007, Cammalleri et al., 2009, Antonucci et al., 2012, Leon-Espinosa et al., 2012, Massi et al., 2012, Huang et al., 2013). To avoid fluorescence crosstalk, fluorophores were imaged sequentially using a confocal microscope (Leica SPE).

Analysis of antibody labeling was performed manually using Fiji (Schindelin et al., 2012). In each individual image stack, layer 5 boundaries were identified by the presence of labeled PCs in the GluA2 channel. To quantify fluorescence intensity across labeled cells, the mean gray value in selected regions of interest (ROIs; ~3 µm diameter) centered on the brightest regions of the cell body was measured. ROIs of the same area were used to determine the average mean grey background (minimum of 15 values for each stack) and subtracted from all measurements. The GluA2 labeling in PCs was used to normalize the GluA2 intensity across slices and animals.

Acute slice preparation

Mice were anesthetized with isoflurane and decapitated once the hind-limb withdrawal reflex was lost. As previously described (Sjöström et al., 2001, Buchanan et al., 2012), the brain was rapidly removed and placed in $< 4^{\circ}\text{C}$ artificial cerebrospinal fluid (ACSF, containing in mM: 125 NaCl, 2.5 KCl; 1 MgCl_2 ; 1.25 NaH_2PO_4 ; 2 CaCl_2 ; 26 NaHCO_3 ; 25 D-glucose and bubbled with 95% O_2 / 5% CO_2 , adjusted to 338 mOsm with glucose). Three-hundred-micron-thick near-coronal slices were cut from visual neocortex with a Leica VT1200S or a Campden Instruments 5000mz-2 vibratome. Slices were heated to 32°C for ~ 15 min and were subsequently left to cool to room temperature for > 1 hour before being transferred to the recording chamber. To improve slice quality, dissection was in some cases carried out with partial replacement of Na^+ and with elevated Mg^{2+} concentration, using a solution containing (in mM): 87 NaCl, 75 sucrose, 2.5 KCl, 7 MgSO_4 , 1.25 NaH_2PO_4 , 0.5 CaCl_2 , 26 NaHCO_3 , and 25 D-glucose.

Electrophysiology

General electrophysiological methods

Neurons were patched with infrared video Dodt contrast using 40x objectives and customized microscopes (SliceScope, Scientifica Ltd). The medial side of primary visual neocortex was targeted based on the presence of a granular layer 4. To target MCs genetically, we used slices from the GIN mouse line (Jackson Labs 3718, Oliva et al., 2000), while BCs were targeted genetically using the G42 mouse line (Jackson Labs 7677, Chattopadhyaya et al., 2004). BCs and MCs were most often targeted by the rounded non-pyramidal appearance of somata in slices from C57BL/6 wild-type mice. L5 PCs were targeted by their large pyramidal somata and

characteristic thick apical dendrite. IN cell identity was always verified *post hoc* by manual reconstruction and morphometry (see **Figure 3.2** and 'Morphological classification of cells' below). All recordings were in L5, as determined by the presence of the conspicuously large somata of L5 PCs.

Whole-cell recordings were obtained using BVC-700A (Dagan Corporation, Minneapolis, MN) or MultiClamp 700B amplifiers (Molecular Devices, Sunnyvale, CA). Voltage and current signals were filtered at 4-10 kHz and acquired at 10-20 kHz using National Instrument PCI-6229 boards and custom software (Sjöström et al., 2001) running in Igor Pro (v. 6.36, WaveMetrics Inc., Lake Oswego, OR). Patch pipettes were pulled from medium-wall capillaries using a Sutter Instruments P-97 or P-1000 electrode puller.

Paired recordings

Presynaptic PCs were patched with pipettes (4-6 M Ω) filled with a gluconate-based current-clamp solution containing (in mM): 5 KCl; 115 K-gluconate; 10 K-HEPES; 4 Mg-ATP; 0.3 Na-GTP; 10 Na₂-phosphocreatine; 0.02-0.04 Alexa Fluor 594, adjusted to pH 7.2-7.4 with KOH and to 310 mOsm with sucrose. Postsynaptic cells were patched with a cesium-based voltage-clamp solution containing (in mM): 100 Cs-gluconate; 5 CsCl; 10 HEPES; 4 Mg-ATP; 0.3 Na-GTP; 10 Na₂-phosphocreatine; 8 NaCl; 5 QX-314-Cl; 5 TEA-Cl; 0.02 Alexa Fluor 594; 0.1 spermine tetrahydrochloride, adjusted to pH 7.2-7.4 with CsOH and to 310 mOsm with sucrose. In some recordings, the internal solution included 0.1% w/v biocytin. When specified, 200 μ M Nasp (Santa Cruz Biotechnology) or 200 μ M DL-AP5 (Sigma) was bath applied. Because neocortical connectivity is sparse (Song et al., 2005), we used quadruple recordings to rapidly find synaptically neuronal pairs (Sjöström et al., 2001, 2003). To assess connectivity, five APs were elicited at 30 Hz

in the presynaptic cell every 10-15 seconds by 5-ms-long ~1.3-nA current injections, and 10-20 traces were averaged. In rectification experiments, postsynaptic cells were clamped for 6-10 seconds at potentials ranging from -100 to +50 mV while evoking 2-5 APs at 30 Hz in the presynaptic PC. Each voltage step was repeated 6-20 times every 10-15 seconds. With Nasp^m wash-in, the postsynaptic cell was held at -80 mV to minimize blockade by intracellular spermine. In experiments measuring synaptic current decay time constants (**Figure 3.6A**), we verified that we did not have spurious differences in animal age or perfusion temperature that could potentially explain the differences in decay kinetics (age in postnatal days, PCs: 14 ± 0.8 ; BCs: 13 ± 0.2 ; MCs: 14 ± 0.6 ; ANOVA $p = 0.25$; perfusion temperature in °C, PCs: 32 ± 0.1 ; BCs: 32 ± 0.05 ; MCs: 32 ± 0.1 ; ANOVA $p = 0.82$; n numbers as in **Figure 3.6A**).

mEPSC recordings

We recorded mEPSCs from BCs in the presence of 20 μ M D-AP5, 20 μ M SR-95531, 1 μ M CGP 54626 and 0.5 μ M TTX-citrate. To block potassium channels and improve the voltage clamp, ACSF was supplemented with 4 mM TEA-Cl in some recordings. Patch pipettes (3-6 M Ω) were filled with the gluconate current-clamp solution (above) or a voltage-clamp solution containing (in mM): 100 Cs-gluconate; 5 CsCl; 10 HEPES; 2 Mg-ATP; 0.3 Na-GTP; 10 Na₂-phosphocreatine; 8 NaCl; 5 QX-314-Cl; 5 TEA-Cl; 20 K₂-ATP; 0.2 EGTA; 0.02 Alexa Fluor 594, adjusted to pH 7.2-7.4 with CsOH and to 310 mOsm with sucrose. The internal solution also included 0.1% w/v biocytin in some cases. High K₂ATP was present to buffer endogenous spermine. In some recordings, 0.5 mM spermine tetrahydrochloride was added to yield a free internal spermine concentration of ~40 μ M (Rozov et al., 2012). For rectification measurements, we used the voltage-clamp internal solution and

mEPSCs were recorded at -60 mV and $+60$ mV. With Naspmm wash-in, we used current-clamp internal solution, and BCs were voltage-clamped at -60 mV throughout. The use of current-clamp solution enabled us to determine intrinsic cellular properties: 500 ms-long current steps ranging from -200 to $+700$ pA were injected at 40 pA increments. Here, cells were only included if resting membrane potential was -65 mV or less.

Dynamic clamp

Conductance clamp experiments were implemented using a second electrophysiology rig computer as a slave, similar to what has previously been described (Kemenes et al., 2011, Yang et al., 2015). To simulate the synaptic current $i_{\text{syn}}(t) = g_{\text{syn}}(t) \cdot (E_{\text{rev}} - V_m(t))$ in real-time, the slave computer ran a custom script in Igor Pro that read two analogue-to-digital inputs (the g_{syn} command from the rig computer and the V_m voltage reading from the amplifier) and wrote one digital-to-analogue output (the i_{syn} current command to the amplifier) of a National Instruments PCI-6229 board at maximal non-synchronized speed using an infinite loop. With NIDAQTools MX (v. 1.06, WaveMetrics), Igor Pro (v. 6.36, WaveMetrics), 32-bit Windows 7 (Microsoft), and a SuperLogics Rack Mount Industrial PC model SL-4U-CL-LLQ35-HA (2.66 GHz Core 2 Quad Processor, 1333 MHz front-side bus), we reliably obtained steady sampling rates close to 30 kHz, effectively achieving real-time dynamic clamp. The conductance waveform $g_{\text{syn}}(t)$ was determined by the master computer and was defined as a double exponential (compare ‘Computer modeling’ below) with fast time constant $\tau_{\text{rise}} = 1.4$ ms and a slow time constant τ_{decay} of either 3 ms or 5 ms, which was close to the synaptic current kinetics we found in BCs and MCs (**Table 3.1**). In reality, AMPAR synaptic conductances rise and decay faster than this; dendritic cable filtering made our time constant measurements

overestimations. However, as we injected the conductances into the soma, these filtered kinetics were more realistic as they accounted for dendritic cable filtering.

BCs were patched as described for paired recordings. We systematically altered the peak conductance, g_{syn} , according to a bisection algorithm to find the first and second rheobase conductance values, g_{rheo1} and g_{rheo2} , which we defined as the lowest conductance values for which one and two spikes, respectively, were obtained (compare 'Computer modeling'). This procedure was thus repeated once each for the two time constant values, $\tau_2 = 3$ ms and $\tau_2 = 5$ ms, where the former value emulated a BC excitatory input while the latter value simulated a slow-decaying excitatory input to an MC, but in the same recorded BC. Our experimental design removed other contributing factors such as filtering by the membrane time constant, τ_M , or differences in short-term plasticity (see Buchanan et al., 2012), and focused solely on the role of excitatory synaptic input kinetics. Working with rheobase conductance values enabled across-cell comparisons, as well as comparisons with the computer model (see **Figure 3.7** and 'Computer modeling' below). With $\tau_2 = 3$ ms as for a CP-AMPA-mediated input to a BC, we obtained $g_{\text{rheo1}} = 1 \pm 0.2$ nS and $g_{\text{rheo2}} = 3.7 \pm 0.9$ nS ($n = 5$ cells). With $\tau_2 = 5$ ms as for a CI-AMPA-mediated input to an MC, we obtained $g_{\text{rheo1}} = 0.8 \pm 0.1$ nS and $g_{\text{rheo2}} = 2 \pm 0.5$ nS (the same $n = 5$ cells). Note that in **Figure 3.7Bii**, we opted to sidestep the electrophysiologist's sign convention that amplifier current injections are represented as upward positive deflections, instead illustrating these as downward negative deflections to simplify comparison with the computer simulation in **Figure 3.7Aii**.

Analysis of electrophysiological data

Stability criteria were applied to all recordings: membrane potential was not

allowed to vary by more than 8 mV, input resistance not by more than 30%, and temperature had to remain within 31-33°C throughout recordings. If not, recordings were discarded or truncated. Experiments with unstable baseline, as assessed using a *t*-test of Pearson's *r* at the $p < 0.05$ significance level, were discarded. Input resistance was measured by a 250-ms-long test pulse of -50 pA in current clamp, or -25 mV in voltage clamp.

In paired recordings, the AMPA current was measured at a 1-ms-long window positioned at the peak of the first EPSC in a train, while the NMDA current was measured 20 ms later. Rectification was defined as the ratio of peak AMPA current at $+40$ mV over AMPA current at -40 mV ($RI_{+40/-40}$). Current at $+40$ mV and -40 mV was interpolated from a straight line between the currents measured at $+35$ and $+50$ mV, and -60 and -30 mV, respectively. To average across experiments, current values were normalized to the value at -60 mV. To quantify the effect of Naspm on PC-BC connections, we determined the ratio of the amplitude of the first EPSC in a train during Naspm wash-in over that during the baseline. Liquid junction potential (10 mV) was accounted for in the off-line analysis.

Analysis of mEPSCs was performed using NeuroMatic 2.8 (<http://www.neuromatic.thinkrandom.com/>) running in Igor Pro. For detection, records were digitally low-pass Butterworth filtered at 2 kHz, and events were detected using threshold crossing of 2.5 standard deviations over background noise (Kudoh and Taguchi, 2002), or 8.0 ± 0.4 pA ($n = 23$). All automatically detected events were individually visually inspected and manually triaged. To limit dendritic filtering, analysis was restricted to events with 20-80% rise times faster than 0.4 ms. To reduce error in estimating the rise time and charge of noisy mEPSCs, individual events were fitted with an empirical equation and measures were taken from the fit

waveform (Bekkers and Stevens, 1996, Bekkers and Clements, 1999). We calculated mEPSC rectification as the ratio of the summed mEPSC charge, i.e. the sum of mEPSC charge from equal lengths of recordings at positive and negative voltages; $RI_{+60/-60, \text{ sum}}$. The effect of Naspm on summed mEPSC charge was assessed by comparing 100-ms-long epochs at the beginning of the recording and 20 min after Naspm wash-in. RI calculation was adjusted for liquid junction potential (11 mV).

Optical methods

Two-photon imaging

Two-photon excitation was achieved using a Chameleon XR (Coherent, Santa Clara, CA, USA) or MaiTai BB (Spectraphysics, Santa Clara, CA, USA) Ti:Sa laser, tuned to 820 nm for Alexa 594 and 880-900 nm for eGFP. Two-photon microscopes were custom-built in house (for details, see Buchanan et al., 2012). The two-photon microscope design was based on Scientifica's SliceScope, Hamamatsu R3896 bialkali photomultipliers, and Cambridge Technologies 6215H 3-mm or Thorlabs GVSM002/M 5-mm galvanometric mirrors. Ti:Sa laser gating was achieved using Thorlabs SH05/SC10 or Uniblitz LS6ZM2/VCM-D1 shutters. Laser power was manually attenuated using a polarizing beam splitter (Thorlabs GL10-B with AHWP05M-980 half-lambda plate) while monitoring output with a PM100A/S121C power meter (Thorlabs). Fluorescence was collected with an FF665 dichroic and an FF01-680/SP-25 emitter from Semrock. Red versus green fluorescence was selected with a t565lpxr (Chroma) or a FF560-Di01 dichroic (Semrock), a ET630/75m (Chroma) red emitter, and a ET525/50m (Chroma) or a FF01-525/45-25 (Semrock) green emitter. Imaging data was acquired using customized variants of

ScanImage v3.5-3.7 (Pologruto et al., 2003) running in Matlab (The MathWorks, Natick, MA, USA) via PCI-6110 boards (National Instruments, Austin, TX).

Morphological classification of cells

After recordings, morphologies were acquired with ScanImage. The preparation was scanned at 2 Hz frame rate (2 ms/line, 512 by 512 pixels) and 3 frames were averaged for each optical section. Neurons were manually reconstructed from 2PLSM imaging stacks using Neuromantic (<http://www.reading.ac.uk/neuromantic/>) as previously described (Blackman et al., 2014). Morphological reconstructions were carried out blinded to electrophysiology results. Boundaries of neocortical layers (**Figure 3.2B, D**) were identified in laser-scanning Dodt-contrast image stacks acquired simultaneously with the 3D 2PLSM fluorescence stacks. L5 was distinguished by the presence of prominent L5 PCs with large somata, L4 by a slightly darker granular band, and layer 1 by a conspicuous absence of cell bodies. Morphologies were quantified using in-house custom software (Buchanan et al., 2012) running in Igor Pro (v. 6.36, WaveMetrics Inc., Lake Oswego, OR), as described below.

To enable the creation of density maps (**Figure 3.2B**), morphologies were first rotated a small amount around the soma to ensure that the pial surface was in “up” position, then they were centered on the L4/L5 boundary, after which the density map was calculated. Each compartment was represented by a two-dimensional Gaussian with amplitude proportional to compartment length and a fixed sigma set to 25 μm . Maps were created by summing all Gaussians for each reconstruction, mirrored to create symmetry, normalizing to permit averaging across reconstructions, gamma corrected to improve visualization of weak densities, assigned a color lookup

table depending on axonal or dendritic identity, and finally merged by the logical OR operation.

Convex hulls of individual reconstructions were constructed by 2D projecting axonal and dendritic arbors separately and then applying a Jarvis walk to each projection. Ensemble convex hulls (**Figure 3.2B**) are convex hulls of all convex hulls, including mirror-image convex hulls, to enable comparison of ensemble hulls with density maps.

For the Sholl analysis (**Figure 3.2C**), reconstructions were first re-centered on their somata and converted to radial coordinates. In 6.5- μm steps, the number of compartments straddling circles of increasing radii was counted (Sholl, 1953). Ensemble Sholl diagrams were averaged without normalization.

BCs were clustered automatically and independently into type 1 and type 2 (**Figure 3.8**) using agglomerative single-linkage hierarchical clustering software custom-made in Igor Pro, with the squared Euclidian distance as linkage metric. BCs were clustered based on the percentage amount of the axon convex hull that was above the boundary between L2/3 and L4. We used this measure as it provided a degree of normalization across reconstructions manually traced by different people; some individuals added a lot of detail, whereas others did not, and this measure was robust in the face of such variability. We used a 25% best-cut selection criterion to assess the number of clusters (Everitt et al., 2011). The Igor Pro built-in fuzzy *c*-means clustering algorithm preset to find $c = 2$ clusters classified BCs exactly the same way.

AMPA uncaging

NPEC-AMPA (200 μM) dissolved in ACSF (1 mM) supplemented with 0.2 μM TTX-citrate and 20 mM HEPES was locally puffed using a patch pipette (4-6 M Ω).

Photolysis was achieved with a violet TTL-gated solid-state laser (405 nm, 150 mW, MonoPower-405-150-MM-TEC, Alphas GmbH, Göttingen, Germany). Photomultipliers were protected from the violet laser using a BLP01-488R-25 long-pass filter (Semrock). The violet laser was always at maximum power as this setting gave the most reproducible pulses in separate laser tests. Power was instead attenuated with a polarizing beam splitter (Thorlabs WPMH05M-405 and GL10-A); laser power at the objective back aperture was measured to ~8 mW with a PM100A/S121C power meter (Thorlabs). A single pulse of 0.1-2 ms was used to release AMPA during each voltage step (-100 mV to +50 mV) — the slow photorelease of AMPA is a property of the NPEC cage (Palma-Cerda et al., 2012) (**Table 3.1**). Each voltage step lasted 6-10 s and the inter-step interval was 15 s. To assess the effect of NaspM bath application, cells were held at -80 mV while uncaging AMPA every 15 s. In separate experiments, the AMPAR-specific blocker NBQX was bath-applied (10 μ M) to verify that uncaging-evoked currents were attributable solely to AMPAR activation. In experiments where we measured the kinetics of uncaging-evoked responses (**Figure 3.6B**), we verified that we did not have spurious differences in animal age or perfusion temperature that could potentially explain the findings (age in postnatal days, PCs: 13 ± 0.4 ; BCs: 13 ± 0.3 ; MCs: 14 ± 0.2 ; ANOVA $p = 0.85$; perfusion temperature in $^{\circ}$ C, PCs: 32 ± 0.04 ; BCs: 32 ± 0.06 ; MCs: 32 ± 0.04 ; ANOVA $p = 0.47$; n numbers as in **Figure 3.6B**). Laser pulse durations were also indistinguishable (PCs: 1.0 ± 0.1 ms; BCs: 1.0 ± 0.1 ms; MCs: 1 ± 0.2 , Kruskal-Wallis $p = 0.4$), as were the uncaging-evoked response amplitudes (PCs: -53 ± 9 pA; BCs: -61 ± 9 pA; MCs: -78 ± 12 pA, ANOVA $p = 0.3$), suggesting that accidental differences in uncaging pulse properties could not explain our findings.

Computer modeling

A BC was modeled as a simplistic leaky integrate-and-fire point neuron with a single double-exponential synaptic input (Dayan and Abbott, 2001). Differential equations were numerically integrated in Igor Pro (v. 6.36, WaveMetrics Inc., Lake Oswego, OR) using the forward Euler method with a time step of $\Delta t = 0.1$ ms. The model was hand-tuned approximately to biologically measured parameters (**Table 3.1** and **Table 3.2**), with membrane time constant $\tau_M = 10$ ms, cell reversal potential $E_{\text{leak}} = 70$ mV, input resistance $R_{\text{in}} = 160$ M Ω , cell capacitance $C_M = 62.5$ pF (implicit from $\tau_M = R_{\text{in}}C_M$), AP threshold $V_{\text{thres}} = -37$ mV, AP amplitude $V_{\text{peak}} = 20$ mV, AP reset voltage $V_{\text{reset}} = -80$ mV, synaptic reversal potential $E_{\text{rev}} = 0$ mV, and synaptic conductance double-exponential fast time constant $\tau_{\text{rise}} = 1.4$ ms. The synaptic conductance double exponential slow time constant was set to $\tau_{\text{decay}} = 3$ ms to simulate a fast-decaying CP-AMPA-mediated synaptic input, or to $\tau_{\text{decay}} = 5$ ms to simulate an excitatory input of MC type but in a cell body with BC intrinsic properties. The goal of this model was thus not biological realism. Rather, since BCs and MCs also vary with respect to e.g. membrane time constant (Buchanan et al., 2012), our modeling approach aimed to tease apart the specific contribution of rapid AMPAR kinetics to BC response properties, in the absence of other contributing factors such as filtering by τ_M and short-term plasticity.

We defined the first and second rheobase conductance values, g_{rheo1} and g_{rheo2} , as the lowest peak synaptic conductances, g_{syn} , for which one and two spikes, respectively, were obtained. This approximated a condition in which multiple excitatory inputs cooperate to bring a postsynaptic BC just beyond threshold for one and for two APs, which had the additional advantage of providing normalization to

enable comparison with conductance clamp experiments (see ‘Dynamic clamp’ above). We determined g_{rheo1} and g_{rheo2} using a bisection algorithm iterated 15 times. This approach established first and second rheobase conductance values to the second decimal place. For fast CP-AMPA-style synaptic decay kinetics typical of excitatory synapses onto BCs ($\tau_{\text{decay}} = 3$), we obtained $g_{\text{rheo1}} = 13.03$ nS, and $g_{\text{rheo2}} = 22.09$ nS. For relatively slow synaptic decay kinetics characteristic of excitatory inputs to MCs ($\tau_{\text{decay}} = 5$), $g_{\text{rheo1}} = 11.15$ nS, and $g_{\text{rheo2}} = 17.76$ nS.

Statistics

Results are reported as mean \pm SEM. Significance levels $p < 0.05$, $p < 0.01$, and $p < 0.001$ are denoted by *, **, and ***, respectively. Non-significant differences are indicated by ‘n.s.’ Boxplots indicate the median value (middle black line), the 25th and 75th percentiles (box), and the highest and lowest values (whiskers), with the black cross denoting the mean.

Unless otherwise stated, we used Student’s t-test for equal means for all pairwise comparisons. If equality of variances F test gave $p < 0.05$, we employed the unequal variances t-test. Individual data sets were tested using one-sample t-test. For multiple comparisons, pairwise comparisons were carried out if one-way ANOVA permitted this at the $p < 0.05$ significance level. For data that was not normally distributed, however, we instead report outcome of the Kruskal-Wallis test, as stated. Multiple pairwise comparisons were corrected *post hoc* using Bonferroni-Dunn’s method. Non-parametric tests were always used in parallel with parametric tests, and were in agreement with respect to significance, although occasionally gave different significance level. Statistical tests were performed in Igor Pro (v. 6.36, WaveMetrics Inc., Lake Oswego, OR).

Acknowledgements

We thank Arnd Roth, Alanna Watt, Marzieh Zonouzi, and Therese Abrahamsson for help and useful discussions. We thank Rochelin Dalangin, Eric Fineberg, and Xinwen Zhu for assistance with morphological reconstructions.

Additional information

Funding

Funder	Grant reference number	Author
McGill University Integrated Program in Neuroscience	Returning Student Award	Txomin Lalanne
The Research Institute of the McGill University Health Centre	Studentship	Txomin Lalanne
University College London	PhD Student Impact Award	Julia V. Oyrer
Fonds de recherche du Québec - Santé	Postdoctoral Scholarship	Jérôme Maheux
Medical Research Council	Programme MR/J002976/1	Grant Mark Farrant
Medical Research Council	Project MR/J012998/1	Grant Mark Farrant
Wellcome Trust	Programme 086185/Z/08/Z	Grant Mark Farrant
Canada Foundation for Innovation	Leaders Opportunity Fund 28331	P. Jesper Sjöström
Canadian Institutes of Health Research	New Investigator Award 288936	P. Jesper Sjöström
Canadian Institutes of Health Research	Operating Grant 126137	P. Jesper Sjöström
European Union Future Emergent Technologies	Brain-i-Nets 243914	P. Jesper Sjöström
Medical Research Council	Career Development	P. Jesper Sjöström

The funders had no role in study design, data collection and interpretation, or the decision to submit the work for publication. The authors declare no conflicting financial interest.

Author contribution

TL carried out paired recordings, dynamic clamp experiments, and AMPA uncaging experiments. JVO carried out immunolabeling and mEPSC recordings. AM, EG, AC, SB, LH, and JM carried out the bulk of morphological reconstructions. TL and JVO analyzed data with help from MF and PJS. PJS carried out the computer modeling, wrote the in-house data acquisition and analysis software, and designed the dynamic clamp setup. PJS and MF conceived the project and designed experiments together with TL and JVO. TL, JVO, MF, and PJS wrote the manuscript.

Ethics

All procedures conformed to the standards and guidelines set in place by the *UK Animals (Scientific Procedures) Act 1986* and the *Canadian Council on Animal Care*, with appropriate licenses. Mice were anesthetized with isoflurane and sacrificed once the hind-limb withdrawal reflex was lost. Transgenic animals had no abnormal phenotype. Every attempt was made to ensure minimum discomfort to the animals at all times.

Figures

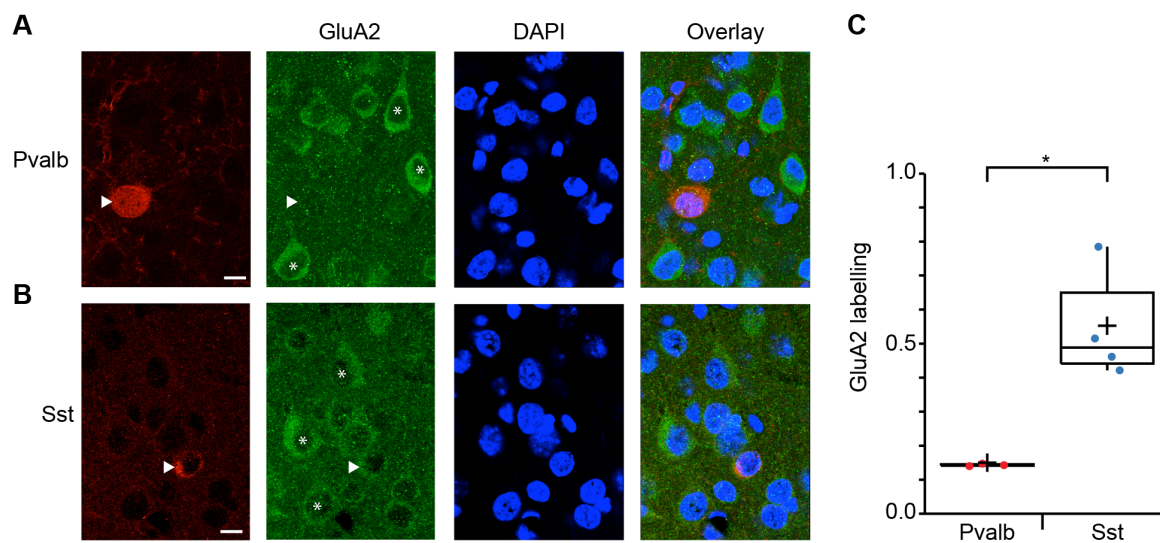


Figure 3.1: Lower GluA2 immunolabeling in Pvalb-positive than in Sst-positive INs

(A) Confocal images of coronal sections of L5 visual neocortex from a P21 WT mouse stained with DAPI and immunolabelled with antibodies against Pvalb and GluA2 (single optical slice). Rightmost image is a composite of the other three. The Pvalb-positive IN (arrowhead) lacks GluA2 labeling. Asterisks indicate PCs labeled for GluA2. Scale bar: 10 μ m.

(B) As in A, but for an Sst-positive IN in an acute slice from another P21 WT mouse. The Sst-positive IN (arrowhead) is positively labeled for GluA2, although less so than in nearby PCs (asterisks).

(C) Boxplot quantifying the significantly lower GluA2 expression in Pvalb-positive compared to Sst-positive INs ($n = 3$ and 4 mice, respectively; see 'Materials and methods').

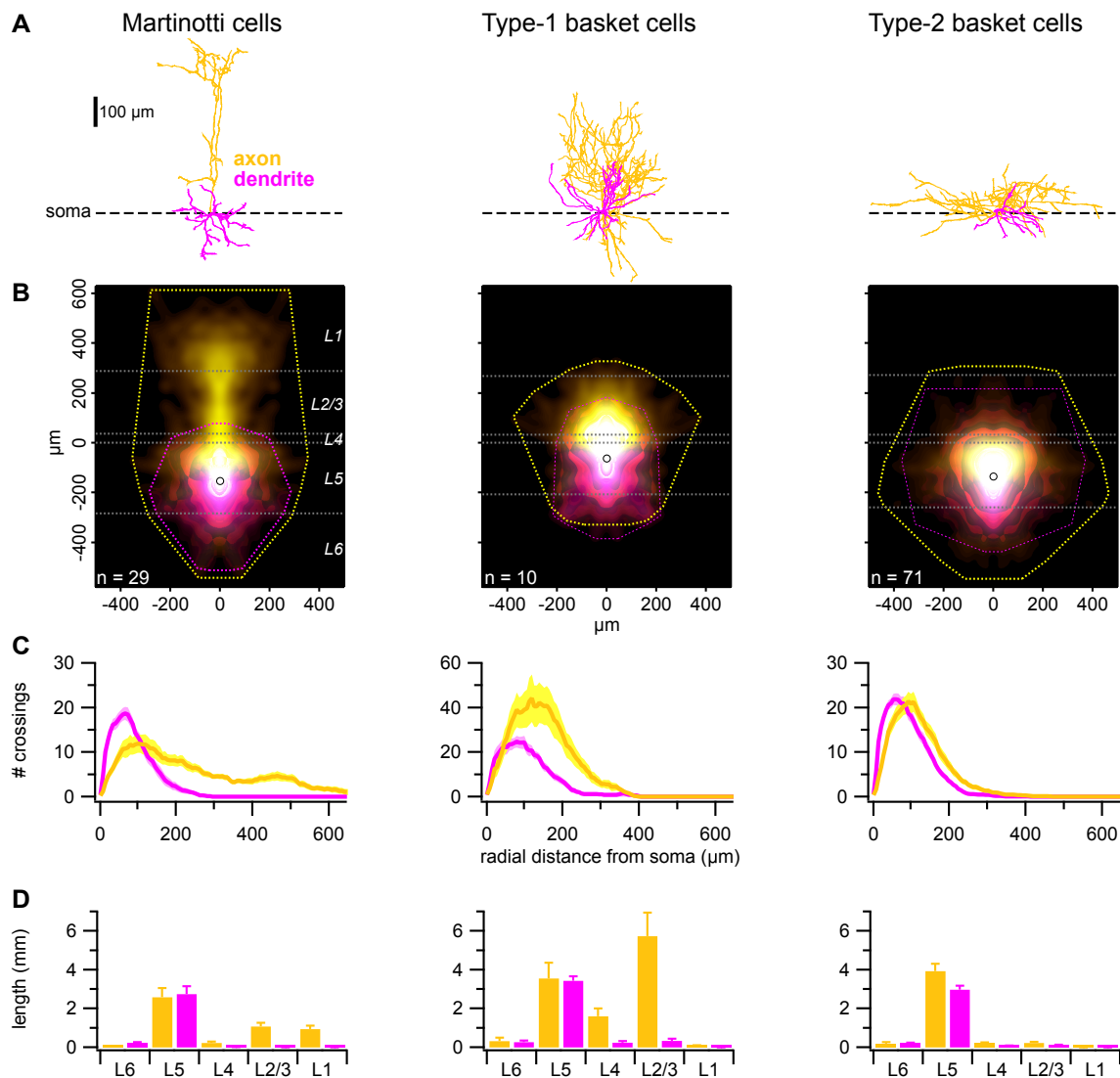


Figure 3.2: Morphology classified recorded INs into MCs and two types of BCs

(A) Sample MC, type-1 and type-2 BC morphologies, aligned on their somata (dashed line).

(B) Ensemble density maps (see ‘Materials and methods’ and Buchanan et al., 2012) of all recorded INs show typical axonal (yellow) and dendritic (magenta) arborisations. Convex hulls (dashed lines) illustrate maximum axonal and dendritic extents. Open circles indicate average position of cell bodies. Horizontal white dashed lines denote the neocortical layer boundaries averaged across cells.

(C) The ensemble Sholl diagrams show the number of axonal (yellow) or dendritic (pink) branches crossing a given radial distance from the soma (Sholl, 1953). The prominent ascending axon of type-1 BCs distinguishes them from the classical type-

2 BCs, whose peak axonal radial density is closer to the soma (Buchanan et al., 2012, Ferreira et al., 2014).

(D) The total length of axonal arbors (yellow) within a neocortical layer distinguished different cell types well, whereas dendritic branching pattern (magenta) was less useful for classification. Axons of type-1 but not of type-2 BCs branched extensively in L2/3 but never reached L1. MC axons, however, consistently reached L1.

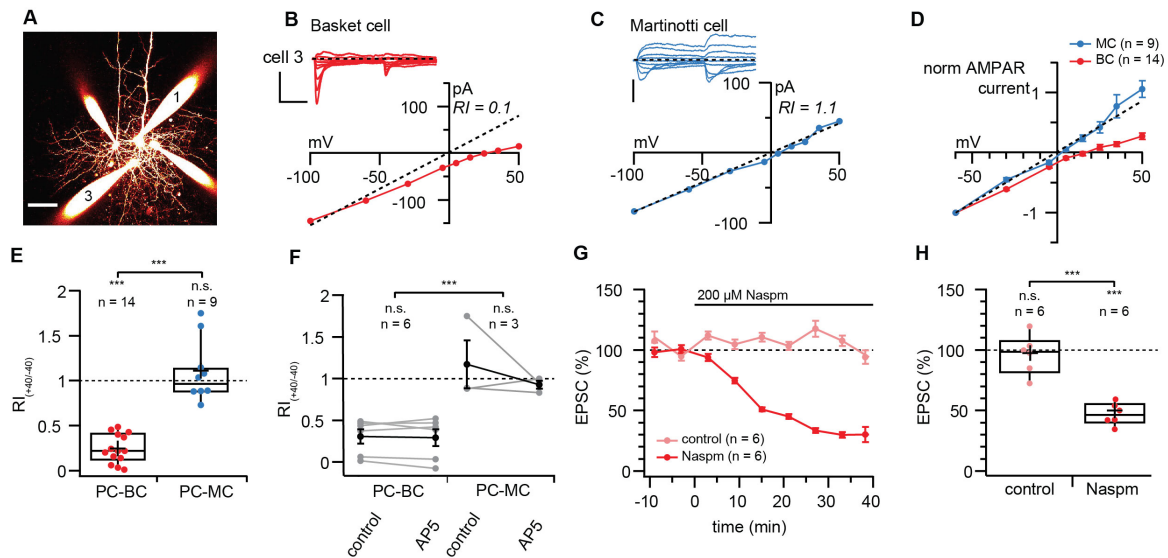


Figure 3.3: Monosynaptic connections from PCs to BCs but not to MCs rectify

(A) 2PLSM maximum intensity projection of a quadruple whole-cell recording in which cell 1 was a PC connected to cell 3, a BC. These cells were identified by morphology and electrophysiology, see ‘Materials and methods’. Scale bar: 50 μm .

(B) Two APs evoked at 30 Hz in PC1 gave rise to short-term depressing synaptic responses in BC3 (inset, average of 10 traces) that rectified at positive membrane potentials. The RI (0.1) was calculated as the ratio of peak synaptic currents at +40 mV and -40 mV, see ‘Materials and methods’. Dashed diagonal line denotes expected IV relationship in the absence of rectification. Scale bars: 10 ms, 100 pA.

(C) As in B, but for a PC-MC connection that characteristically did not show inward rectification. Scale bar: 50 pA.

(D) Normalized and averaged IV curves of PC-BC connections (red) and PC-MC connections (blue) indicated that this difference in outward rectification was specific to synapse type and not a random heterogeneity.

(E) PC-BC synapses (red) were inward rectifying, but PC-MC synapses (blue) were not ($p = 0.35$). The RI of PC-BC pairs was in addition different compared to that of PC-MC connections (Bonferroni corrected). RI in cells recorded from GIN and WT mice were indistinguishable (0.94 ± 0.05 , $n = 3$ vs. 1.2 ± 0.2 , $n = 6$, $p = 0.16$).

(F) In a subset of recordings, we examined whether NMDAR currents biased our CP-AMPA rectification measurements, but we found that AP5 wash-in had no effect on

RI measurements at PC-BC or PC-MC connections (paired two-sample t-tests). As in E, the difference in RI between PC-MC and PC-BC connections was significant.

(G) Ensemble averages show the time course of Nasp^m blockade of PC-BC EPSC (red) compared to stable mock wash-in controls (light red).

(H) While mock wash-in controls were stable ($p = 0.81$ versus 100%), Nasp^m halved PC-BC EPSC amplitude, implying the presence of CP-AMPA_Rs at this connection type.

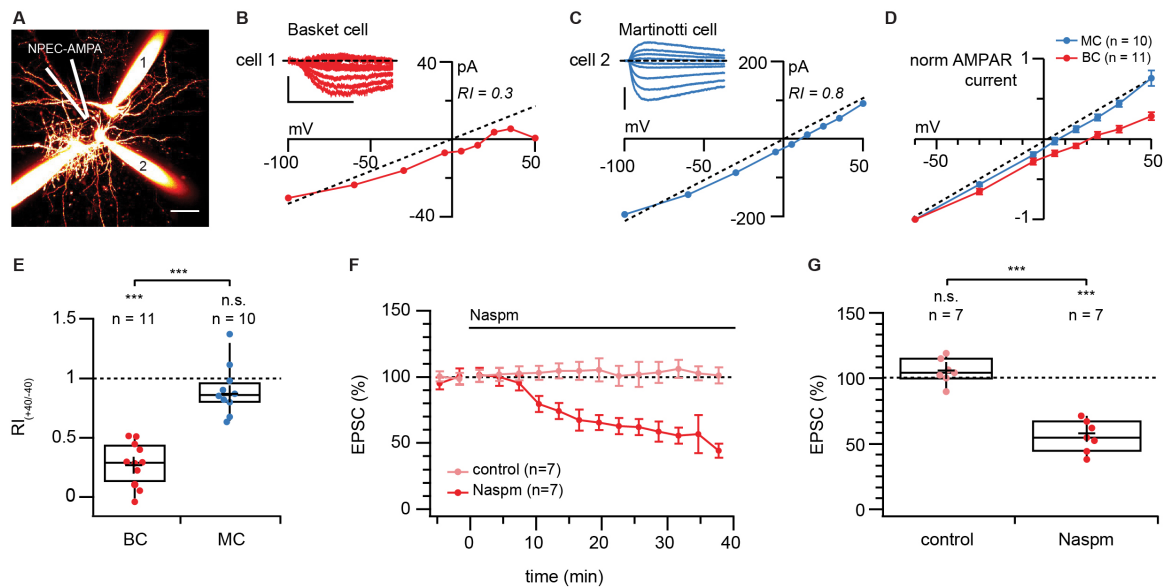


Figure 3.4: AMPA uncaging currents rectify in BCs but not in MCs

(A) 2PLSM maximum intensity projection of a triplet IN recording, with a fourth pipette (white) used for puffing NPEC-AMPA (200 μ M). Cells were morphologically and electrophysiologically identified as BC (cell 1) and MC (cell 2) cells. Scale bar: 50 μ m.

(B) Sub millisecond 405-nm laser pulses elicited AMPAR responses in the BC (cell 1, inset) with slow kinetics — as expected from the NPEC cage (Palma-Cerda et al., 2012) — that rectified at positive membrane potentials, suggesting the presence of CP-AMPA. The RI (0.3) was calculated as the ratio of peak photolysis-evoked currents at +40 mV and at -40 mV ('Materials and methods'). Scale bars: 500 ms, 25 pA.

(C) For the MC recorded in parallel, however, AMPA uncaging responses did not rectify (cell #2, inset). Scale bars: 150 pA.

(D) Normalized and averaged IV curves of AMPA uncaging responses recorded in BCs (red) and in MCs (blue) showed that this difference in inward rectification was specific to cell type, suggesting that CP-AMPA expression is cell-wide in BCs.

(E) NPEC-AMPA photolysis-evoked responses were rectifying in BCs (red) but not in MCs (blue, $p = 0.1$). In addition, the RI measured in BCs was different compared to that recorded in MCs (Bonferroni corrected). RI in cells recorded from GIN and WT mice were indistinguishable (0.90 ± 0.1 , $n = 6$ vs. 0.92 ± 0.1 , $n = 4$, $p = 0.91$).

(F) Ensemble averages show the time course of Nasp^m blockade of AMPA-uncaging-evoked responses (red) compared to stable mock wash-in controls (light red)

(G) While mock wash-in controls were unaffected ($p = 0.21$), Nasp^m decreased NPEC-AMPA photolysis-evoked responses by half, suggesting the widespread presence of CP-AMPA receptors in this cell type.

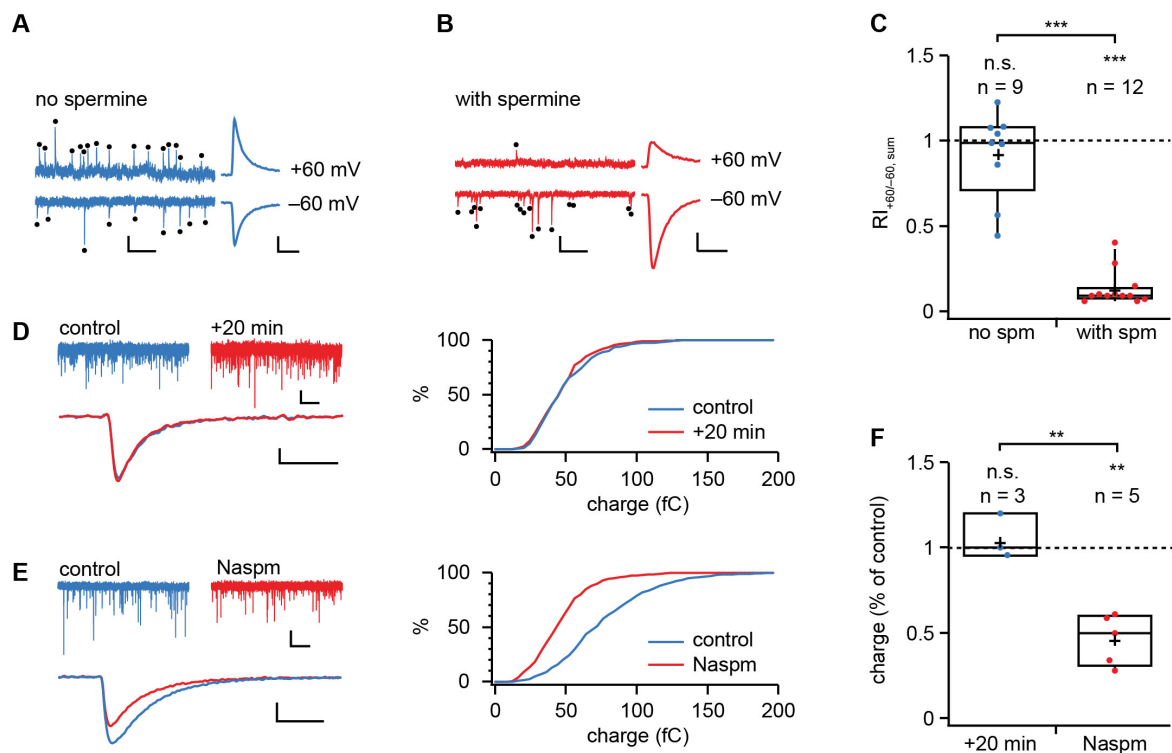


Figure 3.5: Rectification of BC mEPSCs is spermine dependent

(A) Representative BC mEPSCs (black dots) recorded at -60 mV and $+60$ mV using spermine-free internal solution. Scale bars: 100 ms, 50 pA. Right: Average of all mEPSCs at $+60$ mV and count-matched average at -60 mV are of similar absolute amplitudes, suggesting an absence of rectification. Scale bars: 2 ms, 20 pA.

(B) As in A, but for a BC recorded with internal solution supplemented with spermine. Right: Average of all mEPSCs at $+60$ mV is of smaller absolute amplitude than the count-matched average at -60 mV, indicating rectification. Scale bars as in A.

(C) BC mEPSC rectified in the presence (red) but not the absence of spermine (blue, $p = 0.37$ for the comparison to 1), suggesting the presence of CP-AMPA receptors. The RI of mEPSCs was in addition different with compared to without spermine. The rectification index, $RI_{+60/-60, \text{sum}}$, was calculated from summed charge (see 'Materials and methods'). Half of the cells were targeted in the Pvalb-positive G42 mouse line (6/12 for 'with spm' and 5/9 for 'no spm') (Chattopadhyaya et al., 2004).

(D) In this representative control recording at -60 mV, mEPSC charge remained stable for 20 minutes ($p = 0.95$ using Kolmogorov-Smirnov test). Scale bars, top: 500 ms, 20 pA; bottom: 2 ms, 10 pA.

(E) Naspm wash-in reduced mEPSC charge ($p < 0.01$, Kolmogorov-Smirnov), suggesting the presence of CP-AMPARs. Scale bars as in D.

(F) While mEPSC summed charge was unaffected by mock wash-in ($p = 0.56$ for comparison with 100%), bath application of Naspm approximately halved mEPSC summed charge, hinting at a cell-wide presence of CP-AMPARs in BCs. All cells were WT. Mini frequency (12 ± 3 Hz) was typical of BCs (Buchanan et al., 2012).

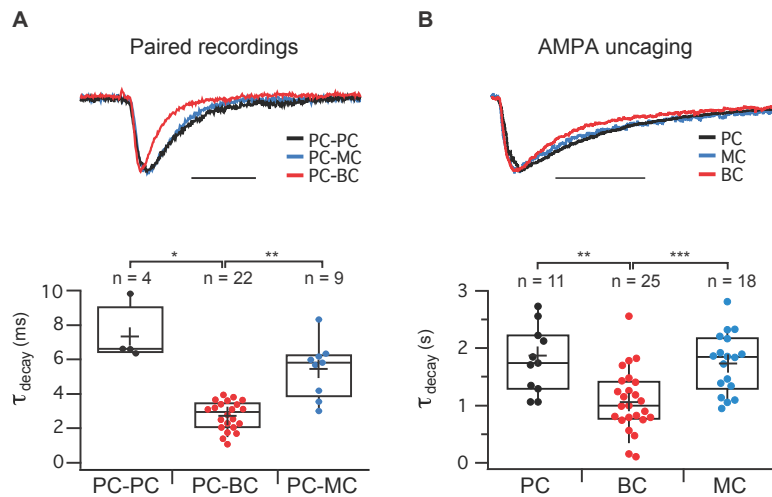


Figure 3.6: AMPAR currents decay faster in BCs than in PCs and MCs

(A) Top: Representative voltage-clamp traces showing faster decay kinetics at a PC-BC synapse (red) than at a PC-PC (black) and a PC-MC connection (blue). Scale bar: 10 ms. Bottom: The decay time constant, τ_{decay} , was faster for PC-BC (red) than for PC-PC (black) and PC-MC (blue) connections. PC-PC and PC-MC connections were indistinguishable with respect to τ_{decay} ($p = 0.09$). PC-BC synapses were measured at -100 mV or at -80 mV, and since decay times at these two voltages were indistinguishable, this data was pooled ($\tau_{\text{decay},-100 \text{ mV}} = 2.8 \pm 0.3 \text{ ms}$, $n = 14$ pairs and $\tau_{\text{decay},-80 \text{ mV}} = 3.2 \pm 0.3 \text{ ms}$, $n = 8$ pairs, $p = 0.22$, data not shown).

(B) Top: Representative voltage-clamp traces showing AMPA-uncaging responses with faster decay kinetics in BCs (red) than in PCs (black) and MCs (blue). Scale bar: 2 s. Bottom: The decay time constant, τ_{decay} , was faster for AMPA uncaging responses in BCs (red) than in PCs (black) and MCs (blue). Data was acquired at either -100 mV or at -80 mV, and was pooled since decay time constants at these two voltages were indistinguishable (BCs: $\tau_{\text{decay},-100 \text{ mV}} = 1.1 \pm 0.2 \text{ s}$, $n = 11$ cells, $\tau_{\text{decay},-80 \text{ mV}} = 1.1 \pm 0.1 \text{ s}$, $n = 14$ cells, $p = 0.9$; MCs: $\tau_{\text{decay},-100 \text{ mV}} = 1.8 \pm 0.1 \text{ s}$, $n = 10$ cells, $\tau_{\text{decay},-80 \text{ mV}} = 1.7 \pm 0.1 \text{ s}$, $n = 8$ cells, $p = 0.8$; PCs: $\tau_{\text{decay},-100 \text{ mV}} = 2.0 \pm 0.3 \text{ s}$, $n = 5$ cells, $\tau_{\text{decay},-80 \text{ mV}} = 1.6 \pm 0.2 \text{ s}$, $n = 6$ cells, $p = 0.2$; data not shown). Uncaging responses recorded in PCs and in MCs were indistinguishable with respect to τ_{decay} ($p = 0.77$).

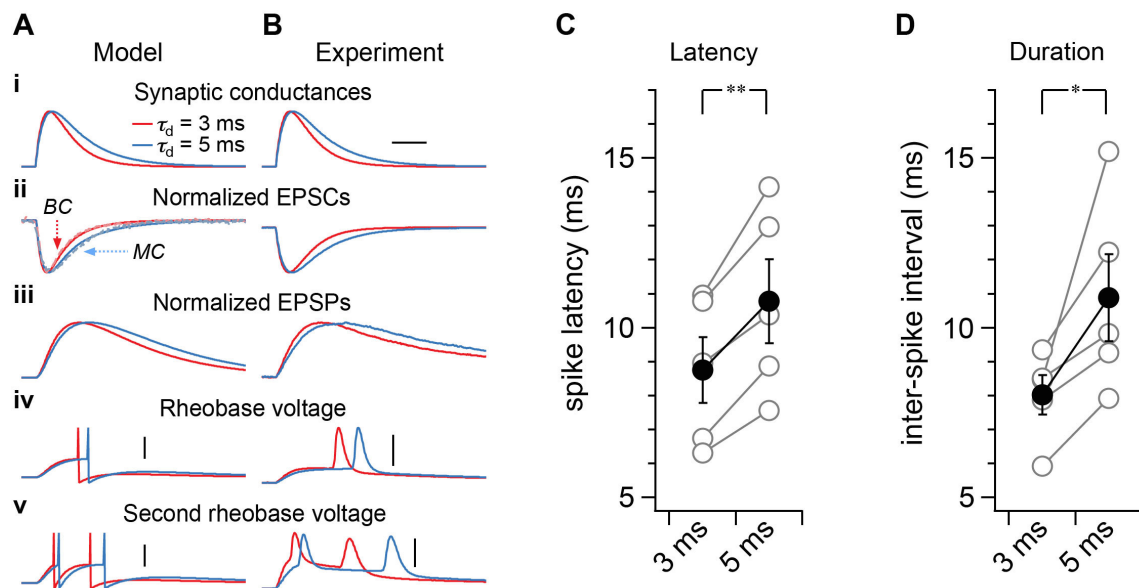


Figure 3.7: Rapid AMPAR kinetics temporally sharpens BC-mediated inhibition

(A) A leaky integrate-and-fire computer model was tuned to average BC intrinsic properties (see ‘Materials and methods’). A single excitatory synaptic conductance (Ai) was modeled based on an excitatory input to a BC with rapid decay, $\tau_{\text{decay}} = 3$ ms, or on an excitatory input to an MC with slow decay, $\tau_{\text{decay}} = 5$ ms. For comparison, model EPSCs are represented together with representative EPSCs recorded in a BC and an MC (Aii, dashed traces). Even though the synaptic conductance rise time constant τ_{rise} was the same in both cases (Table 1), this gave rise to EPSPs with different rise times and peak latencies (Aiii), because of temporal integration. When the peak synaptic conductance amplitude was set to the lowest value at which one spike was evoked (‘rheobase’), fast-decaying conductances consequently produced APs with shorter latencies than slow-decaying conductances did (Aiv). To assess BC response duration, the peak synaptic conductance was increased to the lowest value at which two APs were evoked (denoted the ‘second rheobase’), which resulted in inter-spike intervals of shorter duration with the rapidly decaying input. Scale bars: 5 ms, 20 mV.

(B) To verify the computer model predictions, we carried out conductance clamp experiments (see ‘Materials and methods’), as this allowed us to investigate the consequences of altered synaptic kinetics in a real BC. The same conductance

kinetics was used as in the computer model (Bi), which again gave rise to EPSCs with fast and slow decay (Bii). The resulting EPSPs had different rise times and peak latencies (Bii). This resulted in different AP latency (Biv) and response duration (Bv) in this particular BC, in agreement with the computer model.

(C) In dynamic clamp experiments, the AP latency was consistently shorter with rapidly decaying synaptic kinetics (paired t-test). Grey circles denote measurements from individual BCs ($n = 5$), and black circles are the averages.

(D) Response duration was also robustly shortened by rapidly decaying synaptic conductance (paired t-test).

Table 3.1: Synaptic properties of BCs and MCs

Data was taken from BCs and MCs in **Figure 3.3**, **Figure 3.4** and **Figure 3.6**.

Experiment	Parameter	BC	n	MC	n	p
Paired recording EPSCs	Paired-pulse ratio	0.36 ± 0.03	14	5.6 ± 1	9	***
	τ_{rise} (ms)	1.8 ± 0.3	22	2.0 ± 0.4	9	n.s.
	τ_{decay} (ms)	2.9 ± 0.2	22	5.6 ± 0.5	9	***
	τ_{decay} in AP5 (ms)	2.8 ± 0.3	6	5.2 ± 0.6	3	**
AMPA uncaging EPSCs	τ_{rise} (s)	0.17 ± 0.02	25	0.15 ± 0.02	18	n.s.
	τ_{decay} (s)	1.1 ± 0.1	25	1.7 ± 0.1	18	***
	τ_{decay} in Naspm (s)	1 ± 0.1	7	1.6 ± 0.2	5	*

Table 3.2: Intrinsic Properties of BCs

Data obtained from BCs in Figure 3.5D-F.

Parameter	Value
Spike threshold (mV)	-33 ± 1
Spike height (mV)	55 ± 3
Spike half-width (ms)	0.63 ± 0.07
Spike after-hyperpolarization (mV)	-19 ± 1
Rheobase current (pA)	220 ± 30
Frequency (Hz)	55 ± 10
Accommodation (%)	-5.6 ± 10
Coefficient of variation (%)	8.0 ± 2
Membrane potential, V_M (mV)	-70 ± 2
Input resistance, R_{in} ($M\Omega$)	150 ± 10
Membrane time constant, τ_M (ms)	11 ± 2

Supplemental Figures

Table 3.3: All INs were morphologically identified

Morphologies in **Figure 3.2** were obtained from 81 BCs and 29 MCs, which constitutes the entire IN data set of this study. Paired recordings in **Figure 3.3** included data from two triplet recordings, for which two PCs were connected to the same postsynaptic BC. Additionally, four PC-BC connections used in rectification measurement (**Figure 3.3D, E**) also served as stability controls for Naspm wash-in experiments (**Figure 3.3G, H**). Together, this results in a total of 87 experiments in BCs, even though the total number of reconstructed BC morphologies is 81.

Experiment	BC (n)	MC (n)
Rectification, pairs	14	9
Rectification, NPEC-AMPA uncaging	11	10
Naspm wash-in, pairs	6	NA
Naspm wash-in, pairs (control)	6	NA
Naspm wash-in, NPEC-AMPA uncaging	7	5
Naspm wash-in, NPEC-AMPA uncaging (control)	7	3
NBQX wash-in, NPEC-AMPA uncaging	2	2
Rectification of mEPSCs, no spermine	9	NA
Rectification of mEPSCs, with spermine	12	NA
Naspm wash-in, mEPSCs	5	NA
Naspm wash-in, mEPSCs (control)	3	NA
Dynamic clamp	5	NA
Total	87	29

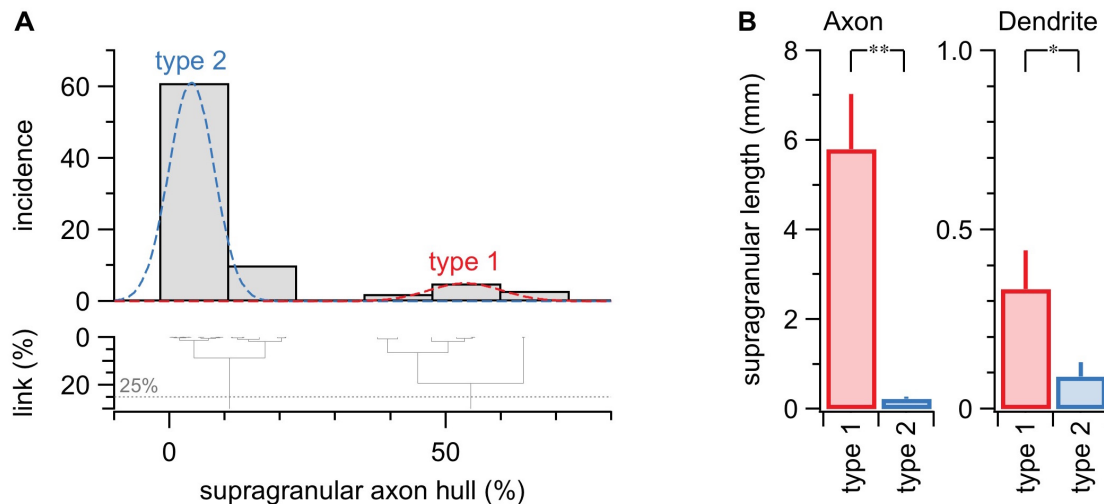


Figure 3.8: Axonal morphology classified BCs into two types

(A) BC morphologies were independently clustered based on the amount axonal branching in supragranular layers (see 'Materials and methods'). The 25% best-cut (dotted line) intersected the dendrogram (bottom) twice, suggesting that BCs should be partitioned into two types. Type 1 (red) had ascending axons ramifying extensively above the border of granular L4, whereas the axonal arbor of type 2 (blue) was largely subgranular (**Figure 2**) (Buchanan et al., 2012, Ferreira et al., 2014).

(B) Total supragranular axon length was considerably different for type-1 and type-2 BCs (5.8 ± 1 mm, $n = 10$, vs. 0.23 ± 0.05 mm, $n = 71$, $p < 0.01$). We also found a small but significant difference in total supragranular dendrite length (330 ± 100 μm vs. 90 ± 40 μm , $p < 0.05$).

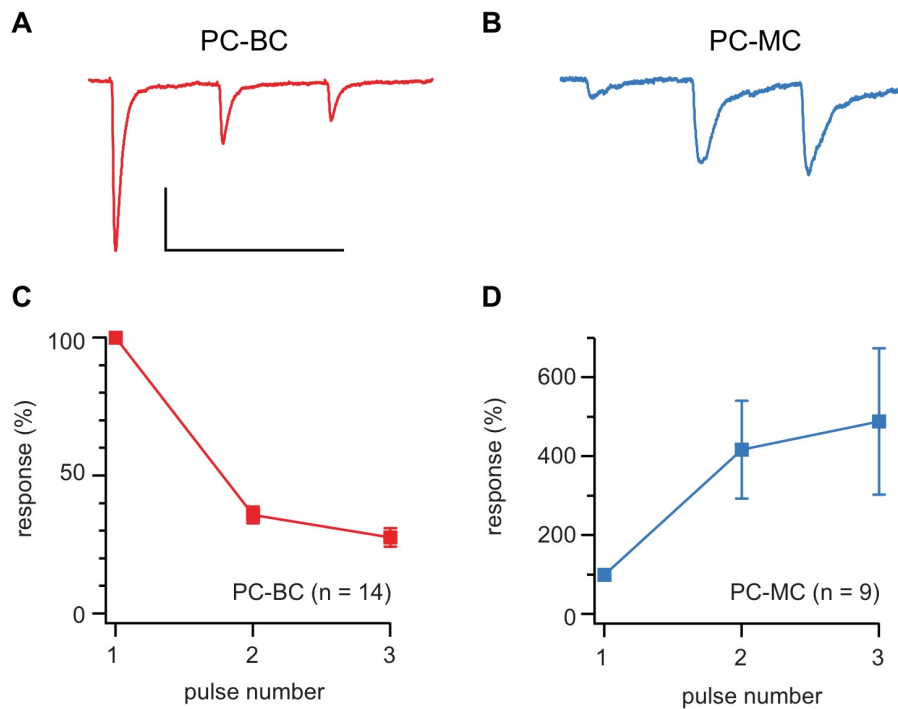


Figure 3.9: PC-BC connections short-term depress whereas PC-MC synapses facilitate

(A) Sample voltage-clamp trace illustrates a PC-BC connection that characteristically exhibits short-term depression (Blackman et al., 2013). Three APs were repeatedly elicited at 30 Hz in the presynaptic PC and 20 postsynaptic sweeps were averaged every 15 seconds. Scale bars: 50 ms, 50 pA.

(B) A PC-MC connection recorded under the same conditions shows typical short-term facilitation (Blackman et al., 2013).

(C) Ensemble average shows that PC-BC short-term depression is robust. Responses were normalized to the first in a train.

(D) In contrast, PC-MC synapses strongly and robustly facilitated. Short-term plasticity properties could thus be used to distinguish MCs from BCs.

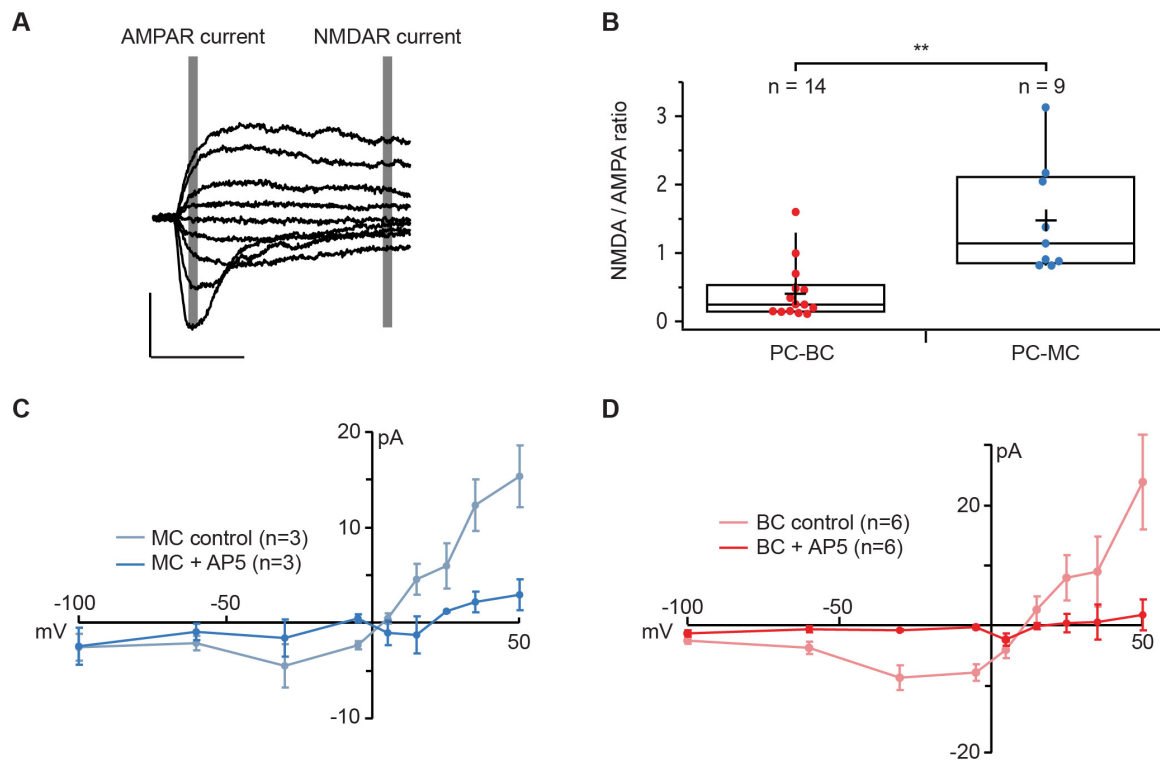


Figure 3.10: Both PC-MC and PC-BC connections have postsynaptic NMDARs

(A) The AMPAR and NMDAR-mediated currents were measured at latencies indicated by grey boxes (see 'Materials and methods'). These sample sweeps are from a PC-MC paired recording. Scale bars: 10 ms, 100 pA.

(B) PC-BC connections (red) had smaller NMDA/AMPA ratios than PC-PC (black) or PC-MC connections (blue), which might seem to suggest that the former have fewer postsynaptic NMDARs. NMDA/AMPA ratio in cells recorded from GIN and WT mice were indistinguishable (0.87 ± 0.03 , $n = 3$ vs. 1.4 ± 0.2 , $n = 6$, $p = 0.07$).

(C) In agreement with the existence of postsynaptic NMDARs at PC-MC connections, an IV relationship characteristic of an NMDAR-mediated current was found in the absence (blue) but not the presence of the NMDAR antagonist AP5 (light blue).

(D) Evidence for postsynaptic NMDARs were found at PC-BC connections as well: an IV relationship characteristic of the NMDAR-mediated current was found in the absence (red) but not the presence of the NMDAR antagonist AP5 (pink). Taken together, our results suggest that PC-BC connections have low NMDA/AMPA ratio because AMPAR-mediated currents are high, not because NMDAR-mediated currents are low.

Additional discussion (not included in manuscript)

Naspm affects PC-MC synapses

Naspm wash-in would be expected to have no effect at PC-MC synapses, since they lack CP-AMPARs. However, as mentioned above those synapses are likely to express presynaptic KARs that are known to contribute to making the synapse short-term facilitating in Sst-positive cells in the hippocampus (**Figure 3.11, C**). To verify it, we performed paired recordings of connected PCs and MCs and measured the EPSCs amplitude overtime while washing-in Naspm. We observed a strong decrease, as illustrated by a sample recording in **Figure 3.11, A**. This results, although preliminary, together with the results of Naspm action on the AMPA-evoked currents in MCs (**Figure 3.11, C**) that only focuses on the postsynaptic side, suggests that presynaptic KARs are indeed present at PC-MC synapses in neocortical L5.

Developmental regulation of CP-AMPARs in PCs

Through the manuscript, we provide information regarding the absence of CP-AMPARs at PC-PC synapses. We summarized all this data in **figure 3.12**. In all experiments performed PC-PC connections gave results similar to that at PC-MC synapses, and globally PCs showed results similar to that of MCs. It has been shown before that CP-AMPARs are present in PC dendrites in the CA1 region of the hippocampus (Mattison et al., 2014). However, literature suggests that CP-AMPARs are developmentally regulated in PCs as in INs (Kumar et al., 2002, Shin et al., 2005, Wang and Gao, 2010, Lu et al., 2014), which may explain why different research teams describe apparently contradictory results Here, we find that, in the age range

studied (P12-P21), PCs do not express CP-AMPARs or at least that they predominantly express CI-AMPARs.

Critical function of CP-AMPARs in FIDI

Finally, we implemented a second phenomenological computer model (**Figure 3.13**). The model was tuned to our paired recording data on the effect of Nasp on PC-BC pairs and shows that, in the context of FIDI and FDDI, so when a PC or a group of PCs connected to a MC and a BC fire APs at high frequency, CP-AMPARs specifically mediate the feed-forward BC-mediated early inhibition onto PCs (**Figure 3.13**). This result is not surprising given the receptors are not expressed at PC-MC synapses, but the model shows that the receptors play a key role in this simple microcircuit.

Additional Figures (not included in the manuscript)

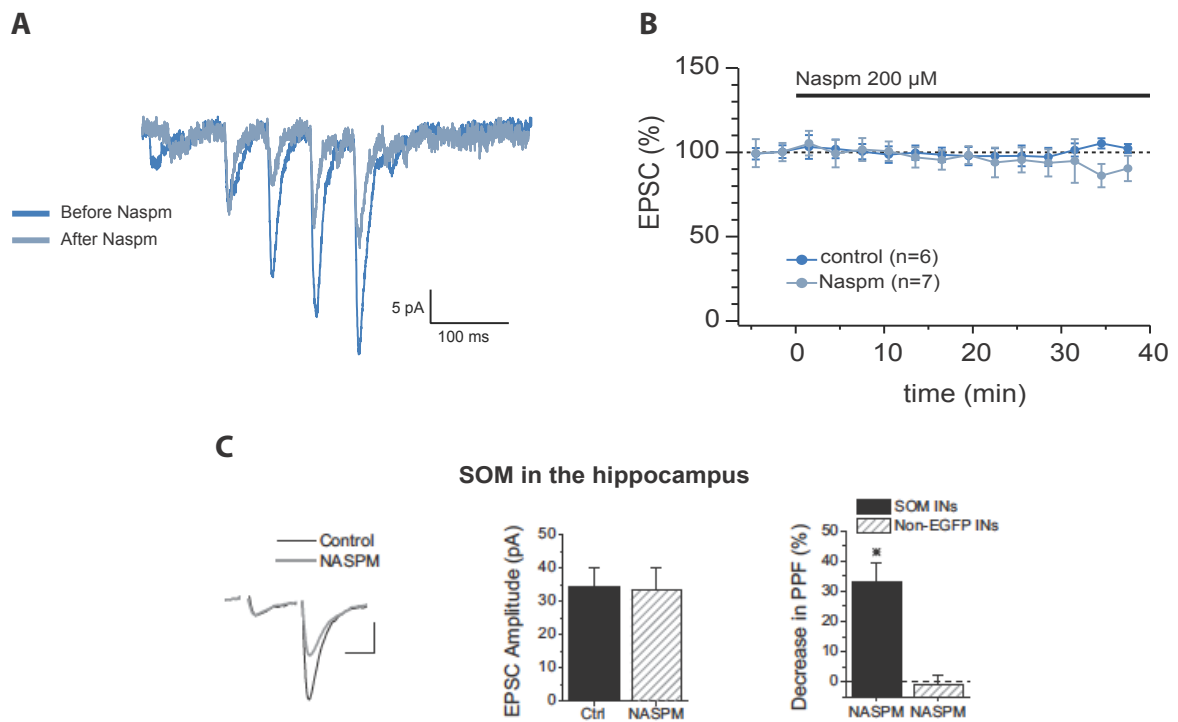


Figure 3.11: Naspnm decreases the amplitude of PC-MC synapses

(A) Sample trace of the EPSCs in a MC when eliciting 5 APs at 30Hz in the presynaptic PC before (dark blue) and after (light blue) Naspnm bath application.

(B) Effect of Naspnm on the AMPA-evoked current in MCs (light blue) compared to control condition without Naspnm (dark blue).

(C) Data from Sun et al., (2009), showing that at excitatory synapses onto Sst-positive cells in the hippocampus, Naspnm decreases the amplitude of the second but not of the first response, indicating a presynaptic locus of Naspnm action. A similar phenomenon may occur at PC-MC synapses in neocortical L5. However, the low release probability and high failure rate observed in paired recordings almost systematically prevents measuring the amplitude of the first response in a train.

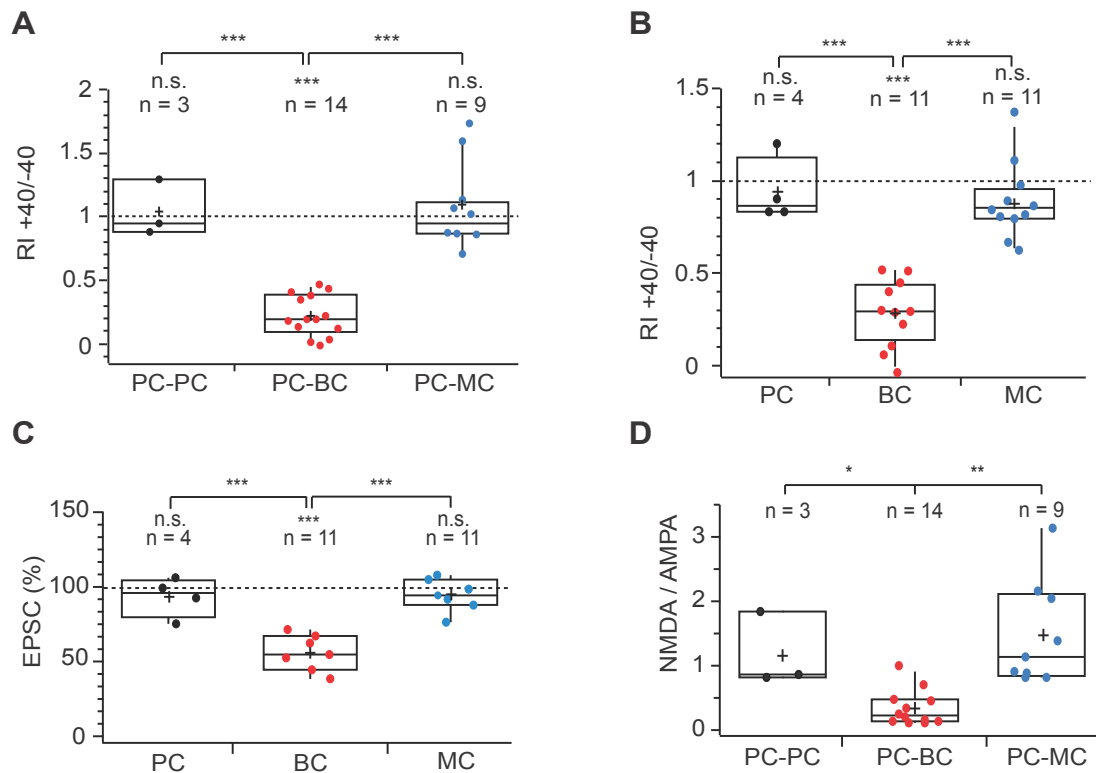


Figure 3.12: PC-PC synapses do not express CP-AMPA

(A) Rectification index of the AMPAR current at PC-PC pairs (black) compared to PC-BC (red) and PC-MC (blue).

(B) Rectification index of the uncaging-evoked current in PCs (black) compared to MCs (blue) and BCs (red).

(C) Effect of Naspam on the uncaging-evoked current in PCs (black), MCs (blue) and BCs (red).

(D) NMDAR/AMPA ratio at PC-PC (black) compared to PC-BC (red) and PC-MC (blue) synapses. Boxplots and statistical tests are as described in results section 1.

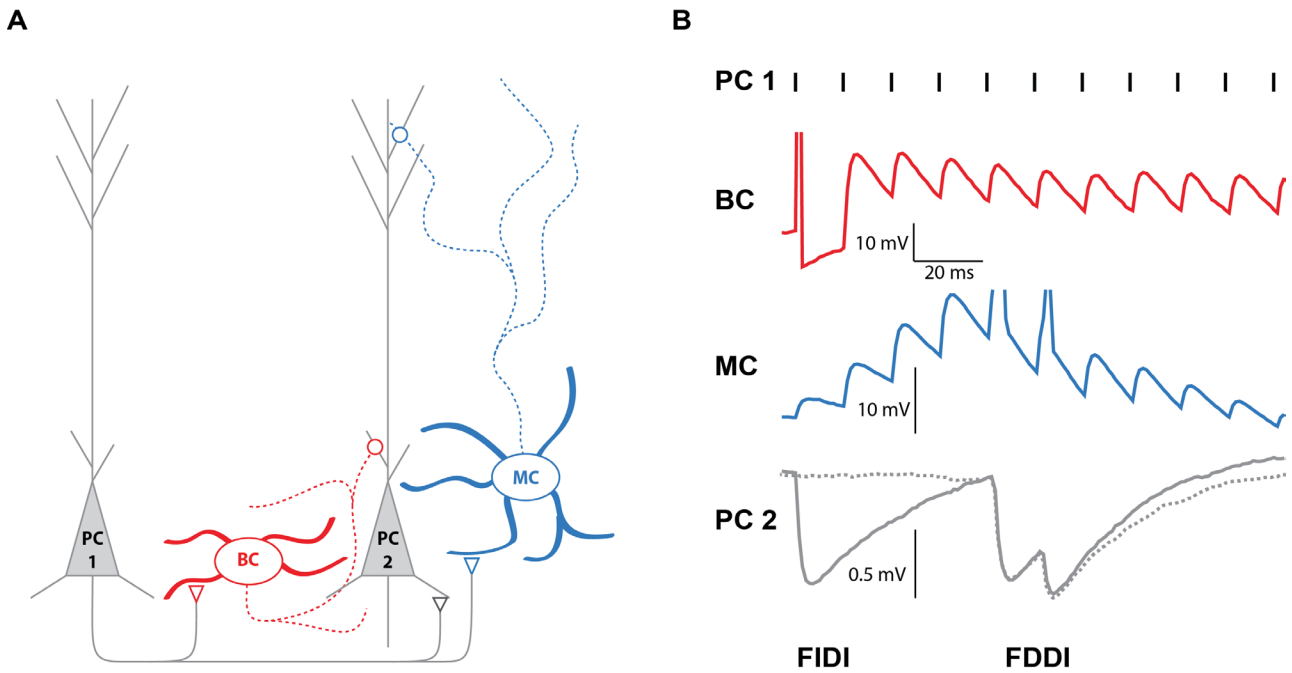


Figure 3.13: Role of CP-AMPA receptors in the BC-mediated early inhibition

(A) Diagram depicting the FDDI and FIDI circuit, as in figure 1.7

(B) Dashed lines indicate the effect of CP-AMPA blockade by Naspm on the circuit: it selectively abolishes the early but not late (MC-mediated) inhibition. The model was tuned to our paired recordings data by Dr. Rui Costa (Edinburgh University).

Target-specific expression of presynaptic NMDARs

Summary

In a project performed by members of the laboratory (Buchanan et al., 2012), and to which I contributed as described below, we found that preNMDARs are specifically expressed at PC-MC and PC-PC, but not at PC-BC synapses (they were expressed at type-1 BCs, but not at classical type-2 BCs). We arrived to this conclusion by using a combination of multiple whole-cell recordings and 2PLSM as well as 2-photon calcium imaging and pharmacology. Furthermore, a computer model, which predictions were confirmed experimentally, demonstrated the implication of those receptors in the FDDI microcircuit (see Buchanan et al., 2012). My contribution to this work consisted in two sets of experiments, one involving pharmacology and quadruple whole-cell recordings, the other based on whole-cell recordings and two-photon Ca^{2+} imaging.

Results

Specificity of MNI-NMDA

In order to activate NMDARs we used MNI-NMDA. The principle of MNI-NMDA uncaging is similar to that of NPEC-AMPA described in **chapter II**. The chief difference is that NMDA is release instead of AMPA, and this allows the experimenter to specifically activate NMDARs. Also, the photolysis rate of the link between the MNI molecule and the caged compound is much faster than that of the NPEC cage (Palma-Cerda et al., 2012). However, MNI-NMDA had not been widely used at the time, so we set out to prove that it specifically acted on NMDARs. In order to block NMDA receptors specifically in the recorded cell we introduced MK801, which antagonizes NMDARs by blocking the channel pore in an activity-

dependent manner, in the recorded cells via the solution contained in the patch pipette. Because MK801 does not readily traverse the cell membrane, it is unlikely to diffuse to other cells (**figure 3.14 A**). MNI-NMDA was then puffed close to those cells using a patch pipette, and 5 laser pulses at 30 Hz were elicited in order to uncage NMDA using the 405 nm laser. The intracellular solution was also supplemented with the calcium-sensitive dye Fluo 5F. NMDARs have the particularity to present non-linearity of their calcium signal (MacDermott et al., 1986, Ascher and Nowak, 1988). We thus imaged and measured with 2PLSM the calcium transients evoked in three conditions that allow us to assess this non-linearity: (a) when eliciting APs directly in the soma via the patch pipette, (b) when uncaging NMDA from MNI-NMDA, or (c) when doing both at the same time. Because NMDARs are maximally activated by a combination of NMDA binding and depolarization, the sum of the two individual stimulations (calcium transient (a) + calcium transient (b)) should be smaller than the calcium signal occurring when the stimulations are combined (calcium transient a+b) (**figure 3.14 B**).

Indeed, the sum of the calcium transients evoked by the two individual stimulations was smaller than the transient measured when evoking both at the same time. When repeating these stimulations in sequence, the activity-dependent blockade by MK801 decreased specifically the calcium transient amplitude evoked by NMDA uncaging as well as the non-linearity (see **figure 3.14 B, C**), while leaving the calcium transients evoked by APs alone unaffected. This demonstrates that the NMDA released by MNI-NMDA photolysis produces a current that is indeed NMDAR-dependent.

PC-PC but not PC-IN synapses express presynaptic NMDARs

The main experiment I carried out for this work demonstrated the absence of presynaptic NMDARs at PC-IN synapses, INs that after reconstruction turned out to be type-2 BCs. As illustrated in **figure 3.15A**, we used again internal MK801, this time introduced only in the presynaptic cell in connected PC-IN pairs. INs were targeted blindly, and since BCs represent ~50% of all INs in visual neocortex L5, the probability to patch BCs is higher than for other INs, which may explain why they turned out to be BCs. Once a connection in the correct direction was found we measured the amplitude of the EPSPs over time while stimulating the presynaptic cell at 30 Hz. After a few minutes, MK801 reliably decreased the amplitude of PC-PC but not PC-IN connections, demonstrating that presynaptic NMDARs are not expressed at PC-BC synapses **figure 3.15C**.

Other lab members carried out similar experiments at PC-MC and PC-PC connections (**figure 3.15B**), where no decrease in amplitude could be observed. In conclusion, this work demonstrates that presynaptic NMDARs are expressed at PC-PC and PC-MC, but not PC-BC and that they play a role in information processing, e.g. in the FDDI microcircuit.

Discussion

Debate on the existence of preNMDARs

Although various studies have provided evidence for the presynaptic location of NMDARs, the subject has been strongly debated. One of the first studies to show a possible expression of preNMDARs was performed in the cerebellum (Casado et al., 2000, Casado et al., 2002). Three years later, another team on the other hand

failed to observe calcium signals from preNMDARs at the same synapses, while they did find them at others (stellate interneuron) (Shin and Linden, 2005). However, these results were themselves disputed by other researchers who argued that the NMDAR-dependent calcium signal observed by Shin and Linden were only indirectly NMDAR-dependent (Christie and Jahr, 2008). They thought that the signals observed arose from the activation of calcium channels indirectly gated by dendritic NMDAR stimulation. By a combination of internal MK801 in the presynaptic cell, Rodriguez-Moreno and colleagues finally provided strong evidence of the presence of preNMDARs (Rodriguez-Moreno and Paulsen, 2008). In the end, it seems that, even though some results may be debated, the most parsimonious explanation is that preNMDARs are expressed at some but not all synapse types, as was demonstrated by (Buchanan et al., 2012).

The developmental regulation of preNMDARs expression may also explain part of those discrepancies. In the mouse visual cortex for example, Corlew et al. (2007) found that excitatory inputs onto PCs express preNMDARs until after the onset of the critical period (~P23) but not later. Furthermore, they observed that the rules governing timing-dependent LTD at those synapses, involving preNMDARs before P23, were independent of preNMDARs after that.

Functions of preNMDARs

The existence of presynaptically located NMDARs raises questions about their functions (Duguid and Sjöström, 2006). Indeed, as developed in chapter I, the postsynaptic location of the receptors allow them to act as coincidence detectors, but this function may not make sense for presynaptically located NMDARs. However, several hypotheses exist. First, preNMDARs may be critical for the induction of LTD

(Casado et al., 2002, Sjöström et al., 2003) and of LTP (Humeau et al., 2003). Also, consistent with their presynaptic location, evidence indicates that they may play important roles in neurotransmitter release (Sjöström et al., 2003, Bardoni et al., 2004, Duguid and Smart, 2004). Finally, again because of their presynaptic location, it has been shown that preNMDARs may act as frequency filters (Sjöström et al., 2003, Bidoret et al., 2009). However, our study provides evidence that they are not equally distributed across synapse types, thus limiting their role, which to specific circuits.

Interestingly, although one could expect a presynaptically located ion channel involved in evoked neurotransmitter release to affect short-term synaptic dynamics, our results seem to argue against that hypothesis. Of course, other factors may counteract the role of preNMDARs and no clear conclusion on the matter can be drawn from this study, but we found preNMDARs at short-term facilitating PC-MC synapses as well as at short-term depressing PC-PC and PC-type 1 BC connections, thus ruling out the possibility that they play a determining role in short-term plasticity at those synapses.

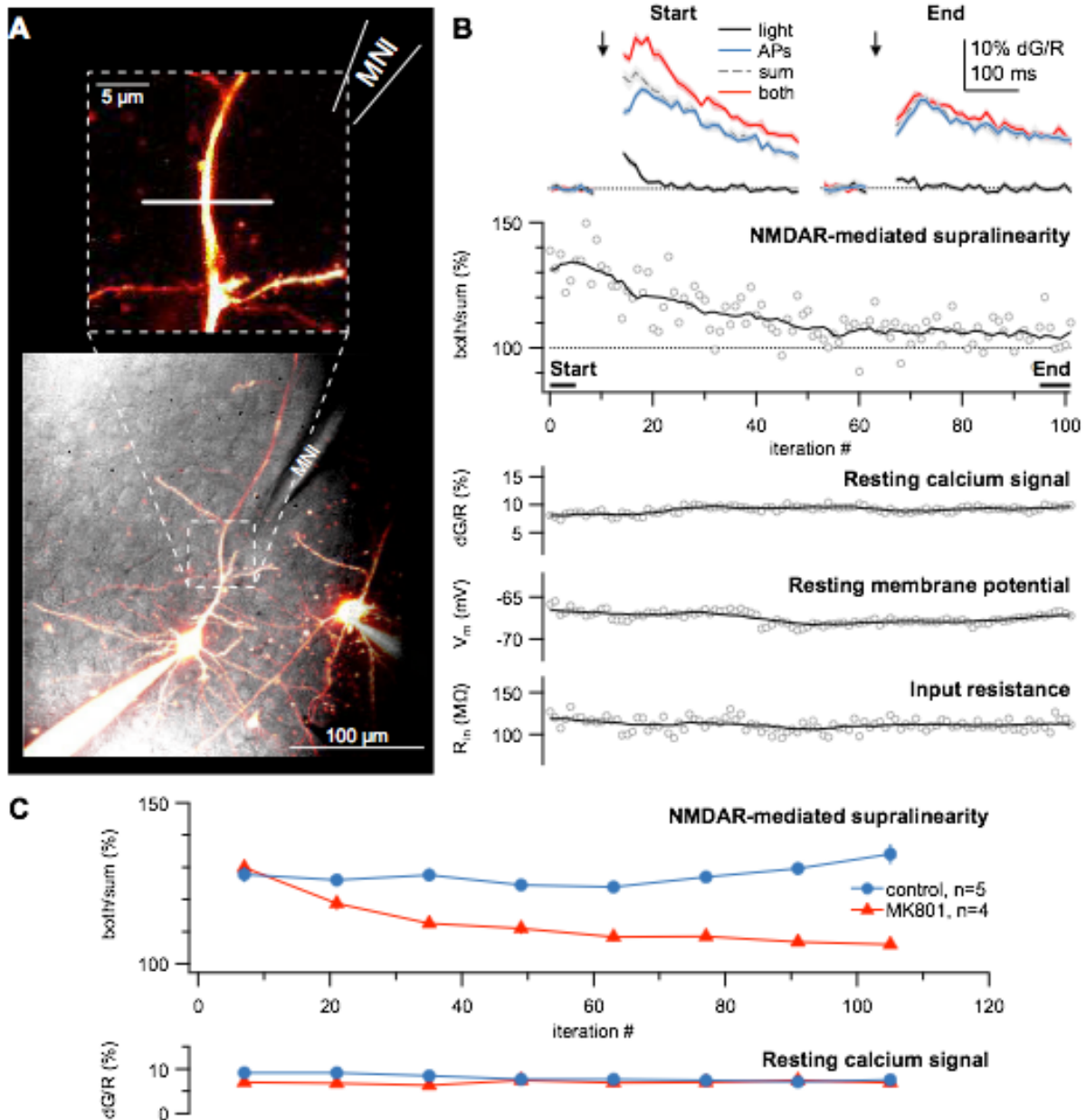


Figure 3.14: MNI-NMDA Specifically Acts on NMDARs

(A) We loaded this neuron with MK801 (Bender et al., 2006, Brasier and Feldman, 2008, Rodriguez-Moreno and Paulsen, 2008) to show the NMDAR specificity of MNI-NMDA. Note how ejection from puff pipette (“MNI”) bends the dendrite, indicating the presence of MNI-NMDA. Line scan and uncaging carried out as for Figure 3.

(B) As expected, NMDAR-mediated dendritic supralinearities (inset top left, $132\% \pm 2.6\%$, $p < 0.001$) were gradually reduced to insignificance (inset top right, 107 ± 3.3 , $p = 0.14$) in the neuron in (A) dialysed with MK801, while basal calcium, membrane potential and input resistance remained stable (see Methods). Each iteration denotes

the delivery of the three types of sweeps: both, light, and APs. The inter-sweep interval was two seconds.

(C) Consistent with a specific action on NMDARs by MNI-NMDA and internal MK801, dendritic calcium supralinearities remained stable in interleaved control cells ($128\% \pm 5.6\%$ vs. $130\% \pm 7.9\%$, $n = 5$, $p = 0.85$), while supralinearities in cells loaded with MK801 were robustly reduced (to $108\% \pm 1.4\%$ compared to the initial $128\% \pm 2.9\%$, $n = 4$, $p < 0.001$; or $p < 0.05$ compared to controls). Internal MK801 did not affect basal calcium signals (dG/R: $9.2\% \pm 1.9\%$ vs. $9.4\% \pm 1.7\%$, $n = 5$, $p = 0.95$). (Buchanan et al., 2012).

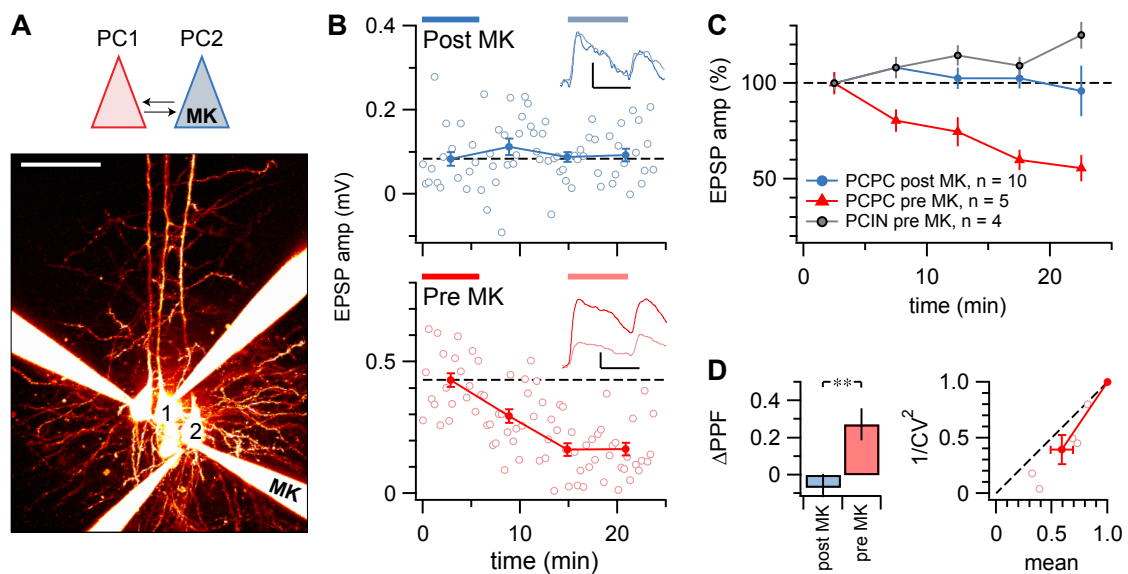


Figure 3.15: NMDAR blockade in pre but not postsynaptic PCs suppresses EPSPs

(A) A reciprocally connected pair of PCs where PC2 was filled with internal MK801 (“MK”) but PC1 was not. Morphology is maximum intensity projection of Alexa-594 fluorescence obtained with 2PLSM, verifying that these neurons were PCs. Scale bar: 25 μ m.

(B) PC1-PC2 connection was unaffected (top; 0.08 ± 0.02 mV vs. 0.09 ± 0.01 mV, $p = 0.71$), whereas PC2-PC1 connection was suppressed (bottom; 0.43 ± 0.03 mV vs. 0.14 ± 0.02 mV, $p < 0.001$), indicating that pre but not postsynaptic MK801 down-regulates neurotransmission. Inset traces are averages comparing 15-21 min and 0-6 min after breakthrough.

(C) Pre but not postsynaptic MK801 consistently suppressed neurotransmission in PC-PC pairs (pre MK: $59\% \pm 10\%$, $n = 5$; post MK: $100\% \pm 4\%$, $n = 10$; $p < 0.01$; averaged over periods indicated in B). Presynaptic MK801 loading in PC-IN pairs was indistinguishable from post MK PC-PC pairs ($120 \pm 20\%$, $n = 4$; $p = 0.27$) but different from pre MK PC-PC pairs ($p < 0.05$).

(D) Pre but not postsynaptic MK801 reduced PPR in PC-PC pairs (compare inset traces in B), consistent with a presynaptic impact of presynaptic MK801. PPR in PC-IN pairs with pre MK801 was not affected (-0.09 ± 0.1 , $p=0.82$).

(E) CV analysis of PC-PC pairs with presynaptic MK801 resulted in data points below the diagonal, confirming the presynaptic locus ($\varphi = 10 \pm 3^\circ$, $p < 0.05$). CV was

unaffected for PC-PC pairs with post MK801 ($\varphi = -20 \pm 24^\circ$, $p = 0.42$) and for PC-IN pairs with pre MK801 ($\varphi = -60 \pm 40^\circ$, $p = 0.26$). For this figure I contributed the PC-IN paired recordings with MK801 in the presynaptic PC (C). From (Buchanan et al., 2012).

Synapse-specific long-term plasticity

Summary

In results section 1, we demonstrate the synapse-specific expression of CP-AMPA receptors as well as a lower NMDAR/AMPA ratio at PC-BC compared to PC-MC or PC-PC connections. In results section 2, we describe the work that showed the existence of presynaptic NMDARs at PC-MC and PC-PC but not PC-type-2 BC synapses. Since CP-AMPA receptors and NMDARs, both pre and postsynaptic, are involved in long-term plasticity, we hypothesized that the different composition in receptors should impact on long-term plasticity at those synapses. We do not intend to describe a complete STDP curve with various timings and frequencies or thoroughly characterize plasticity of these synapse types, but rather test the hypothesis that plasticity may be different, based on the data presented in result sections 1 and 2.

As developed in the introduction, STDP is a paradigm which induction is biologically realistic because it corresponds to patterns of activity that can happen in vivo. Furthermore, the laboratory has an important expertise in this area and I thus greatly benefited from my supervisor's knowledge and technical skills. I started by recording STDP at 50 Hz because it is known to reliably induce LTP at PC-PC synapses regardless of the timing between pre and postsynaptic firing and, if we manage to reproduce it, this result can thus be used as a control, showing that the protocol employed is efficient. As described in **figure 2.6**, once a connection was established, the protocol consisted in recording a baseline period (~10 min), followed by the induction, after which a post-induction period of ~30 min identical to the baseline occurred in order to compare the response amplitudes after to that before the induction. Five APs at 50 Hz were elicited in both the pre and the postsynaptic

cells during the induction, and the timing between spikes in the two cells was either + or – 10 ms.

In the following sections, I describe the results obtained from five different synapse types for which we compared STDP with this 50 Hz induction protocol: PC-PC, PC-BC, PC-MC, as well as inhibitory connections from BCs and MCs to PCs. In all cases, results obtain with a time difference of +10 ms or -10 ms were pooled since the outcome was the same.

Results

STDP at PC-PC synapses

As expected, a STDP induction protocol at 50 Hz (sample recording in **figure 2.6**) induced LTP at L5 PC-PC synapses, regardless of the timing (after/before = $120\% \pm 7\%$, $n = 10$ pairs, $p < 0.05$, **figure 3.14**). These recordings were obtained from both GIN and WT mice, but no difference in the outcome of STDP could be observed with the protocol employed between the two mouse lines. These results provide us with a control of the relevance and efficiency of the protocol. Indeed, we managed to reproduce in paired recordings a classical finding of plasticity at excitatory connections onto excitatory cells with high frequency induction eliciting LTP. We can thus use this data to compare the plasticity induced at PC-IN synapses using the same induction protocol. Interestingly, the short-term plasticity of PC-PC connections was not affected by the induction protocol.

STDP at PC-IN synapses

PC-BC synapses always underwent LTD with the same induction protocol (after/before = $74\% \pm 7\%$, $n = 6$ pairs, $p < 0.05$, **figure 3.14**). Again, these recordings have been performed in GIN and WT mice and no difference in the outcome of plasticity could be observed, indicating that the result does not arise from differences in e.g. genetic background.

At PC-MC synapses, the first EPSP in paired recordings is often almost absent due to low probability of release (Sylwestrak and Ghosh, 2012) and high failure rate of those synapses (Urban-Ciecko et al., 2015), and thus very difficult to analyze (see discussion). As a consequence, in **figure 3.14**, plasticity of the third EPSP induced by a train of 5 APs in the presynaptic PC is shown. Results are similar to that at PC-BC synapses in that LTD was consistently obtained (after/before = $54\% \pm 10\%$, $n = 5$ pairs, $p < 0.05$, **figure 3.14**).

STDP at IN-PC synapses

Although less relevant to the present work, plasticity of IN-PC synapses has been studied much less than PC-PC plasticity (for review, see Kullmann et al., 2012), and can thus provide us with interesting insights regarding information processing in neocortical circuits. We thus recorded STDP of inhibitory synapses from BCs and MCs onto PCs, still with the same exact induction protocol. Interestingly, we found no significant change in the amplitude IPSPs at BC-PC synapses, but a strong potentiation of MC-PC connections was observed. Although preliminary, this result suggests that plasticity of inhibition may be synapse-specific, just like it is for excitation.

Discussion

Here, we show that high frequency stimulation of both PC-BC and PC-MC synapses leads to LTD, while the same protocol induces LTP of PC-PC synapses. These results thus strongly suggest that a synapse-specific long-term plasticity exists in L5 of the developing visual neocortex when considering excitatory synapses onto excitatory or inhibitory cells.

Importantly, CP-AMPA receptors have not been shown to be involved in STDP, and it is somehow conceptually difficult to understand how they could potentially act since they require a hyperpolarization of the postsynaptic cell, cell that on the other hand requires APs to comply with the STDP paradigm. This does not mean that CP-AMPA receptors are not involved in plasticity at PC-BC synapses, but that a different experimental paradigm may have to be employed, such as the classical frequency-dependent plasticity, with which they may induce non-Hebbian plasticity (Lamsa et al., 2007b).

Excitatory connections onto MCs have a very low release probability and high failure rate (Sylwestrak and Ghosh, 2012, Urban-Ciecko et al., 2015). As a consequence, the average amplitude of the first EPSP in a train of stimulations in our recordings was not sufficient for a reliable analysis or even quantification. Since those connections are facilitating we could however measure the amplitude of the subsequent EPSPs. A reliable way to analyze the first EPSP is necessary in order to compare the result to PC-PC and PC-BC synapses (for which we analyzed the amplitude of the first EPSP). Although we did not observe changes in short-term plasticity for a given synapse type caused by the induction protocol, analyzing the first EPSP would avoid hypothetical changes in short-term plasticity and would thus be more adequate. One possibility could be to use extracellular stimulations to

record excitatory connections onto MCs as they allow us to adjust the strength of the stimulation until a first EPSP of decent amplitude is obtained. In the neocortical circuitry this technique does not ensure the nature of the presynaptic cell is known because several neighboring cells are activated, and may thus be less conclusive with regard to synapse-specific plasticity.

A key mechanism that may help explain the difference in plasticity at PC-PC and PC-IN synapses is the reliability of the bAP: if a weak depolarization reaches the synapses, even with high frequency, this may cause a small entry of calcium, triggering LTD instead of LTP. A recent study by Camiré and colleagues has shown that the bAP in hippocampal BCs decreases very rapidly with distance from the soma. As a consequence, LTP induction at distal dendrites (and thus synapses onto distal dendrites) in BCs requires a strong depolarization that allows internal calcium stores to be recruited (here provided by extracellular stimulation and CP-AMPA activation) (Camiré and Topolnik, 2014). In contrast, Christina Chou, a student in Dr. Sjöström laboratory has performed a combination of whole-cell recordings and 2-photon calcium imaging of the bAP in neocortical L5 BCs and found that they propagate with very little, if any, attenuation in distal dendrites. Although still preliminary, this finding suggests that the mechanisms underlying plasticity may be different between hippocampal and neocortical BCs. Nevertheless, the comparison of the bAP propagation in neocortical L5 between PCs, BCs and MCs as well as determining the location of the synapses, or at least the distribution of putative excitatory contacts would help nail down the role of the postsynaptic bAP in the synapse-specific STDP we observed.

Interestingly, the Topolnik lab could obtain LTP of excitatory connections onto hippocampal BCs and this required calcium from both CP-AMPA and from internal

stores. I thus performed paired recordings of STDP at PC-BC synapses including cyclopiazonic acid in the bath (which opens internal stores), but found no change in STDP with a 50 Hz induction protocol. The differences between our experiments may be due to the techniques employed, but also to the paradigm, since these authors did not look at STDP but frequency-dependent plasticity. Furthermore, it is also possible that hippocampal and neocortical BCs behave differently.

An interesting work by Lu et al. (2007) demonstrates that in L2/3 or the rat somatosensory neocortex, excitatory connections from PCs to fast-spiking cells (chiefly BCs), showed LTD regardless of the timing when recording STDP. Although the protocol is slightly different, the result is in agreement with our data at L5 PC-BC synapses. However, in the same study, another group of INs underwent LTP or LTD depending on the timing, just like PC-PC connections do. Unfortunately, we cannot compare those cells to our MCs because this identification criterion used in the study (AP threshold) does not correspond to MCs only, but rather encompasses several morphologically identified IN types. This may help explain why our results — which only focused on morphologically identified MCs — differ from those of Lu and colleagues (Lu et al., 2007) with regards to non-fast-spiking INs.

Another important factor that has to be taken into account when studying STDP is neuromodulation. Although we do not stimulate the release of neuromodulators or apply neuromodulators, it has been shown that they can drastically affect STDP, including in neocortical INs (Seol et al., 2007, Huang et al., 2012, Huang et al., 2013). Thus, even for a given synapse type, at a specific frequency of induction and for a precise timing of pre and postsynaptic activation, LTP and LTD can be obtained depending on the neuromodulator environment.

Finally, as described above, STDP varies with cell type, location of the synapse, frequency, brain region and neuromodulation. Unfortunately, the study of STDP also generally suffers from the vast diversity of induction protocols that can be found in the literature. These differences can take various forms, such as the number of spikes used, the number of repetitions, the frequency, and the delay between the whole-cell configuration and the induction (see **Chapter II**). Although this diversity of efficient protocols can be seen as evidence that STDP is a widespread phenomenon, this may render comparison between studies difficult and unreliable. This can create confusion in the field and may lead to disagreements in the literature.

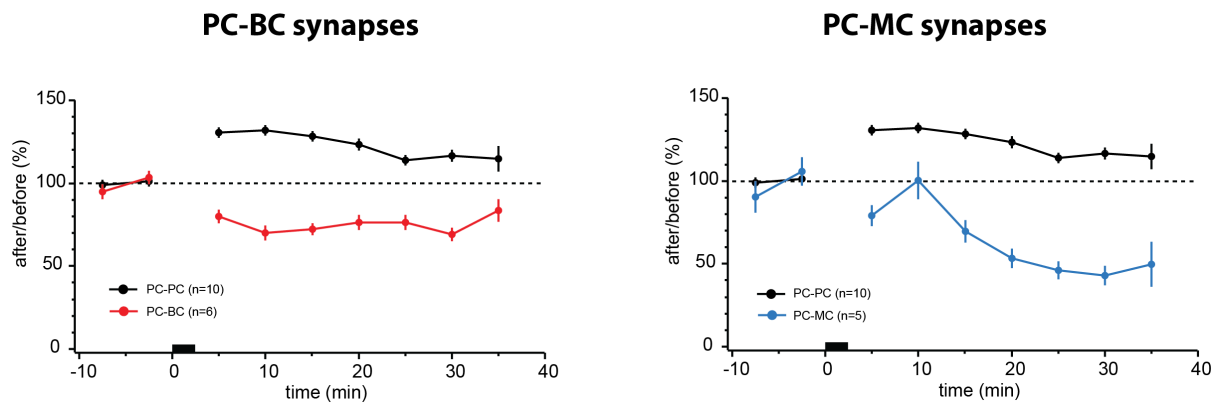


Figure 3.16: STDP at PC-PC and PC-IN synapses

While a 50 Hz induction protocol reliably induced LTP of PC-PC synapses (black, after/before = $120\% \pm 7\%$, $n = 10$ pairs, $p < 0.05$), the same protocol consistently led to LTD at both PC-BC (left, red, after/before = $74\% \pm 7\%$, $n = 6$ pairs, $p < 0.05$ and PC_MC (right, blue) synapses (after/before = $54\% \pm 10\%$, $n = 5$ pairs, $p < 0.05$).

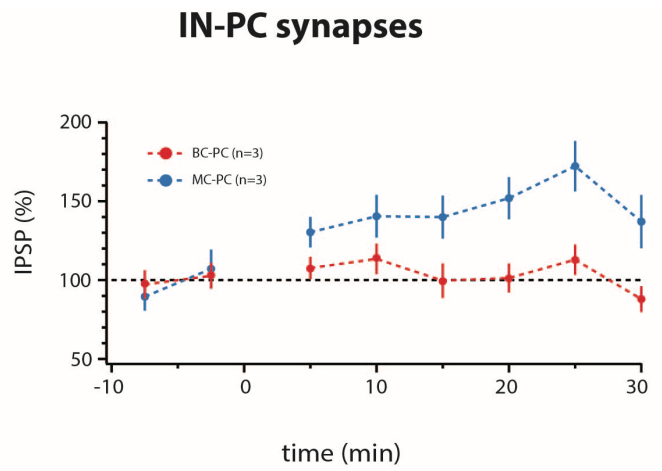


Figure 3.17: STDP at IN-PC synapses

The same 50 Hz induction protocol applied at BC-PC (red) did not produce any change in IPSPs amplitude. However, at MC-PC synapses (blue), a strong LTP of inhibition was observed.

Chapter IV: Concluding remarks

Using a combination of paired recordings, 2PLSM and uncaging, I demonstrate that in neocortical L5 CP-AMPARs are not expressed by all INs: PC-BC synapses express CP-AMPARs, while PC-MC and PC-PC connections predominantly carry CI-AMPARs. Furthermore, combining computer modeling and dynamic clamp recordings, we also find that CP-AMPARs may sharpen BC-mediated feed-forward inhibition. Moreover, PC-BC synapses seem to express less postsynaptic NMDARs than PC-MC and PC-PC connections do, relative to their amount of AMPARs. The Sjöström lab previously demonstrated that PC-MC and PC-PC but not PC-BC connections express preNMDARs (see Buchanan et al., 2012). Finally, based on this data we emit the hypothesis that long-term plasticity may differ between those synapse types, due to the established roles of CP-AMPARs and NMDARs in plasticity. Here we observed that plasticity differs between excitatory inputs onto excitatory or inhibitory cells of the BC and MC types.

The present thesis consists of three distinct results sections, but these are interlinked, as they all share a common context. For example, all results relate to specific aspects of synaptic transmission or plasticity at the same three types of connections in neocortical L5: PC-PC, PC-BC and PC-MC synapses (**figure 4.1**). Importantly, the thesis focuses on CP-AMPARs, and results on NMDARs as well as plasticity are only presented as supplementary information. Even though we tried to relate synaptic composition to long-term plasticity, no direct link could be established. Although we observed a synapse-specific plasticity, the outcome was only different when comparing PC-PC and PC-IN synapses, but not between PC-BC and PC-MC connections. Indeed, while PC-PC and PC-MC connections seemed to have similar

synaptic compositions in pre and postsynaptic NMDARs and AMPARs, PC-BC connections differed on those points. Yet, PC-BC and PC-MC synapses showed the same outcome in plasticity. Thus the different plasticity at PC-PC and PC-IN synapses cannot only be explained by the composition in AMPARs and NMDARs.

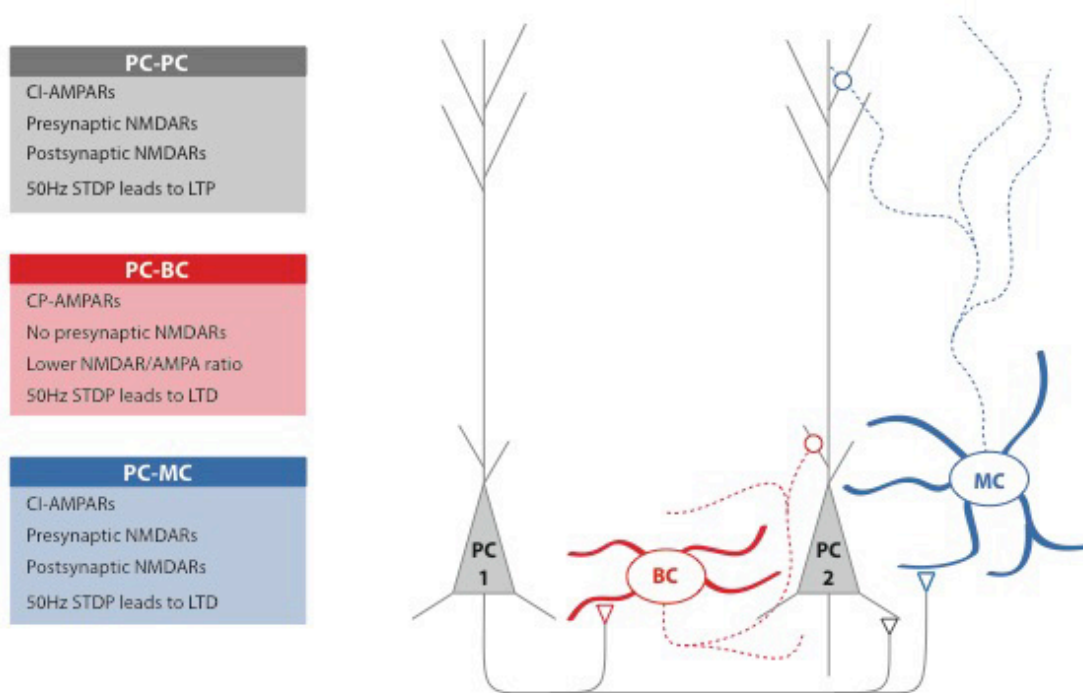


Figure 4.1: Conclusion

On the one hand we found a synapse-specific expression of CP-AMPA at PC-BC synapses only while PC-PC and PC-MC synapses carry CI-AMPA. On the other hand we observe that preNMDARs are specifically expressed at PC-PC and PC-MC but not PC-BC synapses. We also observed a lower NMDAR/AMPA at PC-BC compared to PC-PC and PC-MC synapses, suggesting the former express less NMDARs. Finally, in an attempt to link synaptic composition and plasticity, we found that while a high frequency STDP induction protocol leads to LTP of PC-PC connections, both PC-BC and PC-MC synapses consistently undergo LTD when using the same protocol.

Appendices

Appendix 1: List of publications

(* indicates co-authorship)

Lalanne T*, Oyrer J*, Mancino A, Farrant M & Sjöström PJ: Synapse-specific expression of calcium-permeable AMPA receptors in neocortical Layer V inhibitory neurons. (2015), submitted to *Journal of Physiology*

Contribution: I performed most of the experiments, i.e. all paired recordings, AMPA uncaging and dynamic clamp recordings. I also analyzed all the corresponding data and wrote the manuscript.

Lalanne T, Abrahamsson T, & Sjöström PJ: Using quadruple whole-cell recordings to study spike-timing-dependent plasticity in acute neocortical slices. (2015), in press (*Cold Spring Harbor Laboratory Protocols*)

Contribution: I performed the experiments, analyzed the data and wrote the manuscript.

Lalanne T*, Abrahamsson T*, Watt AJ & Sjöström PJ: In-vitro investigation of synaptic plasticity (2015), in press (*Cold Spring Harbor Laboratory Press*)

Contribution: I wrote the manuscript together with the other authors.

Guangfu W, Daniel RW, Weiguo Y, Yiqing W, Lana C. M, **Lalanne T**, Jiang X, Ying S, Qian-Quan S & Zhu JJ: An optogenetics- and imaging-assisted simultaneous multiple patch-clamp recordings system for decoding complex neural circuits (2015) *Nature Protocols*, 10(3):397-412. doi: 10.1038/nprot.2015.019

Contribution: I performed multiple whole-cell recordings and gave input that contributed in improving the technology. I also participated in writing the manuscript.

Blackman AV, Abrahamsson T, Costa RP, **Lalanne T** & Sjöström PJ: Target-cell-specific short-term plasticity in local circuits. (2013) *Frontiers in Synaptic Neuroscience* 5:11, DOI: 10.3389/fnsyn.2013.00011

Contribution: I participated in writing the manuscript.

Buchanan KA, Blackman AV, Moreau AW, Elgar D, Costa RP, **Lalanne T**, Tudor Jones AA, Oyrer J & Sjöström PJ: Target-Specific Expression of Presynaptic NMDA Receptors in Neocortical Microcircuits. (2012) *Neuron* 75:451-466

Contribution: I performed paired recordings, MNI-glutamate uncaging and calcium imaging to show the absence of presynaptic NMDARs at PC-IN connections and the specificity of MNI-NMDA uncaging.

Appendix 2: List of posters and presentations

(* indicates the presenting author)

Posters

Lalanne T*, Oyrer J, Gregor E, Mancino A, Burwell S, Farrant M & Sjöström PJ: Synapse-specific expression of calcium-permeable AMPA receptors in neocortical layer-5 sharpens basket cell-mediated inhibition (2015) *Annual meeting of the Society for Neuroscience*

Lalanne T, Oyrer J*, Costa RP, Chung AJ, Farrant M & Sjöström PJ: Calcium-permeable AMPA receptors and synapse-specific plasticity in the neocortical layer-5 microcircuit. (2014) *Proceedings of the Physiological Society*, London, UK

Lalanne T*, Oyrer J, Costa RP, Chung AJ, Farrant M & Sjöström PJ: Synapse-specific plasticity in the neocortical layer-5 microcircuit. (2014) *Association for Canadian Neuroscience meeting, Montreal, Quebec, Canada*

Lalanne T, Oyrer J*, Chung AJ, Sjöström PJ & Farrant M: Calcium-permeable AMPARs in local circuits of mouse visual neocortex. (2013) *Annual meeting of the Society for Neuroscience*

Lalanne T*, Oyrer J, Chung A, Farrant M & Sjöström PJ: Synapse-specific expression of Cp-AMPA receptors in neocortical inhibitory neurons. (2013) *Annual retreat of the Integrated Program in Neuroscience of McGill University*, Montreal, Quebec, Canada

Sjöström PJ*, Moreau AW, Buchanan KA, Blackman AV, Elgar D, Costa RP, **Lalanne T**, Tudor Jones AA & Oyrer J: Target-specific expression of presynaptic NMDA receptors in neocortical microcircuits. (2013) *FENS Featured Regional Meeting*, Prague, Czech Republic

Moreau AW*, Buchanan KA, Blackman AV, Elgar D, Costa RP, **Lalanne T**, Tudor Jones AA, Oyrer J & Sjöström PJ: Target-specific expression of presynaptic NMDA receptors in neocortical microcircuits. (2013) *11e Colloque de la Société des Neurosciences*, Lyon, France

Blackman AV*, Buchanan KA, Moreau AW, Elgar D, Costa RP, **Lalanne T**, Tudor Jones AA, Oyrer J & Sjöström PJ: Target-specific expression of presynaptic NMDA receptors in neocortical microcircuits. (2012) *Annual meeting of the Society for Neuroscience*

Presentations

Lalanne T*, Synapse-specific expression of Cp-AMPA receptors in neocortical inhibitory neurons (2015). Invited seminar hosted by Dr. Bo Li and Dr. Hiro Furukawa at the *Cold Spring Harbor Laboratory*, Laurel Hollow, NY, USA.

Lalanne T*, Synapse-specific expression of Cp-AMPA receptors in neocortical inhibitory neurons (2015). Invited seminar hosted by Dr. Lisa Topolnik at the Mental Health Research Institute of Laval University, Quebec, Quebec, Canada.

Lalanne T*, Synapse-specific plasticity and expression of Cp-AMPA receptors in neocortical microcircuits. (2014) *Workshop on novel tools to study the neocortical circuits*, Meon Springs, United Kingdom

Lalanne T*, Synapse-specific expression of Cp-AMPA receptors in neocortical inhibitory neurons (2014). *The Molecular Neuroscience Group meeting*, Montreal, Quebec, Canada

Lalanne T*, Techniques of the 21st Century. (2012) Invited presentation at *the Retreat of the Integrated Program in neuroscience of McGill University*, Montreal, Quebec, Canada

References

Abbott LF, Nelson SB (2000) Synaptic plasticity: taming the beast. *Nature Neuroscience* 3:1178-1183.

Abbott LF, Regehr WG (2004) Synaptic computation. *Nature* 431:796-803.

Ady V, Perroy J, Tricoire L, Piochon C, Dadak S, Chen X, Dusart I, Fagni L, Lambolez B, Levenes C (2014) Type 1 metabotropic glutamate receptors (mGlu1) trigger the gating of GluD2 delta glutamate receptors. *EMBO Rep* 15:103-109.

Andjelic S, Gallopin T, Cauli B, Hill EL, Roux L, Badr S, Hu E, Tamas G, Lambolez B (2009) Glutamatergic nonpyramidal neurons from neocortical layer VI and their comparison with pyramidal and spiny stellate neurons. *J Neurophysiol* 101:641-654.

Angulo MC, Lambolez B, Audinat E, Hestrin S, Rossier J (1997) Subunit composition, kinetic, and permeation properties of AMPA receptors in single neocortical nonpyramidal cells. *J Neurosci* 17:6685-6696.

Angulo MC, Staiger JF, Rossier J, Audinat E (1999) Developmental synaptic changes increase the range of integrative capabilities of an identified excitatory neocortical connection. *J Neurosci* 19:1566-1576.

Antonucci F, Alpar A, Kacza J, Caleo M, Verderio C, Giani A, Martens H, Chaudhry FA, Allegra M, Grosche J, Michalski D, Erck C, Hoffmann A, Harkany T, Matteoli M, Hartig W (2012) Cracking down on inhibition: selective removal of GABAergic interneurons from hippocampal networks. *J Neurosci* 32:1989-2001.

Aponte Y, Bischofberger J, Jonas P (2008) Efficient Ca²⁺ buffering in fast-spiking basket cells of rat hippocampus. *J Physiol* 586:2061-2075.

Ascher P, Nowak L (1988) The role of divalent cations in the N-methyl-D-aspartate responses of mouse central neurones in culture. *J Physiol* 399:247-266.

Ascoli GA, Alonso-Nanclares L, Anderson SA, Barrionuevo G, Benavides-Piccione R, Burkhalter A, Buzsaki G, Cauli B, Defelipe J, Fairen A, Feldmeyer D, Fishell G, Fregnac Y, Freund TF, Gardner D, Gardner EP, Goldberg JH, Helmstaedter M, Hestrin S, Karube F, Kisvarday ZF, Lambolez B, Lewis DA, Marin O, Markram H, Munoz A, Packer A, Petersen CC, Rockland KS, Rossier J, Rudy B, Somogyi P, Staiger JF, Tamas G, Thomson AM, Toledo-Rodriguez M, Wang Y, West DC, Yuste R (2008) Petilla terminology: nomenclature of features of GABAergic interneurons of the cerebral cortex. *Nat Rev Neurosci* 9:557-568.

Atallah BV, Bruns W, Carandini M, Scanziani M (2012) Parvalbumin-expressing interneurons linearly transform cortical responses to visual stimuli. *Neuron* 73:159-170.

Atasoy D, Ertunc M, Moulder KL, Blackwell J, Chung C, Su J, Kavalali ET (2008) Spontaneous and evoked glutamate release activates two populations of NMDA receptors with limited overlap. *J Neurosci* 28:10151-10166.

Ayalon G, Stern-Bach Y (2001) Functional assembly of AMPA and kainate receptors is mediated by several discrete protein-protein interactions. *Neuron* 31:103-113.

Bar-Ilan L, Gidon A, Segev I (2012) The role of dendritic inhibition in shaping the plasticity of excitatory synapses. *Front Neural Circuits* 6:118.

Barbour B, Brunel N, Hakim V, Nadal JP (2007) What can we learn from synaptic weight distributions? *Trends in neurosciences* 30:622-629.

Barbour B, Isope P (2000) Combining loose cell-attached stimulation and recording. *J Neurosci Methods* 103:199-208.

Bardoni R, Torsney C, Tong CK, Prandini M, MacDermott AB (2004) Presynaptic NMDA receptors modulate glutamate release from primary sensory neurons in rat spinal cord dorsal horn. *J Neurosci* 24:2774-2781.

Bats C, Soto D, Studniarczyk D, Farrant M, Cull-Candy SG (2012) Channel properties reveal differential expression of TARPed and TARPlless AMPARs in stargazer neurons. *Nat Neurosci* 15:853-861.

Beaulieu C, Colonnier M (1985) A comparison of the number of neurons in individual laminae of cortical areas 17, 18 and posteromedial suprasylvian (PMLS) area in the cat. *Brain Res* 339:166-170.

Beaulieu C, Kisvarday Z, Somogyi P, Cynader M, Cowey A (1992) Quantitative distribution of GABA-immunopositive and -immunonegative neurons and synapses in the monkey striate cortex (area 17). *Cereb Cortex* 2:295-309.

Bekkers JM, Clements JD (1999) Quantal amplitude and quantal variance of strontium-induced asynchronous EPSCs in rat dentate granule neurons. *J Physiol* 516 (Pt 1):227-248.

Bekkers JM, Stevens CF (1996) Cable properties of cultured hippocampal neurons determined from sucrose-evoked miniature EPSCs. *J Neurophysiol* 75:1250-1255.

Bender VA, Bender KJ, Brasier DJ, Feldman DE (2006) Two coincidence detectors for spike timing-dependent plasticity in somatosensory cortex. *J Neurosci* 26:4166-4177.

Berger TK, Silberberg G, Perin R, Markram H (2010) Brief bursts self-inhibit and correlate the pyramidal network. *PLoS biology* 8.

Berretta N, Jones RS (1996) Tonic facilitation of glutamate release by presynaptic N-methyl-D-aspartate autoreceptors in the entorhinal cortex. *Neuroscience* 75:339-344.

Bi GQ, Poo MM (1998) Synaptic modifications in cultured hippocampal neurons: dependence on spike timing, synaptic strength, and postsynaptic cell type. *Journal of Neuroscience* 18:10464-10472.

Bidoret C, Ayon A, Barbour B, Casado M (2009) Presynaptic NR2A-containing NMDA receptors implement a high-pass filter synaptic plasticity rule. *Proceedings of the National Academy of Sciences of the United States of America* 106:14126-14131.

Blackman AV, Abrahamsson T, Costa RP, Lalanne T, Sjöström PJ (2013) Target Cell-Specific Short-Term Plasticity in Local Circuits. *Frontiers in Synaptic Neuroscience* 5.

Blackman AV, Grabuschnig S, Legenstein R, Sjöström PJ (2014) A comparison of manual neuronal reconstruction from biocytin histology or 2-photon imaging: morphometry and computer modeling. *Front Neuroanat* 8:65.

Bliss TV, Collingridge GL (1993) A synaptic model of memory: long-term potentiation in the hippocampus. *Nature* 361:31-39.

Bliss TV, Lømo T (1973) Long-lasting potentiation of synaptic transmission in the dentate area of the anaesthetized rabbit following stimulation of the perforant path. *Journal of Physiology* 232:331-356.

Bortone DS, Olsen SR, Scanziani M (2014) Translaminar inhibitory cells recruited by layer 6 corticothalamic neurons suppress visual cortex. *Neuron* 82:474-485.

Bourque CW (2008) Central mechanisms of osmosensation and systemic osmoregulation. *Nat Rev Neurosci* 9:519-531.

Bowie D, Lange GD, Mayer ML (1998) Activity-dependent modulation of glutamate receptors by polyamines. *J Neurosci* 18:8175-8185.

Bowie D, Mayer ML (1995) Inward rectification of both AMPA and kainate subtype glutamate receptors generated by polyamine-mediated ion channel block. *Neuron* 15:453-462.

Brasier DJ, Feldman DE (2008) Synapse-specific expression of functional presynaptic NMDA receptors in rat somatosensory cortex. *J Neurosci* 28:2199-2211.

Buchanan KA, Blackman AV, Moreau AW, Elgar D, Costa RP, Lalanne T, Tudor Jones AA, Oyrer J, Sjöström PJ (2012) Target-Specific Expression of Presynaptic NMDA Receptors in Neocortical Microcircuits. *Neuron* 75:451-466.

Buchanan KA, Mellor JR (2007) The development of synaptic plasticity induction rules and the requirement for postsynaptic spikes in rat hippocampal CA1 pyramidal neurones. *The Journal of physiology* 585:429-445.

Buchanan KA, Mellor JR (2010) The activity requirements for spike timing-dependent plasticity in the hippocampus. *Frontiers in Synaptic Neuroscience* 2.

Burnashev N, Zhou Z, Neher E, Sakmann B (1995) Fractional calcium currents through recombinant GluR channels of the NMDA, AMPA and kainate receptor subtypes. *J Physiol* 485 (Pt 2):403-418.

Callaway EM (1998) Local circuits in primary visual cortex of the macaque monkey. *Annu Rev Neurosci* 21:47-74.

Camire O, Topolnik L (2014) Dendritic calcium nonlinearities switch the direction of synaptic plasticity in fast-spiking interneurons. *J Neurosci* 34:3864-3877.

Cammalleri M, Martini D, Timperio AM, Bagnoli P (2009) Functional effects of somatostatin receptor 1 activation on synaptic transmission in the mouse hippocampus. *J Neurochem* 111:1466-1477.

Cardin JA, Carlen M, Meletis K, Knoblich U, Zhang F, Deisseroth K, Tsai LH, Moore CI (2009) Driving fast-spiking cells induces gamma rhythm and controls sensory responses. *Nature* 459:663-667.

Casado M, Dieudonne S, Ascher P (2000) Presynaptic N-methyl-D-aspartate receptors at the parallel fiber-Purkinje cell synapse. PNAS 97:11593-11597.

Casado M, Isope P, Ascher P (2002) Involvement of presynaptic N-methyl-D-aspartate receptors in cerebellar long-term depression. Neuron 33:123-130.

Cathala L, Holderith NB, Nusser Z, DiGregorio DA, Cull-Candy SG (2005) Changes in synaptic structure underlie the developmental speeding of AMPA receptor-mediated EPSCs. Nat Neurosci 8:1310-1318.

Cauli B, Audinat E, Lambolez B, Angulo MC, Ropert N, Tsuzuki K, Hestrin S, Rossier J (1997) Molecular and physiological diversity of cortical nonpyramidal cells. The Journal of neuroscience : the official journal of the Society for Neuroscience 17:3894-3906.

Celio MR (1986) Parvalbumin in most gamma-aminobutyric acid-containing neurons of the rat cerebral cortex. Science 231:995-997.

Chattopadhyaya B, Di Cristo G, Higashiyama H, Knott GW, Kuhlman SJ, Welker E, Huang ZJ (2004) Experience and activity-dependent maturation of perisomatic GABAergic innervation in primary visual cortex during a postnatal critical period. J Neurosci 24:9598-9611.

Christie JM, Jahr CE (2008) Dendritic NMDA receptors activate axonal calcium channels. *Neuron* 60:298-307.

Clopath C, Büsing L, Vasilaki E, Gerstner W (2010) Connectivity reflects coding: a model of voltage-based STDP with homeostasis. *Nat Neurosci* 13:344-352.

Collingridge GL, Lester RA (1989) Excitatory amino acid receptors in the vertebrate central nervous system. *Pharmacological reviews* 41:143-210.

Collingridge GL, Peineau S, Howland JG, Wang YT (2010) Long-term depression in the CNS. *Nat Rev Neurosci* 11:459-473.

Colquhoun D, Jonas P, Sakmann B (1992) Action of brief pulses of glutamate on AMPA/kainate receptors in patches from different neurones of rat hippocampal slices. *J Physiol* 458:261-287.

Conde F, Lund JS, Jacobowitz DM, Baimbridge KG, Lewis DA (1994) Local circuit neurons immunoreactive for calretinin, calbindin D-28k or parvalbumin in monkey prefrontal cortex: distribution and morphology. *J Comp Neurol* 341:95-116.

Constantinople CM, Bruno RM (2013) Deep cortical layers are activated directly by thalamus. *Science* 340:1591-1594.

Corlew R, Wang Y, Ghermazien H, Erisir A, Philpot BD (2007) Developmental switch in the contribution of presynaptic and postsynaptic NMDA receptors to long-term depression. *J Neurosci* 27:9835-9845.

Cotman CW, Monaghan DT, Ganong AH (1988) Excitatory amino acid neurotransmission: NMDA receptors and Hebb-type synaptic plasticity. *Annu Rev Neurosci* 11:61-80.

Cull-Candy S, Kelly L, Farrant M (2006) Regulation of Ca²⁺-permeable AMPA receptors: synaptic plasticity and beyond. *Curr Opin Neurobiol* 16:288-297.

da Costa NM, Martin KA (2011) How thalamus connects to spiny stellate cells in the cat's visual cortex. *J Neurosci* 31:2925-2937.

Davie JT, Kole MH, Letzkus JJ, Rancz EA, Spruston N, Stuart GJ, Hausser M (2006) Dendritic patch-clamp recording. *Nature protocols* 1:1235-1247.

Dayan P, Abbott LF (2001) *Theoretical Neuroscience: Computational and Mathematical Modeling of Neural Systems*. Cambridge, MA, USA: The MIT Press.

Debanne D, Boudkkazi S, Campanac E, Cudmore RH, Giraud P, Fronzaroli-Molinieres L, Carlier E, Caillard O (2008) Paired-recordings from

synaptically coupled cortical and hippocampal neurons in acute and cultured brain slices. *Nature protocols* 3:1559-1568.

DeFelipe J (2013) Cajal and the discovery of a new artistic world: the neuronal forest. *Prog Brain Res* 203:201-220.

DeFelipe J, Farinas I (1992) The pyramidal neuron of the cerebral cortex: morphological and chemical characteristics of the synaptic inputs. *Progress in neurobiology* 39:563-607.

DeFelipe J, Lopez-Cruz PL, Benavides-Piccione R, Bielza C, Larranaga P, Anderson S, Burkhalter A, Cauli B, Fairen A, Feldmeyer D, Fishell G, Fitzpatrick D, Freund TF, Gonzalez-Burgos G, Hestrin S, Hill S, Hof PR, Huang J, Jones EG, Kawaguchi Y, Kisvarday Z, Kubota Y, Lewis DA, Marin O, Markram H, McBain CJ, Meyer HS, Monyer H, Nelson SB, Rockland K, Rossier J, Rubenstein JL, Rudy B, Scanziani M, Shepherd GM, Sherwood CC, Staiger JF, Tamas G, Thomson A, Wang Y, Yuste R, Ascoli GA (2013) New insights into the classification and nomenclature of cortical GABAergic interneurons. *Nat Rev Neurosci* 14:202-216.

Demeulemeester H, Arckens L, Vandesande F, Orban GA, Heizmann CW, Pochet R (1991) Calcium binding proteins and neuropeptides as molecular markers of GABAergic interneurons in the cat visual cortex. *Exp Brain Res* 84:538-544.

Donevan SD, Rogawski MA (1995) Intracellular polyamines mediate inward rectification of Ca(2+)-permeable alpha-amino-3-hydroxy-5-methyl-4-isoxazolepropionic acid receptors. PNAS 92:9298-9302.

Duguid I, Sjöström PJ (2006) Novel presynaptic mechanisms for coincidence detection in synaptic plasticity. Curr Opin Neurobiol 16:312-322.

Duguid IC, Smart TG (2004) Retrograde activation of presynaptic NMDA receptors enhances GABA release at cerebellar interneuron-Purkinje cell synapses. NatNeurosci 7:525-533.

Dumitriu D, Cossart R, Huang J, Yuste R (2007) Correlation between axonal morphologies and synaptic input kinetics of interneurons from mouse visual cortex. Cereb Cortex 17:81-91.

Everitt BS, Landau S, Leese M, Stahl D (2011) Cluster Analysis. Chichester, UK: John Wiley & Sons Ltd.

Feldman DE (2012) The spike-timing dependence of plasticity. Neuron 75:556-571.

Feldmeyer D, Egger V, Lübke J, Sakmann B (1999) Reliable synaptic connections between pairs of excitatory layer 4 neurones within a single 'barrel' of developing rat somatosensory cortex. J Physiol 521 Pt 1:169-190.

Ferreira TA, Blackman AV, Oyrer J, Jayabal S, Chung AJ, Watt AJ, Sjostrom PJ, van Meyel DJ (2014) Neuronal morphometry directly from bitmap images. *Nature methods* 11:982-984.

Fino E, Venance L (2010) Spike-timing dependent plasticity in the striatum. *Frontiers in Synaptic Neuroscience* 2.

Fino E, Yuste R (2011) Dense inhibitory connectivity in neocortex. *Neuron* 69:1188-1203.

Fleming JJ, England PM (2010) AMPA receptors and synaptic plasticity: a chemist's perspective. *Nat Chem Biol* 6:89-97.

Fogarty M, Grist M, Gelman D, Marin O, Pachnis V, Kessaris N (2007) Spatial genetic patterning of the embryonic neuroepithelium generates GABAergic interneuron diversity in the adult cortex. *J Neurosci* 27:10935-10946.

Fortune ES, Rose GJ (2001) Short-term synaptic plasticity as a temporal filter. *Trends Neurosci* 24:381-385.

Froemke RC, Poo MM, Dan Y (2005) Spike-timing-dependent synaptic plasticity depends on dendritic location. *Nature* 434:221-225.

Fuhrmann G, Segev I, Markram H, Tsodyks M (2002) Coding of temporal information by activity-dependent synapses. *J Neurophysiol* 87:140-148.

Fukaya M, Tsujita M, Yamazaki M, Kushiya E, Abe M, Akashi K, Natsume R, Kano M, Kamiya H, Watanabe M, Sakimura K (2006) Abundant distribution of TARP gamma-8 in synaptic and extrasynaptic surface of hippocampal neurons and its major role in AMPA receptor expression on spines and dendrites. *Eur J Neurosci* 24:2177-2190.

Fukuda T, Kosaka T (2000) Gap junctions linking the dendritic network of GABAergic interneurons in the hippocampus. *J Neurosci* 20:1519-1528.

Galarreta M, Hestrin S (1999) A network of fast-spiking cells in the neocortex connected by electrical synapses. *Nature* 402:72-75.

Geiger JR, Lubke J, Roth A, Frotscher M, Jonas P (1997) Submillisecond AMPA receptor-mediated signaling at a principal neuron-interneuron synapse. *Neuron* 18:1009-1023.

Geiger JR, Melcher T, Koh DS, Sakmann B, Seeburg PH, Jonas P, Monyer H (1995) Relative abundance of subunit mRNAs determines gating and Ca²⁺ permeability of AMPA receptors in principal neurons and interneurons in rat CNS. *Neuron* 15:193-204.

Gentet LJ, Kremer Y, Taniguchi H, Huang ZJ, Staiger JF, Petersen CC (2012) Unique functional properties of somatostatin-expressing GABAergic neurons in mouse barrel cortex. *Nat Neurosci* 15:607-612.

Gerstner W, Kempter R, van Hemmen JL, Wagner H (1996) A neuronal learning rule for sub-millisecond temporal coding. *Nature* 383:76-81.

Gidon A, Segev I (2012) Principles governing the operation of synaptic inhibition in dendrites. *Neuron* 75:330-341.

Goldberg JH, Lacefield CO, Yuste R (2004) Global dendritic calcium spikes in mouse layer 5 low threshold spiking interneurons: implications for control of pyramidal cell bursting. *J Physiol* 558:465-478.

Goldberg JH, Tamas G, Aronov D, Yuste R (2003a) Calcium microdomains in aspiny dendrites. *Neuron* 40:807-821.

Goldberg JH, Tamas G, Yuste R (2003b) Ca^{2+} imaging of mouse neocortical interneurone dendrites: Ia-type K^+ channels control action potential backpropagation. *J Physiol* 551:49-65.

Golding NL, Staff NP, Spruston N (2002) Dendritic spikes as a mechanism for cooperative long-term potentiation. *Nature* 418:326-331.

Gonchar Y, Burkhalter A (1997) Three distinct families of GABAergic neurons in rat visual cortex. *Cereb Cortex* 7:347-358.

Gonchar Y, Wang Q, Burkhalter A (2007) Multiple distinct subtypes of GABAergic neurons in mouse visual cortex identified by triple immunostaining. *Front Neuroanat* 1:3.

Greger IH, Khatri L, Kong X, Ziff EB (2003) AMPA receptor tetramerization is mediated by Q/R editing. *Neuron* 40:763-774.

Gupta A, Wang Y, Markram H (2000) Organizing principles for a diversity of GABAergic interneurons and synapses in the neocortex. *Science* 287:273-278.

Hardie J, Spruston N (2009) Synaptic depolarization is more effective than back-propagating action potentials during induction of associative long-term potentiation in hippocampal pyramidal neurons. *J Neurosci* 29:3233-3241.

Harris KD, Mrsic-Flogel TD (2013) Cortical connectivity and sensory coding. *Nature* 503:51-58.

Harris KD, Shepherd GM (2015) The neocortical circuit: themes and variations. *Nat Neurosci* 18:170-181.

Hebb DO (1949) *The Organization of Behavior*. New York: Wiley.

Hendry SH, Schwark HD, Jones EG, Yan J (1987) Numbers and proportions of GABA-immunoreactive neurons in different areas of monkey cerebral cortex. *J Neurosci* 7:1503-1519.

Hestrin S (1993) Different glutamate receptor channels mediate fast excitatory synaptic currents in inhibitory and excitatory cortical neurons. *Neuron* 11:1083-1091.

Hof PR, Glezer, II, Conde F, Flagg RA, Rubin MB, Nimchinsky EA, Vogt Weisenhorn DM (1999) Cellular distribution of the calcium-binding proteins parvalbumin, calbindin, and calretinin in the neocortex of mammals: phylogenetic and developmental patterns. *J Chem Neuroanat* 16:77-116.

Holmgren C, Harkany T, Svennenfors B, Zilberter Y (2003) Pyramidal cell communication within local networks in layer 2/3 of rat neocortex. *J Physiol* 551:139-153.

Huang S, Huganir RL, Kirkwood A (2013) Adrenergic gating of Hebbian spike-timing-dependent plasticity in cortical interneurons. *J Neurosci* 33:13171-13178.

Huang S, Treviño M, He K, Ardiles A, Pasquale Rd, Guo Y, Palacios A, Huganir R, Kirkwood A (2012) Pull-push neuromodulation of LTP and LTD enables bidirectional experience-induced synaptic scaling in visual cortex. *Neuron* 73:497-510.

Hughes GM, Tauc L (1968) A direct synaptic connexion between the left and right giant cells in *Aplysia*. *J Physiol* 197:511-527.

Hull C, Isaacson JS, Scanziani M (2009) Postsynaptic mechanisms govern the differential excitation of cortical neurons by thalamic inputs. *J Neurosci* 29:9127-9136.

Hume RI, Dingledine R, Heinemann SF (1991) Identification of a site in glutamate receptor subunits that controls calcium permeability. *Science* 253:1028-1031.

Humeau Y, Shaban H, Bissière S, Lüthi A (2003) Presynaptic induction of heterosynaptic associative plasticity in the mammalian brain. *Nature* 426:841-845.

Ikeda K, Nagasawa M, Mori H, Araki K, Sakimura K, Watanabe M, Inoue Y, Mishina M (1992) Cloning and expression of the epsilon 4 subunit of the NMDA receptor channel. *FEBS Lett* 313:34-38.

Ishii T, Moriyoshi K, Sugihara H, Sakurada K, Kadotani H, Yokoi M, Akazawa C, Shigemoto R, Mizuno N, Masu M, et al. (1993) Molecular characterization of the family of the N-methyl-D-aspartate receptor subunits. *J Biol Chem* 268:2836-2843.

Jackson AC, Milstein AD, Soto D, Farrant M, Cull-Candy SG, Nicoll RA (2011) Probing TARP modulation of AMPA receptor conductance with polyamine toxins. *J Neurosci* 31:7511-7520.

Jiang X, Wang G, Lee AJ, Stornetta RL, Zhu JJ (2013) The organization of two new cortical interneuronal circuits. *Nat Neurosci* 16:210-218.

Jonas P, Racca C, Sakmann B, Seeburg PH, Monyer H (1994) Differences in Ca²⁺ permeability of AMPA-type glutamate receptor channels in neocortical neurons caused by differential GluR-B subunit expression. *Neuron* 12:1281-1289.

Jonas P, Sakmann B (1992) Glutamate receptor channels in isolated patches from CA1 and CA3 pyramidal cells of rat hippocampal slices. *J Physiol* 455:143-171.

Kaesler PS, Regehr WG (2014) Molecular mechanisms for synchronous, asynchronous, and spontaneous neurotransmitter release. *Annu Rev Physiol* 76:333-363.

Kaiser KM, Lübke J, Zilberter Y, Sakmann B (2004) Postsynaptic calcium influx at single synaptic contacts between pyramidal neurons and bitufted interneurons in layer 2/3 of rat neocortex is enhanced by backpropagating action potentials. *J Neurosci* 24:1319-1329.

Kakegawa W, Kohda K, Yuzaki M (2007) The delta2 'ionotropic' glutamate receptor functions as a non-ionotropic receptor to control cerebellar synaptic plasticity. *J Physiol* 584:89-96.

Kamboj SK, Swanson GT, Cull-Candy SG (1995) Intracellular spermine confers rectification on rat calcium-permeable AMPA and kainate receptors. *J Physiol* 486 (Pt 2):297-303.

Kapfer C, Glickfeld LL, Atallah BV, Scanziani M (2007) Supralinear increase of recurrent inhibition during sparse activity in the somatosensory cortex. *Nat Neurosci* 10:743-753.

Karube F, Kubota Y, Kawaguchi Y (2004) Axon branching and synaptic bouton phenotypes in GABAergic nonpyramidal cell subtypes. *J Neurosci* 24:2853-2865.

Kato AS, Gill MB, Ho MT, Yu H, Tu Y, Siuda ER, Wang H, Qian YW, Nisenbaum ES, Tomita S, Brecht DS (2010) Hippocampal AMPA receptor gating controlled by both TARP and cornichon proteins. *Neuron* 68:1082-1096.

Kätzel D, Zemelman BV, Buetfering C, Wölfel M, Miesenböck G (2011) The columnar and laminar organization of inhibitory connections to neocortical excitatory cells. *Nature neuroscience* 14:100-107.

Kawaguchi Y, Karube F, Kubota Y (2006) Dendritic branch typing and spine expression patterns in cortical nonpyramidal cells. *Cereb Cortex* 16:696-711.

Kawaguchi Y, Kubota Y (1996) Physiological and morphological identification of somatostatin- or vasoactive intestinal polypeptide-containing cells among GABAergic cell subtypes in rat frontal cortex. *J Neurosci* 16:2701-2715.

Kawaguchi Y, Kubota Y (1997) GABAergic cell subtypes and their synaptic connections in rat frontal cortex. *Cerebral cortex* 7:476-486.

Keinanen K, Wisden W, Sommer B, Werner P, Herb A, Verdoorn TA, Sakmann B, Seeburg PH (1990) A family of AMPA-selective glutamate receptors. *Science* 249:556-560.

Kemenes I, Marra V, Crossley M, Samu D, Staras K, Kemenes G, Nowotny T (2011) Dynamic clamp with StdpC software. *Nature protocols* 6:405-417.

Kepecs A, Fishell G (2014) Interneuron cell types are fit to function. *Nature* 505:318-326.

Kessarlis N, Magno L, Rubin AN, Oliveira MG (2014) Genetic programs controlling cortical interneuron fate. *Curr Opin Neurobiol* 26:79-87.

Kirkwood A, Bear MF (1994) Hebbian synapses in visual cortex. *Journal of Neuroscience* 14:1634-1645.

Kirkwood A, Dudek SM, Gold JT, Aizenman CD, Bear MF (1993) Common forms of synaptic plasticity in the hippocampus and neocortex in vitro. *Science* 260:1518-1521.

Kirkwood A, Lee HK, Bear MF (1995) Co-regulation of long-term potentiation and experience-dependent synaptic plasticity in visual cortex by age and experience. *Nature* 375:328-331.

Kisvarday ZF (1992) GABAergic networks of basket cells in the visual cortex. *Prog Brain Res* 90:385-405.

Ko H, Hofer SB, Pichler B, Buchanan KA, Sjöström PJ, Mrcic-Flogel TD (2011) Functional specificity of local synaptic connections in neocortical networks. *Nature* 473:87-91.

Kochubey O, Lou X, Schneggenburger R (2011) Regulation of transmitter release by Ca(2+) and synaptotagmin: insights from a large CNS synapse. *Trends Neurosci* 34:237-246.

Koester HJ, Johnston D (2005) Target cell-dependent normalization of transmitter release at neocortical synapses. *Science* 308:863-866.

Koh DS, Burnashev N, Jonas P (1995) Block of native Ca²⁺-permeable AMPA receptors in rat brain by intracellular polyamines generates double rectification. *J Physiol* 486 (Pt 2):305-312.

Koike M, Iino M, Ozawa S (1997) Blocking effect of 1-naphthyl acetyl spermine on Ca²⁺-permeable AMPA receptors in cultured rat hippocampal neurons. *Neuroscience research* 29:27-36.

Koike M, Tsukada S, Tsuzuki K, Kijima H, Ozawa S (2000) Regulation of kinetic properties of GluR2 AMPA receptor channels by alternative splicing. *J Neurosci* 20:2166-2174.

Kooijmans RN, Self MW, Wouterlood FG, Belien JA, Roelfsema PR (2014) Inhibitory interneuron classes express complementary AMPA-receptor patterns in macaque primary visual cortex. *J Neurosci* 34:6303-6315.

Kudoh SN, Taguchi T (2002) A simple exploratory algorithm for the accurate and fast detection of spontaneous synaptic events. *Biosens Bioelectron* 17:773-782.

Kullmann DM, Lamsa KP (2007) Long-term synaptic plasticity in hippocampal interneurons. *Nat Rev Neurosci* 8:687-699.

Kullmann DM, Moreau AW, Bakiri Y, Nicholson E (2012) Plasticity of inhibition. *Neuron* 75:951-962.

Kumar SS, Bacci A, Kharazia V, Huguenard JR (2002) A developmental switch of AMPA receptor subunits in neocortical pyramidal neurons. *J Neurosci* 22:3005-3015.

Kutsuwada T, Kashiwabuchi N, Mori H, Sakimura K, Kushiya E, Araki K, Meguro H, Masaki H, Kumanishi T, Arakawa M, et al. (1992) Molecular diversity of the NMDA receptor channel. *Nature* 358:36-41.

Kwak S, Weiss JH (2006) Calcium-permeable AMPA channels in neurodegenerative disease and ischemia. *Curr Opin Neurobiol* 16:281-287.

Lamsa K, Irvine EE, Giese KP, Kullmann DM (2007a) NMDA receptor-dependent long-term potentiation in mouse hippocampal interneurons shows a unique dependence on Ca^{2+} /calmodulin-dependent kinases. *J Physiol* 584:885-894.

Lamsa KP, Heeroma JH, Somogyi P, Rusakov DA, Kullmann DM (2007b) Anti-Hebbian long-term potentiation in the hippocampal feedback inhibitory circuit. *Science* 315:1262-1266.

Lamsa KP, Kullmann DM, Woodin MA (2010) Spike-timing dependent plasticity in inhibitory circuits. *Frontiers in Synaptic Neuroscience* 2.

Lee HK, Barbarosie M, Kameyama K, Bear MF, Huganir RL (2000) Regulation of distinct AMPA receptor phosphorylation sites during bidirectional synaptic plasticity. *Nature* 405:955-959.

Lefort S, Tomm C, Floyd Sarria JC, Petersen CC (2009) The excitatory neuronal network of the C2 barrel column in mouse primary somatosensory cortex. *Neuron* 61:301-316.

Lei S, McBain CJ (2002) Distinct NMDA receptors provide differential modes of transmission at mossy fiber-interneuron synapses. *Neuron* 33:921-933.

Leon-Espinosa G, DeFelipe J, Munoz A (2012) Effects of amyloid-beta plaque proximity on the axon initial segment of pyramidal cells. *J Alzheimers Dis* 29:841-852.

Lerma J (1992) Spermine regulates N-methyl-D-aspartate receptor desensitization. *Neuron* 8:343-352.

Letzkus JJ, Kampa BM, Stuart GJ (2006) Learning rules for spike timing-dependent plasticity depend on dendritic synapse location. *J Neurosci* 26:10420-10429.

Lisman J, Spruston N (2005) Postsynaptic depolarization requirements for LTP and LTD: a critique of spike timing-dependent plasticity. *Nat Neurosci* 8:839-841.

Liu SJ, Cull-Candy SG (2002) Activity-dependent change in AMPA receptor properties in cerebellar stellate cells. *J Neurosci* 22:3881-3889.

Lomeli H, Mosbacher J, Melcher T, Hoyer T, Geiger JR, Kuner T, Monyer H, Higuchi M, Bach A, Seeburg PH (1994) Control of kinetic properties of AMPA receptor channels by nuclear RNA editing. *Science* 266:1709-1713.

Lu J, Tucciarone J, Lin Y, Huang ZJ (2014) Input-specific maturation of synaptic dynamics of parvalbumin interneurons in primary visual cortex. *PNAS* 111:16895-16900.

Lu JT, Li CY, Zhao JP, Poo MM, Zhang XH (2007) Spike-timing-dependent plasticity of neocortical excitatory synapses on inhibitory interneurons depends on target cell type. *J Neurosci* 27:9711-9720.

MacDermott AB, Mayer ML, Westbrook GL, Smith SJ, Barker JL (1986) NMDA-receptor activation increases cytoplasmic calcium concentration in cultured spinal cord neurones. *Nature* 321:519-522.

Mahanty NK, Sah P (1998) Calcium-permeable AMPA receptors mediate long-term potentiation in interneurons in the amygdala. *Nature* 394:683-687.

Malinow R, Tsien RW (1990) Presynaptic enhancement shown by whole-cell recordings of long-term potentiation in hippocampal slices. *Nature* 346:177-180.

Markram H (1997) A network of tufted layer 5 pyramidal neurons. *Cerebral Cortex* 7:523-533.

Markram H, Gerstner W, Sjöström PJ (2011) A history of spike-timing-dependent plasticity. *Frontiers in Synaptic Neuroscience* 3:1-24.

Markram H, Lübke J, Frotscher M, Sakmann B (1997) Regulation of synaptic efficacy by coincidence of postsynaptic APs and EPSPs. *Science* 275:213-215.

Markram H, Toledo-Rodriguez M, Wang Y, Gupta A, Silberberg G, Wu C (2004) Interneurons of the neocortical inhibitory system. *Nat Rev Neurosci* 5:793-807.

Massey PV, Bashir ZI (2007) Long-term depression: multiple forms and implications for brain function. *Trends Neurosci* 30:176-184.

Massi L, Lagler M, Hartwich K, Borhegyi Z, Somogyi P, Klausberger T (2012) Temporal dynamics of parvalbumin-expressing axo-axonic and basket cells in the rat medial prefrontal cortex in vivo. *J Neurosci* 32:16496-16502.

Matta JA, Pelkey KA, Craig MT, Chittajallu R, Jeffries BW, McBain CJ (2013) Developmental origin dictates interneuron AMPA and NMDA receptor subunit composition and plasticity. *Nat Neurosci* 16:1032-1041.

Mattison HA, Bagal AA, Mohammadi M, Pulimood NS, Reich CG, Alger BE, Kao JP, Thompson SM (2014) Evidence of calcium-permeable AMPA receptors in dendritic spines of CA1 pyramidal neurons. *J Neurophysiol* 112:263-275.

Mayer ML, Westbrook GL (1987) Permeation and block of N-methyl-D-aspartic acid receptor channels by divalent cations in mouse cultured central neurones. *J Physiol* 394:501-527.

Meliza CD, Dan Y (2006) Receptive-field modification in rat visual cortex induced by paired visual stimulation and single-cell spiking. *Neuron* 49:183-189.

Meyerson JR, Kumar J, Chittori S, Rao P, Pierson J, Bartesaghi A, Mayer ML, Subramaniam S (2014) Structural mechanism of glutamate receptor activation and desensitization. *Nature* 514:328-334.

Miles R, Poncer JC (1996) Paired recordings from neurones. *Curr Opin Neurobiol* 6:387-394.

Milstein AD, Zhou W, Karimzadegan S, Bredt DS, Nicoll RA (2007) TARP subtypes differentially and dose-dependently control synaptic AMPA receptor gating. *Neuron* 55:905-918.

Mittmann W, Koch U, Hausser M (2005) Feed-forward inhibition shapes the spike output of cerebellar Purkinje cells. *J Physiol* 563:369-378.

Molnar G, Olah S, Komlosi G, Fule M, Szabadics J, Varga C, Barzo P, Tamas G (2008) Complex Events Initiated by Individual Spikes in the Human Cerebral Cortex. *PLoS biology* 6:e222.

Monaghan DT, Bridges RJ, Cotman CW (1989) The excitatory amino acid receptors: their classes, pharmacology, and distinct properties in the function of the central nervous system. *Annu Rev Pharmacol Toxicol* 29:365-402.

Monyer H, Sprengel R, Schoepfer R, Herb A, Higuchi M, Lomeli H, Burnashev N, Sakmann B, Seeburg PH (1992) Heteromeric NMDA receptors: molecular and functional distinction of subtypes. *Science* 256:1217-1221.

Moriyoshi K, Masu M, Ishii T, Shigemoto R, Mizuno N, Nakanishi S (1991) Molecular cloning and characterization of the rat NMDA receptor. *Nature* 354:31-37.

Morris RG, Anderson E, Lynch GS, Baudry M (1986) Selective impairment of learning and blockade of long-term potentiation by an N-methyl-D-aspartate receptor antagonist, AP5. *Nature* 319:774-776.

Mountcastle VB (1997) The columnar organization of the neocortex. *Brain* 120 (Pt 4):701-722.

Moyer JR, Jr., Brown TH (1998) Methods for whole-cell recording from visually preselected neurons of perirhinal cortex in brain slices from young and aging rats. *J Neurosci Methods* 86:35-54.

Müller-Dahlhaus F, Ziemann U, Classen J (2010) Plasticity resembling spike-timing dependent synaptic plasticity: the evidence in human cortex. *Frontiers in Synaptic Neuroscience* 2:12.

Murayama M, Perez-Garci E, Nevian T, Bock T, Senn W, Larkum ME (2009) Dendritic encoding of sensory stimuli controlled by deep cortical interneurons. *Nature* 457:1137-1141.

Nabavi S, Fox R, Proulx CD, Lin JY, Tsien RY, Malinow R (2014) Engineering a memory with LTD and LTP. *Nature* 511:348-352.

Nelson SB, Sjöström PJ, Turrigiano GG (2002) Rate and timing in cortical synaptic plasticity. *Philos Trans R Soc Lond B Biol Sci* 357:1851-1857.

Nicoll RA (1988) The coupling of neurotransmitter receptors to ion channels in the brain. *Science* 241:545-551.

Nissen W, Szabo A, Somogyi J, Somogyi P, Lamsa KP (2010) Cell type-specific long-term plasticity at glutamatergic synapses onto hippocampal interneurons expressing either parvalbumin or CB1 cannabinoid receptor. *J Neurosci* 30:1337-1347.

Nowak L, Bregestovski P, Ascher P, Herbet A, Prochiantz A (1984) Magnesium gates glutamate-activated channels in mouse central neurones. *Nature* 307:462-465.

O'Connor DH, Clack NG, Huber D, Komiyama T, Myers EW, Svoboda K (2010) Vibrissa-based object localization in head-fixed mice. *J Neurosci* 30:1947-1967.

Oliva AA, Jr., Jiang M, Lam T, Smith KL, Swann JW (2000) Novel hippocampal interneuronal subtypes identified using transgenic mice that express green fluorescent protein in GABAergic interneurons. *J Neurosci* 20:3354-3368.

Oren I, Nissen W, Kullmann DM, Somogyi P, Lamsa KP (2009) Role of ionotropic glutamate receptors in long-term potentiation in rat hippocampal CA1 oriens-lacunosum moleculare interneurons. *J Neurosci* 29:939-950.

Osakada F, Callaway EM (2013) Design and generation of recombinant rabies virus vectors. *Nature protocols* 8:1583-1601.

Osswald IK, Galan A, Bowie D (2007) Light triggers expression of philanthotoxin-insensitive Ca²⁺-permeable AMPA receptors in the developing rat retina. *J Physiol* 582:95-111.

Palma-Cerda F, Auger C, Crawford DJ, Hodgson AC, Reynolds SJ, Cowell JK, Swift KA, Cais O, Vyklicky L, Corrie JE, Ogden D (2012) New

caged neurotransmitter analogs selective for glutamate receptor sub-types based on methoxynitroindoline and nitrophenylethoxycarbonyl caging groups. *Neuropharmacology* 63:624-634.

Parra P, Gulyas AI, Miles R (1998) How many subtypes of inhibitory cells in the hippocampus? *Neuron* 20:983-993.

Pawlak V, Greenberg DS, Sprekeler H, Gerstner W, Kerr JN (2013) Changing the responses of cortical neurons from sub- to suprathreshold using single spikes in vivo. *eLife* 2:e00012.

Pawlak V, Wickens JR, Kirkwood A, Kerr JND (2010) Timing is not everything: neuromodulation opens the STDP gate. *Frontiers in Synaptic Neuroscience* 2:12.

Peled ES, Newman ZL, Isacoff EY (2014) Evoked and spontaneous transmission favored by distinct sets of synapses. *Curr Biol* 24:484-493.

Pellegrini-Giampietro DE, Gorter JA, Bennett MV, Zukin RS (1997) The GluR2 (GluR-B) hypothesis: Ca²⁺-permeable AMPA receptors in neurological disorders. *Trends Neurosci* 20:464-470.

Perin R, Berger TK, Markram H (2011) A synaptic organizing principle for cortical neuronal groups. *Proceedings of the National Academy of Sciences of the United States of America* 108:5419-5424.

Perin R, Markram H (2013) A computer-assisted multi-electrode patch-clamp system. *Journal of visualized experiments* : JoVE e50630.

Pfeffer CK, Xue M, He M, Huang ZJ, Scanziani M (2013) Inhibition of inhibition in visual cortex: the logic of connections between molecularly distinct interneurons. *Nat Neurosci* 16:1068-1076.

Pologruto TA, Sabatini BL, Svoboda K (2003) ScanImage: flexible software for operating laser scanning microscopes. *Biomed Eng Online* 2:13.

Pouille F, Scanziani M (2001) Enforcement of temporal fidelity in pyramidal cells by somatic feed-forward inhibition. *Science* 293:1159-1163.

Pouille F, Scanziani M (2004) Routing of spike series by dynamic circuits in the hippocampus. *Nature* 429:717-723.

Ragnarsson L, Mortensen M, Dodd PR, Lewis RJ (2002) Spermine modulation of the glutamate(NMDA) receptor is differentially responsive to conantokins in normal and Alzheimer's disease human cerebral cortex. *J Neurochem* 81:765-779.

Richards BA, Aizenman CD, Akerman CJ (2010) In vivo spike-timing-dependent plasticity in the optic tectum of *Xenopus laevis*. *Frontiers in Synaptic Neuroscience* 2.

Roberts PD, Leen TK (2010) Anti-hebbian spike-timing-dependent plasticity and adaptive sensory processing. *Front Comput Neurosci* 4:156.

Rodriguez-Moreno A, Paulsen O (2008) Spike timing-dependent long-term depression requires presynaptic NMDA receptors. *Nat Neurosci* 11:744-745.

Rozov A, Sprengel R, Seeburg PH (2012) GluA2-lacking AMPA receptors in hippocampal CA1 cell synapses: evidence from gene-targeted mice. *Frontiers in molecular neuroscience* 5:22.

Rubio-Garrido P, Perez-de-Manzo F, Porrero C, Galazo MJ, Clasca F (2009) Thalamic input to distal apical dendrites in neocortical layer 1 is massive and highly convergent. *Cereb Cortex* 19:2380-2395.

Salussolia CL, Wollmuth LP (2012) Flip-flopping to the membrane. *Neuron* 76:463-465.

Sara Y, Bal M, Adachi M, Monteggia LM, Kavalali ET (2011) Use-dependent AMPA receptor block reveals segregation of spontaneous and evoked glutamatergic neurotransmission. *J Neurosci* 31:5378-5382.

Scheuss V, Bonhoeffer T (2014) Function of dendritic spines on hippocampal inhibitory neurons. *Cereb Cortex* 24:3142-3153.

Schindelin J, Arganda-Carreras I, Frise E, Kaynig V, Longair M, Pietzsch T, Preibisch S, Rueden C, Saalfeld S, Schmid B, Tinevez JY, White DJ, Hartenstein V, Eliceiri K, Tomancak P, Cardona A (2012) Fiji: an open-source platform for biological-image analysis. *Nature Methods* 9:676-682.

Schneggenburger R (1996) Simultaneous measurement of Ca²⁺ influx and reversal potentials in recombinant N-methyl-D-aspartate receptor channels. *Biophysical journal* 70:2165-2174.

Scorcioni R, Polavaram S, Ascoli GA (2008) L-Measure: a web-accessible tool for the analysis, comparison and search of digital reconstructions of neuronal morphologies. *Nature protocols* 3:866-876.

Seol GH, Ziburkus J, Huang S, Song L, Kim IT, Takamiya K, Huganir RL, Lee H-K, Kirkwood A (2007) Neuromodulators control the polarity of spike-timing-dependent synaptic plasticity. *Neuron* 55:919-929.

Shimuta M, Yoshikawa M, Fukaya M, Watanabe M, Takeshima H, Manabe T (2001) Postsynaptic modulation of AMPA receptor-mediated synaptic responses and LTP by the type 3 ryanodine receptor. *Mol Cell Neurosci* 17:921-930.

Shin HG, Lu Z (2005) Mechanism of the voltage sensitivity of IRK1 inward-rectifier K⁺ channel block by the polyamine spermine. *J Gen Physiol* 125:413-426.

Shin J, Shen F, Huguenard JR (2005) Polyamines modulate AMPA receptor-dependent synaptic responses in immature layer v pyramidal neurons. *J Neurophysiol* 93:2634-2643.

Shin JH, Linden DJ (2005) An NMDA receptor/nitric oxide cascade is involved in cerebellar LTD but is not localized to the parallel fiber terminal. *J Neurophysiol* 94:4281-4289.

Sholl A, Uttley AM (1953) Pattern discrimination and the visual cortex. *Nature* 171:387-388.

Sholl DA (1953) Dendritic organization in the neurons of the visual and motor cortices of the cat. *J Anat* 87:387-406.

Silberberg G, Markram H (2007) Disynaptic inhibition between neocortical pyramidal cells mediated by Martinotti cells. *Neuron* 53:735-746.

Sjöström PJ, Häusser M (2006) A cooperative switch determines the sign of synaptic plasticity in distal dendrites of neocortical pyramidal neurons. *Neuron* 51:227-238.

Sjöström PJ, Nelson SB (2002) Spike timing, calcium signals and synaptic plasticity. *Curr Opin Neurobiol* 12:305-314.

Sjöström PJ, Rancz EA, Roth A, Häusser M (2008) Dendritic Excitability and Synaptic Plasticity. *Physiological Reviews* 88:769-840.

Sjöström PJ, Turrigiano GG, Nelson SB (2001) Rate, timing, and cooperativity jointly determine cortical synaptic plasticity. *Neuron* 32:1149-1164.

Sjöström PJ, Turrigiano GG, Nelson SB (2003) Neocortical LTD via coincident activation of presynaptic NMDA and cannabinoid receptors. *Neuron* 39:641-654.

Smart TG, Paoletti P (2012) Synaptic neurotransmitter-gated receptors. *Cold Spring Harbor perspectives in biology* 4.

Sobolevsky AI (2015) Structure and gating of tetrameric glutamate receptors. *J Physiol* 593:29-38.

Sommer B, Kohler M, Sprengel R, Seeburg PH (1991) RNA editing in brain controls a determinant of ion flow in glutamate-gated channels. *Cell* 67:11-19.

Somogyi P, Tamas G, Lujan R, Buhl EH (1998) Salient features of synaptic organisation in the cerebral cortex. *Brain Res Brain Res Rev* 26:113-135.

Song S, Miller KD, Abbott LF (2000) Competitive Hebbian learning through spike-timing-dependent synaptic plasticity. *Nat Neurosci* 3:919-926.

Song S, Sjöström PJ, Reigl M, Nelson S, Chklovskii DB (2005) Highly nonrandom features of synaptic connectivity in local cortical circuits. *PLoS biology* 3:e68.

Soto D, Coombs ID, Kelly L, Farrant M, Cull-Candy SG (2007) Stargazin attenuates intracellular polyamine block of calcium-permeable AMPA receptors. *Nat Neurosci* 10:1260-1267.

Stuart GJ, Häusser M (2001) Dendritic coincidence detection of EPSPs and action potentials. *Nature Neuroscience* 4:63-71.

Stuart GJ, Sakmann B (1994) Active propagation of somatic action potentials into neocortical pyramidal cell dendrites. *Nature* 367:69-72.

Studniarczyk D, Coombs I, Cull-Candy SG, Farrant M (2013) TARP gamma-7 selectively enhances synaptic expression of calcium-permeable AMPARs. *Nat Neurosci* 16:1266-1274.

Sun HY, Bartley AF, Dobrunz LE (2009) Calcium-permeable presynaptic kainate receptors involved in excitatory short-term facilitation onto somatostatin interneurons during natural stimulus patterns. *J Neurophysiol* 101:1043-1055.

Sun QQ, Wang X, Yang W (2014) Laserspritzer: a simple method for optogenetic investigation with subcellular resolutions. *PLoS one* 9:e101600.

Sutton MA, Schuman EM (2009) Partitioning the synaptic landscape: distinct microdomains for spontaneous and spike-triggered neurotransmission. *Sci Signal* 2:pe19.

Svoboda K, Yasuda R (2006) Principles of two-photon excitation microscopy and its applications to neuroscience. *Neuron* 50:823-839.

Swanson GT, Kamboj SK, Cull-Candy SG (1997) Single-channel properties of recombinant AMPA receptors depend on RNA editing, splice variation, and subunit composition. *J Neurosci* 17:58-69.

Sylwestrak EL, Ghosh A (2012) Elfn1 regulates target-specific release probability at CA1-interneuron synapses. *Science* 338:536-540.

Szabo A, Somogyi J, Cauli B, Lambolez B, Somogyi P, Lamsa KP (2012) Calcium-permeable AMPA receptors provide a common mechanism for LTP in glutamatergic synapses of distinct hippocampal interneuron types. *J Neurosci* 32:6511-6516.

Tao Y, Chen YJ, Shen C, Luo Z, Bates CR, Lee D, Marchetto S, Gao TM, Borg JP, Xiong WC, Mei L (2013) Erbin interacts with TARP gamma-2 for surface expression of AMPA receptors in cortical interneurons. *Nat Neurosci* 16:290-299.

Testa-Silva G, Verhoog MB, Goriounova NA, Loebel A, Hjorth J, Baayen JC, de Kock CP, Mansvelder HD (2010) Human synapses show a

wide temporal window for spike-timing-dependent plasticity. *Front Synaptic Neurosci* 2:12.

Thomson AM, Deuchars J, West DC (1993) Large, deep layer pyramid-pyramid single axon EPSPs in slices of rat motor cortex display paired pulse and frequency-dependent depression, mediated presynaptically and self-facilitation, mediated postsynaptically. *J Neurophysiol* 70:2354-2369.

Thomson AM, West DC, Wang Y, Bannister AP (2002) Synaptic connections and small circuits involving excitatory and inhibitory neurons in layers 2-5 of adult rat and cat neocortex: triple intracellular recordings and biocytin labelling in vitro. *Cereb Cortex* 12:936-953.

Toledo-Rodriguez M, Goodman P, Illic M, Wu C, Markram H (2005) Neuropeptide and calcium-binding protein gene expression profiles predict neuronal anatomical type in the juvenile rat. *J Physiol* 567:401-413.

Toth K, McBain CJ (1998) Afferent-specific innervation of two distinct AMPA receptor subtypes on single hippocampal interneurons. *Nat Neurosci* 1:572-578.

Traynelis SF, Wollmuth LP, McBain CJ, Menniti FS, Vance KM, Ogden KK, Hansen KB, Yuan H, Myers SJ, Dingledine R (2010) Glutamate receptor ion channels: structure, regulation, and function. *Pharmacological reviews* 62:405-496.

Trussell LO, Fischbach GD (1989) Glutamate receptor desensitization and its role in synaptic transmission. *Neuron* 3:209-218.

Turecek R, Vlcek K, Petrovic M, Horak M, Vlachova V, Vyklicky L, Jr. (2004) Intracellular spermine decreases open probability of N-methyl-D-aspartate receptor channels. *Neuroscience* 125:879-887.

Tzounopoulos T, Kim Y, Oertel D, Trussell LO (2004) Cell-specific, spike timing-dependent plasticities in the dorsal cochlear nucleus. *Nat Neurosci* 7:719-725.

Tzounopoulos T, Rubio ME, Keen JE, Trussell LO (2007) Coactivation of pre- and postsynaptic signaling mechanisms determines cell-specific spike-timing-dependent plasticity. *Neuron* 54:291-301.

Urban-Ciecko J, Fanselow EE, Barth AL (2015) Neocortical somatostatin neurons reversibly silence excitatory transmission via GABA_B receptors. *Curr Biol* 25:722-731.

van Welie I, Smith IT, Watt AJ (2011) The metamorphosis of the developing cerebellar microcircuit. *Curr Opin Neurobiol* 21:245-253.

Varela JA, Sen K, Gibson J, Fost J, Abbott LF, Nelson SB (1997) A quantitative description of short-term plasticity at excitatory synapses in layer 2/3 of rat primary visual cortex. *J Neurosci* 17:7926-7940.

Varshney LR, Sjöström PJ, Chklovskii DB (2006) Optimal Information Storage in Noisy Synapses under Resource Constraints. *Neuron* 52:409-423.

Wahle P (1993) Differential regulation of substance P and somatostatin in Martinotti cells of the developing cat visual cortex. *J Comp Neurol* 329:519-538.

Wang HX, Gao WJ (2010) Development of calcium-permeable AMPA receptors and their correlation with NMDA receptors in fast-spiking interneurons of rat prefrontal cortex. *J Physiol* 588:2823-2838.

Wang Y, Gupta A, Toledo-Rodriguez M, Wu CZ, Markram H (2002) Anatomical, physiological, molecular and circuit properties of nest basket cells in the developing somatosensory cortex. *Cereb Cortex* 12:395-410.

Wang Y, Toledo-Rodriguez M, Gupta A, Wu C, Silberberg G, Luo J, Markram H (2004) Anatomical, physiological and molecular properties of Martinotti cells in the somatosensory cortex of the juvenile rat. *J Physiol* 561:65-90.

Washburn MS, Dingledine R (1996) Block of alpha-amino-3-hydroxy-5-methyl-4-isoxazolepropionic acid (AMPA) receptors by polyamines and polyamine toxins. *J Pharmacol Exp Ther* 278:669-678.

Watanabe S, Kusama-Eguchi K, Kobayashi H, Igarashi K (1991) Estimation of polyamine binding to macromolecules and ATP in bovine lymphocytes and rat liver. *J Biol Chem* 266:20803-20809.

Watt AJ, Cuntz H, Mori M, Nusser Z, Sjöström PJ, Häusser M (2009) Traveling waves in developing cerebellar cortex mediated by asymmetrical Purkinje cell connectivity. *Nat Neurosci* 12:463-473.

Wickersham IR, Lyon DC, Barnard RJ, Mori T, Finke S, Conzelmann KK, Young JA, Callaway EM (2007) Monosynaptic restriction of transsynaptic tracing from single, genetically targeted neurons. *Neuron* 53:639-647.

Wolters A, Schmidt A, Schramm A, Zeller D, Naumann M, Kunesch E, Benecke R, Reiners K, Classen J (2005) Timing-dependent plasticity in human primary somatosensory cortex. *J Physiol* 565:1039-1052.

Wonders CP, Anderson SA (2006) The origin and specification of cortical interneurons. *Nat Rev Neurosci* 7:687-696.

Wonders CP, Taylor L, Welagen J, Mbata IC, Xiang JZ, Anderson SA (2008) A spatial bias for the origins of interneuron subgroups within the medial ganglionic eminence. *Dev Biol* 314:127-136.

Wright A, Vissel B (2012) The essential role of AMPA receptor GluR2 subunit RNA editing in the normal and diseased brain. *Frontiers in molecular neuroscience* 5:34.

Xu NL, Ye CQ, Poo MM, Zhang XH (2006) Coincidence detection of synaptic inputs is facilitated at the distal dendrites after long-term potentiation induction. *J Neurosci* 26:3002-3009.

Xu T-X, Yao W-D (2010) D1 and D2 dopamine receptors in separate circuits cooperate to drive associative long-term potentiation in the prefrontal cortex. *Proc Natl Acad Sci USA* 107:16366-16371.

Yang Y, Adowski T, Ramamurthy B, Neef A, Xu-Friedman MA (2015) High-speed dynamic-clamp interface. *J Neurophysiol* 113:2713-2720.

Zucker RS, Regehr WG (2002) Short-term synaptic plasticity. *Annu Rev Physiol* 64:355-405.